POLSKA AKADEMIA NAUK
INSTYTUT FIZYKI
POLSKIE TOWARZYSTWO FIZYCZNE

ACTA PHYSICA POLONICA

MIESIĘCZNIK

Vol. XX—Fasc. 4

WARSZAWA 1961

PAŃSTWOWE WYDAWNICTWO NAUKOWE

PAŃSTWOWE WYDAWNICTWO NAUKOWE — Oddział w Krakowie
Kraków, ul. Smoleńsk 14

Nakład 917 + 143 egz.	*Podpisano do druku 20 maja 1961*
Ark. wyd. 7 ark. druk. 5 7/8	*Druk ukończono w maju 1961*
Papier druk. sat. 80 g, kl. III, 70 × 100 cm	*Zam. prod. 88/61.*
Do składania 3 lutego 1961	*Cena zł 30,—*

DRUKARNIA NARODOWA W KRAKOWIE, ul. Manifestu Lipcowego 19

AN ATTEMPT TO CALCULATE THE REACTION $^{14}N(d, p)^{15}N^*$ BY THE BORN FIRST APPROXIMATION

By Ryszard Kołodziejski

Institute of Theoretical Physics, Warsaw

(Received July 29, 1959; revised manuscript received October 26, 1960)

The stripping differential cross sections are calculated for the case when the $2S$ level of ^{15}N is formed. Thomas' variational method is applied and the angular distribution of the emerging protons is calculated by the Born first approximation for four values of the range of the Yukawa potential. The proton-target nucleus forces are found to be at least just as important as the neutron-target nucleus forces. The angular distributions as obtained for the emerging protons and the absolute values of the differential cross sections are entirely different from the experimental values. The calculations give some hint that in stripping reactions the capture process takes place only on the edge of the nucleus.

The differential cross section for the reaction $^{14}N(d, p)^{15}N^*$ was measured by Warburton and Mc Gruer (1956), who used 14.8 MeV deuterons and measured the stripping differential cross section also for the case when the $2S$ level ($E=8.32$ MeV) of the ^{15}N nucleus is formed by neutron capture. It is interesting to compare their experimental results with the results of calculations carried out by the Born first approximation. In the present calculations, both proton-neutron interaction (potential V_{PN}) and proton-target nucleus interaction (potential V_{PT}) are taken into account. Thus, in our calculations we retain the two terms $\langle f|V_{PT}|i\rangle$ and $\langle f|V_{PN}|i\rangle$ in Owen and Fulton's exact formula (1957) for the stripping differential cross section:

$$\frac{d\sigma}{d\Omega} = \frac{1}{2}\,\frac{(2J+1)}{(2J_0+1)}\,\frac{1}{(2\pi)^2}\,\frac{(M+M_T)^2}{(2M+M_T)^2}\,\frac{v_p}{v_d}\,|\langle f|V_{PT}|i\rangle + \\ + \langle f|V_{PN}|i\rangle + \langle f|H_1^f G H_1^i|i\rangle|^2 \tag{1}$$

Eq. (1) is identical with the Owen and Fulton (1957) formula for a target-nucleus of finite mass M_T averaged over the initial spin orientations and summed over the final spin orientations. The symbols J_0 and J therein denote the ground state spin of ^{14}N and the $2S$ level ($E=8.32$ MeV) spin of ^{15}N, respectively. The velocities v_p and v_d are the relative velocities (as referred to the centre of mass of the final or initial nucleus) of the proton and deuteron.

The operators H_1^i and H_1^f in the third term of eq. (1) are given by

$$H_1^i = V_{NT} + V_{PT} \tag{2}$$

$$H_1^f = V_{PN} + V_{PT} \tag{3}$$

The symbol G in the third term in eq. (1) denotes the Green function for the full Hamiltonian of our problem. The matrix elements of eq. (1) are taken between the initial and final state wave functions. These are of the form

$$\psi_i = (2\pi)^{-3/2} \Phi_d(\vec{r}_P - \vec{r}_N)\zeta(\xi) \exp\left[i\tfrac{1}{2}\vec{k}_d(\vec{r}_N + \vec{r}_P) - i\vec{k}_d\vec{r}_T\right], \tag{4}$$

$$\psi_f = (2\pi)^{-3/2} \eta(\vec{r}_N - \vec{r}_T)\,\zeta(\xi) \exp\left[i\vec{k}_p\vec{r}_P - i\vec{k}_p\vec{r}_T\frac{M_T}{M+M_T} - i\vec{k}_p\vec{r}_N\frac{M}{M+M_T}\right]. \tag{5}$$

The function $\Phi_d(\vec{r}_N - \vec{r}_P)$ in (4) is the wave function of the deuteron.

The functions $\zeta(\xi)$ and $\eta_N(\vec{r}_N - \vec{r}_T)\zeta(\xi)$ are the ground state wave function of ^{14}N and the 2S-level wave function of ^{15}N, respectively. The wave vectors $\vec{k}_d$ and $\vec{k}_p$ are the deuteron and emerging proton wave vectors in the centre of mass system. The magnitudes of these vectors are:

$$k_d = \frac{M_T}{M_d+M_T}\left(\frac{2M_d\varepsilon_d}{\hbar^2}\right)^{1/2}\left(\frac{E_d^{(\mathrm{lab.})}}{\varepsilon_d}\right)^{1/2}$$

$$\simeq \frac{2M_T}{2M+M_T}\,2.316\times10^{12}\,\mathrm{cm}^{-1}\cdot\left(\frac{14.8\,\mathrm{MeV}}{2.226\,\mathrm{MeV}}\right)^{1/2}. \tag{6}$$

$$k_p = \left(\frac{2ME_p}{\hbar^2}\right)^{1/2} = 2.316\times10^{12}\,\mathrm{cm}^{-1}\cdot\left(\frac{24.829\,\mathrm{MeV}}{2.226\,\mathrm{MeV}}\right)^{1/2}. \tag{7}$$

We assume

$$M_d \simeq 2M,$$

where M is the nucleon mass and M_d — that of the deuteron. The energy E_p of the emerging proton in the centre of mass system is given by

$$\frac{M_T E_d^{(\mathrm{lab.})}}{M_d+M_T} - \varepsilon_d + \varepsilon_N = \frac{2M+M_T}{M+M_T}E_p, \tag{8}$$

where $\varepsilon_d = 2.226$ MeV, and $\varepsilon_N = 2.518$ MeV.

ε_d and ε_N denote the deuteron binding energy and the binding energy of the captured neutron. In order to calculate ε_N we assume the value 10.834 MeV for the last neutron binding energy in the ground state of ^{15}N (Ajzenberg and Lauritsen 1952).

For the relative velocities v_p/v_d ratio, we have the formula

$$\frac{v_p}{v_d} = \frac{(2M+M_T)\,M_T M_d k_p}{(M_d+M_T)\,(M+M_T)\,Mk_d} \simeq \frac{2M_T k_p}{(M+M_T)\,k_d} \tag{9}$$

Thus, the formula for the Born stripping differential cross section is finally obtained in the form

$$\frac{(2J_0+1)}{(2J+1)}\frac{d\sigma_{\text{Born}}}{d\Omega}=\frac{M_T(M+M_T)\,k_p}{(2\pi)^2\,(2M+M_T)^2k_d}\,|\langle f|V_{PT}|i\rangle+\langle f|V_{PN}|i\rangle|^2 \tag{10}$$

In order to evaluate the matrix elements $\langle f|V_{PT}|i\rangle$ and $\langle f|V_{PN}|i\rangle$, we assume, for the deuteron, the Hulthèn function:

$$\Phi_d(\vec{r}_P-\vec{r}_N)=N_d\frac{e^{-\alpha r}-e^{-\beta r}}{r}, \tag{11}$$

wherein $\alpha=2.316\times10^{12}\ \text{cm}^{-1}$, and $\beta=12.68\times10^{12}\ \text{cm}^{-1}$.

The normalization constant N_d is given by

$$N_d=\left[\frac{\alpha\beta(\alpha+\beta)}{2\pi(\beta-\alpha)^2}\right]^{1/2}. \tag{12}$$

The Yukawa potential V_{PN} associated with this function has the depth V_0 and the range r_0 given by

$$V_0=\frac{\hbar^2K^2}{M}=68\,\text{MeV}. \tag{13}$$

$$r_0=\frac{1}{\mu_d}=1.18\times10^{-13}\,\text{cm}. \tag{14}$$

Therefore, the potential V_{PN} can be written as follows

$$V_{PN}=g_{PN}\frac{e^{-\mu_d|\vec{r}_P-\vec{r}_N|}}{|\vec{r}_P-\vec{r}_N|}. \tag{15}$$

The constant g_{PN} which, similarly to the constant g of the V_{PT} potential, appears in our formula (10), can be expressed thus:

$$g_{PN}=\frac{K^2}{\mu_d},$$

wherein

$$K^2=(2.316\times10^{12}\text{cm}^{-1})^2\,\frac{68\,\text{MeV}}{2.226\,\text{MeV}}.$$

It is convenient to assume the Wilson function for the bound neutron. We have thus

$$\eta_N(\vec{r}_N-\vec{r}_T)=N_Ne^{-\gamma|\vec{r}_N-\vec{r}_T|}, \tag{16}$$

with

$$N_N=\left(\frac{\gamma^3}{\pi}\right)^{1/2}$$

Assuming the potential V_{NT} to be of the form

$$V_{NT} = g \frac{e^{-\mu|r_N - r_T|}}{|\vec{r}_N - \vec{r}_T|} . \tag{17}$$

we find by the Thomas (1937) variational treatment the following two relations for the constants γ, g and μ:

$$\gamma = \tfrac{1}{2}(\varkappa_N - \tfrac{1}{2}\mu) + \tfrac{1}{2}(\varkappa_N^2 + 5\varkappa_N\mu + \tfrac{9}{4}\mu^2)^{1/2}, \tag{18}$$

$$g = \frac{2(\varkappa_N + \gamma)\,(\varkappa_N + \gamma + \mu)^2}{(2\gamma + \mu)^2} . \tag{19}$$

wherein $\varkappa_N$ denotes the magnitude of the bound neutron wave vector $\vec{\varkappa}_N$; the latter is given by

$$\varkappa_N = \left(\frac{2.518\,\mathrm{MeV}}{\hbar^2} \cdot \frac{2MM_T}{M + M_T}\right)^{1/2} \simeq 2.316 \times 10^{12}\,\mathrm{cm}^{-1} \left(\frac{2 \times 2.518\,\mathrm{MeV}}{2.226\,\mathrm{MeV}}\right)^{1/2} .$$

The postulate of charge independence of nuclear forces suggests the assumption of equality of the neutron-target nucleus and proton-target nucleus interactions. Hence, in our calculations we take the potential V_{PT} to be of form (17). Using the momentum space representation for the functions V_{PN}, V_{PT}, $\Phi_d(\vec{r}_P - \vec{r}_N)$, $\eta_N(r_N - \vec{r}_T)$ we obtain, by the Dalitz (1951) and Lewis (1956) formulas, the following expressions for the matrix elements:

$$\langle f\,|V_{PN}|\,i\rangle = \frac{2^5\pi^2 N_N N_d g_{PN}\gamma}{\left[\gamma^2 + \left(\vec{k}_d - \frac{M_T}{M + M_T}\,\vec{k}_p\right)^2\right]^2 \left|\vec{k}_p - \frac{1}{2}\,\vec{k}_d\right|} \times$$

$$\times \left\{\operatorname{arctg} \frac{|\vec{k}_p - \tfrac{1}{2}\vec{k}_d|}{\mu_d + \alpha} - \operatorname{arctg} \frac{|\vec{k}_p - \tfrac{1}{2}\vec{k}_d|}{\mu_d + \beta}\right\} \tag{20}$$

$$\langle f\,|V_{PT}|\,i\rangle = 2^4\pi^2 N_N N_d g \left\{\frac{\frac{1}{2}\frac{\partial \eta_1\lambda_1}{\partial\gamma} - \xi_1\frac{\partial\xi_1}{\partial\gamma}}{(\eta_1\lambda_1 - \xi_1^2)^{3/2}} \operatorname{arctg} \frac{(\eta_1\lambda_1 - \xi_1^2)^{1/2}}{\xi_1} + \right.$$

$$+ \frac{\lambda_1\eta_1\frac{\partial\xi_1}{\partial\gamma} - \frac{1}{2}\frac{\partial\eta_1\lambda_1}{\partial\gamma}\xi_1}{(\eta_1\lambda_1 - \xi_1^2)\,\eta_1\lambda_1} - \frac{\frac{1}{2}\frac{\partial\eta_2\lambda_2}{\partial\gamma} - \xi_2\frac{\partial\xi_2}{\partial\gamma}}{(\eta_2\lambda_2 - \xi_2^2)^{3/2}} \operatorname{arctg} \frac{(\eta_2\lambda_2 - \xi_2^2)^{1/2}}{\xi_2}$$

$$\left. - \frac{\lambda_2\eta_2\frac{\partial\xi_2}{\partial\gamma} - \frac{1}{2}\frac{\partial\eta_2\lambda_2}{\partial\gamma}\xi_2}{(\eta_2\lambda_2 - \xi_2^2)\,\eta_2\lambda_2}\right\} \tag{21}$$

where ξ_1 and $\eta_1\lambda_1$ are given as follows:

$$\xi_1 = \left[\left(\vec{k}_p - \frac{1}{2}\,\vec{k}_d\right)^2 + (\alpha + \mu)^2\right]\gamma + \left[\gamma^2 + \left(\vec{k}_d - \frac{M_T}{M_T + M}\,\vec{k}_p\right)^2 + \mu^2\right]\alpha +$$

$$+ \left[\gamma^2 + \left(\vec{k}_p\frac{M}{M_T + M} + \frac{1}{2}\,\vec{k}_d\right)^2 + \alpha^2\right]\mu \tag{22}$$

$$\eta_1\lambda_1 = \left[\left(\vec{k}_p - \frac{1}{2}\vec{k}_d\right)^2 + (\alpha+\mu)^2\right]\left[\left(\frac{M}{M_T+M}\vec{k}_p - \vec{k}_d\right)^2 + (\gamma+\mu)^2\right] \times$$

$$\times \left[\left(\frac{M}{M_T+M}\vec{k}_p + \frac{1}{2}\vec{k}_d\right)^2 + (\gamma+\alpha)^2\right] \qquad (23)$$

The formulas for ξ_2 and $\eta_2\lambda_2$ are analogous to those for ξ_1 and $\eta_1\lambda_1$; however, the symbol α therein should be replaced by β. Tables I and II give the results of calculations and the experimental data.

TABLE I

Angle	Calculated differential cross section $\frac{2J_0+1}{2J+1}\frac{d\sigma}{d\Omega}\left[\frac{\text{barn}}{\text{ster}}\right]$ Range of the potentials V_{NT}, V_{PT}				Experim. diff. cross section $\frac{d\sigma}{d\Omega}\left[\frac{\text{barn}}{\text{ster}}\right]$
	2×10^{-13} cm.	3×10^{-13} cm.	4.7×10^{-13} cm.	6×10^{-13} cm.	
$\theta=0°$	0.80	1.02	1.46	1.55	0.04
$\theta=10°$	0.70	0.86	1.20	1.25	0.014
$\theta=20°$	0.50	0.56	0.71	0.71	0.001
$\theta=40°$	0.18	0.17	0.17	0.16	0.004

Table I contains the angular distributions of protons from the reaction $^{14}N(d, p)^{15}N^*$. Here, the symbol $^{15}N^*$ denotes the excited state of the ^{15}N nucleus, which is formed by the capture of a neutron in the $2S$ level. These angular distributions correspond to four ranges $r = 1/\mu$ of the potentials V_{PT} and V_{NT}. For each range of the potentials V_{PT} and V_{NT}, the four values of the stripping differential cross section fix the shape of the angular protons distribution. These four values of the differential cross section are given for angles $\theta = 0°$, $10°$, $20°$, $40°$ which the vector $\vec{k}_p$ subtends with the vector $\vec{k}_d$. In the last column of table I, the experimental values of the stripping differential cross section are included. From Table I it is readily seen that the experimental angular proton distribution is much more strongly peaked in the forward direction than the theoretical one. The same remains true even if we disregard the V_{PT} interaction.

TABLE II

Range of the potentials V_{PT}, V_{NT}	Values of the ratio $\frac{\langle f\|V_{PT}\|i\rangle}{\langle f\|V_{PN}\|i\rangle}$			
	Angle $\theta=0°$	Angle $\theta=10°$	Angle $\theta=20°$	Angle $\theta=40°$
2×10^{-13} cm.	0.55	0.59	0.70	1.16
3×10^{-13} cm.	0.59	0.64	0.76	0.29
4.7×10^{-13} cm.	0.81	0.84	1.01	1.64
6×10^{-13} cm.	0.81	0.86	1.04	1.68

From the Table II it can be concluded that, in the stripping reaction, the proton-target nucleus forces are at least just as important as the neutron-target nucleus forces. The Born first approximation tells us even more. Namely, for smaller binding energies of the captured neutrons (e.g., for $\varepsilon_N = 1.26$ MeV) the matrix element $\langle f|V_{PT}|i\rangle$ in eq. (10) can be quite decisive in fixing the shape of the angular distributions of the emerging protons. This situation arises on account of the resonances which occur at this small binding energy, and which sometimes yield monstrous stripping differential cross sections. The fact that no such effect occurs experimentally can serve as a hint that the capture process takes place on the edge of the nucleus only.

REFERENCES

Dalitz, R. H., *Proc. Roy. Soc.*, A. **206**, 506 (1951).
Fulton, T. and Owen, G. E., *Phys. Rev.*, **108**, 789 (1957).
Lauritsen, T. and Ajzenberg, F., *Rev. mod. Phys.*, **24**, 321 (1952).
Lewis, R. R., *Phys. Rev.*, **102**, 537 (1956).
Thomas, L. R., *Phys. Rev.*, **51**, 202 (1937).
Warburton and Mc Gruer, *Phys. Rev.*, **105**, 639 (1956).

DIPOLE ARRANGEMENT IN PEROVSKITE-TYPE FERROELECTRICS

By A. Jaśkiewicz

Institute of Experimental Physics, Wrocław University, Wrocław

And H. Konwent

Institute of Theoretical Physics, Wrocław University, Wrocław

(Received September 7, 1960)

A method of investigating the dipole arrangement when perovskite-type crystals transform from non-polar to polar state is proposed. Thermal fluctuations cause thermal dipoles to be formed when the crystal begins to undergo transformation. A thermal dipole thus formed gives rise to an electric field in its surrounding favouring some directions for displacement of neighbouring ions. Discussion of ABO_3 substances with ferroelectrically active B ion indicate that there is one possible ferroelectric arrangement and three antiferroelectric ones. The ferro- or antiferroelectric arrangement is shown to depend on the polarizability of the A ion and on the lattice constant.

1. Introduction

The structure of perovskite attracts much attention owing to its simplicity. The chemical formula of substances with this structure is ABO_3, where A is a di- or monovalent metal and B a tetra- or pentavalent one. It is assumed that the ionic binding is more pronounced than the covalent one. Among these substances, there are ferroelectrics as well as antiferroelectrics.

A ferroelectric crystal is characterized by the presence of spontaneous polarization, i.e. all elementary dipoles are aligned in one direction. An antiferroelectric crystal exhibits no spontaneous polarization. In an antiferroelectric, dipoles oriented in the same direction form chains along the direction of polarization, but two neighbouring chains are polarized antiparallel. Such chain polarization, results in the total absence of macroscopic polarization.

It is commonly assumed, that the thermal dipoles in ABO_3 crystals are formed by ion displacement. When all the ions are displaced in the same direction, thermal parallel dipoles are formed. If neighbouring ions are displaced in opposite directions, antiparallel dipoles are formed. An ion leading to the formation of a dipole is termed ferroelectrically active. In the materials under consideration, an A or B ion can be ferroelectrically active

(Venevcev and Zhdanov 1956). Ion displacement takes place along one of the axes, parallel to a cube edge, a face diagonal, or a body diagonal.

The aim of the present paper is to investigate the mechanism of formation of ferro- and antiferroelectric arrangement in crystals of the perovskite-type structure, when only the B ion is ferroelectrically active.

Assume the crystal under investigation to trasform from the non-polar to the polar phase. At sufficiently low temperature, a B ion is displaced and thus a thermal dipole is formed. This dipole produces an electric field in its neighbourhood. The electric field induces elastic dipoles in nieghbouring A and O ions. The electric field produced by the elastic dipoles and by the thermal dipole acts on the nearest B ions and so facilitates the formation of further thermal dipoles. The direction of the B ion displacements depends on the direction of the electric field and therefore the orientation of the thermal dipoles formed depends on the direction of the electric field. By evaluating the electric field at the B ion sites, we can obtain the thermal dipole arrangement and the state of the polar substance.

2. *Polarization of the elementary cell*

In Mason and Matthias' theory (Mason and Matthias 1948) and in the theory of Piekara (Piekara 1954), the B ion is displaced into one of the six positions of minimum potential energy lying on the mutually perpendicular axes. In the cubic phase, the B ion occupies the symmetric position in an elementary cell, because its thermal energy is greater than the potential barrier U between the minimums of potential energy.

At temperature $T \sim U/k$, owing to thermal fluctuations, one B ion may be displaced to an asymmetric position, giving rise to an electric dipole. This dipole may induce elastic dipoles in the surrounding ions of the elementary cell. Such a polarized cell acts on the neighbouring ones as a polarizing agent.

We consider an elementary cell of a perovskite-type single crystal with cubic symmetry. In the lattice, the A ions occupy the corners of the cube, the B ions are at the cube centre, and the O ions are at the face centre (i.e. we have a simple cubic lattice of A ions, face centred by O ions, and body centred by B ions, Fig. I).

It is assumed that the B ion is displaced along the z-axis in the positive direction, giving rise to a thermal electric dipole with moment $m = m_z$. Throughout the present paper,

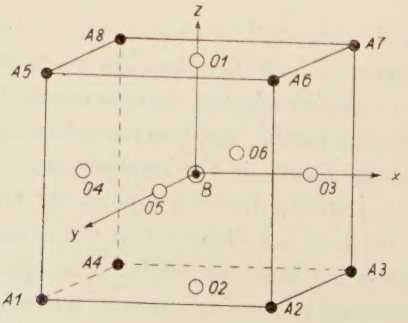

Fig. 1. Elementary cell of perovskite-type cubic crystal

this dipole will be treated as a point dipole. In evaluating its electric field, we make use of the well known formula for the field of a point dipole

$$\vec{E} = \frac{3\vec{r}(\vec{r}\,\vec{m}) - \vec{m}r^2}{r^5}. \tag{1}$$

The induced moment p_i in the ion of type i at the point (x, y, z) is computed from the equation

$$\vec{p}(x, y, z) = \alpha_i \vec{E}(x, y, z), \tag{2}$$

where α_i is the polarizability of an ion of type i. The coordinate system is shown in Fig. 1.

The coordinates of the ions in an elementary cell with lattice constant a are given as follows:

$$\begin{aligned}
&A1\left(-\frac{a}{2}, \frac{a}{2}, -\frac{a}{2}\right), && A5\left(-\frac{a}{2}, \frac{a}{2}, \frac{a}{2}\right),\\
&A2\left(\frac{a}{2}, \frac{a}{2}, -\frac{a}{2}\right), && A6\left(\frac{a}{2}, \frac{a}{2}, \frac{a}{2}\right),\\
&A3\left(\frac{a}{2}, -\frac{a}{2}, -\frac{a}{2}\right), && A7\left(\frac{a}{2}, -\frac{a}{2}, \frac{a}{2}\right),\\
&A4\left(-\frac{a}{2}, -\frac{a}{2}, -\frac{a}{2}\right), && A8\left(-\frac{a}{2}, -\frac{a}{2}, \frac{a}{2}\right),
\end{aligned} \tag{3}$$

$$\begin{aligned}
&O1\left(0, 0, \frac{a}{2}\right), && O4\left(-\frac{a}{2}, 0, 0\right),\\
&O2\left(0, 0, -\frac{a}{2}\right), && O5\left(0, \frac{a}{2}, 0\right),\\
&O3\left(\frac{a}{2}, 0, 0\right), && O6\left(0, -\frac{a}{2}, 0\right),
\end{aligned}$$

$$B(0, 0, 0).$$

The fields acting on the ions of type A and O are

$$E_x^{A1} = -E_x^{A2} = -E_x^{A3} = E_x^{A4} = -E_x^{A5} = E_x^{A6} = E_x^{A7} = -E_x^{A8} = \frac{8m_z}{3\sqrt{3}\,a^3},$$

$$-E_y^{A1} = -E_y^{A2} = E_y^{A3} = E_y^{A4} = E_y^{A5} = E_y^{A6} = -E_y^{A7} = -E_y^{A8} = \frac{8m_z}{3\sqrt{3}\,a^3},$$

$$\begin{aligned}
&E_z^{A1} = E_z^{A2} = E_z^{A3} = E_z^{A4} = E_z^{A5} = E_z^{A6} = E_z^{A7} = E_z^{A8} = 0,\\
&E_x^{O1} = E_x^{O2} = E_x^{O3} = E_x^{O4} = E_x^{O5} = E_x^{O6} = 0,\\
&E_y^{O1} = E_y^{O2} = E_y^{O3} = E_y^{O4} = E_y^{O5} = E_y^{O6} = 0,
\end{aligned} \tag{4}$$

$$E_z^{O1} = E_z^{O2} = \frac{16 m_z}{a^3},$$

$$E_z^{O3} = E_z^{O4} = E_z^{O5} = E_z^{O6} = -\frac{8 m_z}{a^3}.$$

Denoting the ionic polarizabilities α_A, α_O for the ions A and O, respectively, we obtain the following values for the dipole moments induced in the ions of the cell under consideration:

$$p_x^{A1} = -p_x^{A2} = -p_x^{A3} = p_x^{A4} = -p_x^{A5} = p_x^{A6} = p_x^{A7} = -p_x^{A8} = \alpha_A \frac{8 m_z}{3\sqrt{3}\, a^3},$$

$$-p_y^{A1} = -p_y^{A2} = p_y^{A3} = p_y^{A4} = p_y^{A5} = p_y^{A6} = -p_y^{A7} = -p_y^{A8} = \alpha_A \frac{8 m_z}{3\sqrt{3}\, a^3},$$

$$p_z^{A1} = p_z^{A2} = p_z^{A3} = p_z^{A4} = p_z^{A5} = p_z^{A6} = p_z^{A7} = p_z^{A8} = 0,$$

$$p_x^{O1} = p_x^{O2} = p_x^{O3} = p_x^{O4} = p_x^{O5} = p_x^{O6} = 0, \tag{5}$$

$$p_y^{O1} = p_y^{O2} = p_y^{O3} = p_y^{O4} = p_y^{O5} = p_y^{O6} = 0,$$

$$p_z^{O1} = p_z^{O2} = \alpha_O \frac{16 m_z}{a^3},$$

$$p_z^{O3} = p_z^{O4} = p_z^{O5} = p_z^{O6} = -\alpha_O \frac{8 m_z}{a^3},$$

where p_x^{A1} is the x-component of the dipole moment induced in ion $A1$.

3. *Electric field at B ion sites*

In order to evaluate the polarization induced by the polarized cell in the surrounding ones, we take into account the interaction between the nearest neighbours. The polarized cell is surrounded by six adjoining cells with the faces in common. Polarization of each joint face is already known, the latter being part of the polarized cell. The cells are numbered as follows: the cell adjoining to the face centered by the $O1$ ion gets number one, that adjoining to the face centered by the $O2$ ion gets number two, etc... The remaining cells have polarized corners and edges. The influence of these corners and edges on the cells they have in common is relatively small and therefore in further considerations may be neglected.

The polarization induced in the surrounding cells by the polarized cell may be easily computed if the electric fields are known. Therefore, now proceed to compute the electric fields acting on the B ions at the symmetry positions in the cells numbered 1, 2, 3, 4, 5, and 6 due to the dipoles in the polarized cell. With regard to the symmetry conditions, we compute separately the electric field acting on the cells 1 and 2 and on the remaining ones.

The electric field strength at the centre of cells 1 and 2 due to the dipoles induced in ion A of the zero cell (polarized cell) is given by

$$E_x = E_y = 0, \qquad E_z = -\frac{512}{27} \frac{\alpha_A m_z}{a^6}. \tag{6}$$

The electric field strength due to the dipoles induced in ion O at the centre of cells 1 and 2 is given by

$$E_x = E_y = 0, \qquad E_z = 256 \frac{\alpha_O m_z}{a^6}. \tag{7}$$

The electric field at the centre of cells 1 and 2 due to the thermal dipole of the zero cell is

$$E_x = E_y = 0, \qquad E_z = 2 \frac{m_z}{a^3}. \tag{8}$$

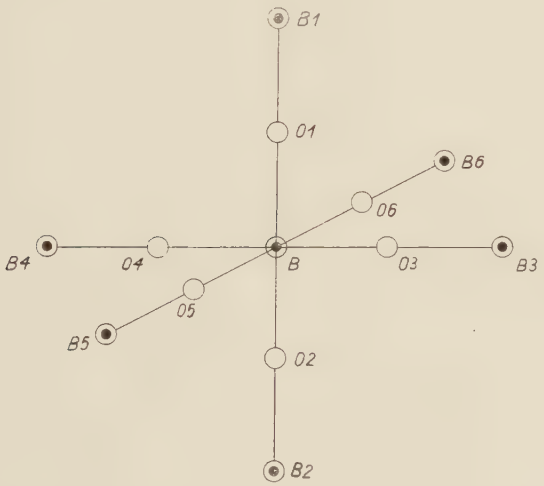

Fig. 2. Configuration of the B ions nearest to the primarily displaced B ion

The total electric field at the centre of cells 1 and 2 is

$$E_x^{(1)} = E_y^{(1)} = 0, \qquad E_z = \left(256 \frac{\alpha_O}{a^3} + 2 - \frac{512}{27} \frac{\alpha_A}{a^3}\right) \frac{m_z}{a^3}. \tag{9}$$

We are now able to compute the electric field at the centre of cells 3, 4, 5, and 6 given rise to by the dipoles induced in the O ions:

$$E_x = E_y = 0, \qquad E_z = 64 \frac{\alpha_O m_z}{a^6}. \tag{10}$$

The field due to the dipoles induced in the A ions is

$$E_x = E_y = E_z = 0. \tag{11}$$

The electric field due to the thermal dipole of the zero cell is

$$E_x = E_y = 0, \qquad E_z = -\frac{m_z}{a^3}. \tag{12}$$

The total electric field at the center of cells 3, 4, 5 and 6 is

$$E_x^{(3)} = E_y^{(3)} = 0, \quad E_z^{(3)} = \left(64\frac{\alpha_O}{a^3} - 1\right)\frac{m_z}{a^3}. \tag{13}$$

We see that, at the sites of the B ions in cells 1 and 2 electric fields are acting which tend to displace the B ion in the positive direction along the z-axis, and others tending to displace it in the negative direction. The field acting in the positive direction is produced by the dipoles induced in the O ions (eq. (6)). Hence the resulting field depends on the same parameters as eqs. (6), (7) and (8). The $B1$ ion is displaced in the positive direction if the following condition is fulfilled:

$$E_z^{(1)} > 0. \tag{14}$$

For the displacement of the $B1$ ion in the negative direction we have

$$E_z^{(1)} < 0. \tag{15}$$

Considering the electric fields acting on the B ions in the side cells, we see that the field due to the dipole induced in the O ion as given by eq. (10) is oriented in the positive direction along the z-axis, whereas the field produced by the thermal dipole of the zero cell, as given by eq. (12), is oriented in the negative direction. The electric field produced by the A ions is zero, as is obvious from eq. (11). The electric fields given by eqs. (10) and (12), respectively, compete to displace the B ion in the positive or negative direction. The B ion will undergo displacement in the positive direction if the following condition is fulfilled:

$$E_z^{(3)} > 0. \tag{16}$$

The B ion is displaced in the negative direction if

$$E_z^{(3)} < 0. \tag{17}$$

The four conditions (14), (15), (16) and (17) yield four possible arrangements of the dipoles in the ferroelectric and antiferroelectric state. For a given crystal structure, we obtain the ferroelectric state (Fig. 3*a*) if the conditions (14) and (16) are fulfilled. Pairwise, the

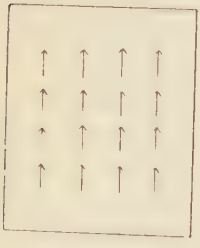

Fig. 3a

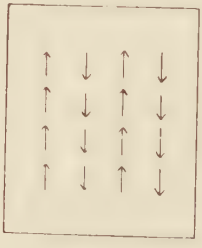

Fig. 3b

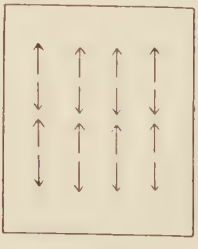

Fig. 3c

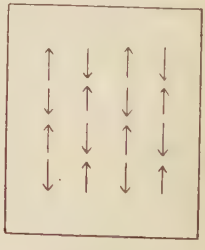

Fig. 3d

Fig. 3. Possible thermal dipole configurations for perovskite crystal when B ion is displaced from its original position

Fig. 3a. $E_z^{(1)} > 0$, $E_z^{(3)} > 0$, Fig. 3b. $E_z^{(1)} > 0$, $E_z^{(3)} < 0$,

Fig. 3c. $E_z^{(1)} < 0$, $E_z^{(3)} > 0$, Fig. 3d. $E_z^{(1)} < 0$, $E_z^{(3)} < 0$.

conditions: (14), (17); (15), (16); (15), (17) yield the antiferroelectric arrangement as presented in Figs. 3*b*, 3*c* and 3*d*, respectively. The three configurations 3*a*, 3*b* and 3*d* were discussed by Kinase (Kinase 1955) using the local field method.

The resulting fields $E_z^{(1)}$ and $E_z^{(3)}$ will cause permanent ion displacement if the energy of the thermal dipole thus formed in the electric field $E_z^{(1)}$ or $E_z^{(3)}$ is of the order of the thermal energy.

4. *Applications*

For ABO_3 substances, the polarizability of the O ion is $\alpha_O = 2.38 \times 10^{-24}\,\mathrm{cm}^3$ (cf. Slater 1951). Since the polarizability of the oxygen ion is known, we can write the conditions for a ferroelectric arrangement of the crystal in the form dependent on the lattice constant and the polarizability of the A ion. The conditions, in this new form, are readily applied to any particular ABO_3 substance.

From eqs. (14) and (16), using eqs. (9) and (13), we easily derive the inequalities which must be fulfilled for the substance to be in the ferroelectric state:

$$\alpha_A < 48.4 \times 10^{-24}\,\mathrm{cm}^3 \tag{18}$$

$$a < 5.35 \times 10^{-8}\,\mathrm{cm} \tag{19}$$

In $BaTiO_3$ and $KNbO_3$ crystals, the B ion is known to be ferroelectrically active; therefore, our results may be applied to these crystals. Since, in these crystals, the polarizability of the A ion and lattice constant fulfill conditions (18) and (19), these substances are ferroelectric.

An antiferroelectric arrangement results if, for a given crystal, inequality (18) or (19) is not fulfilled. As the polarizabilities of all known ions are of the order of that of oxygen ion, it is highly likely that condition (18) should be fulfilled. Therefore it may be anticipated that if the thermal dipoles are formed by the B ions only, ABO_3 crystals will present the ferroelectric state.

5. *Conclusion*

In this paper, we proposed a method of investigating the dipole arrangement occurring when a crystal transforms from the non-polar to the polar state. We discussed the dipole arrangement which will develop then. As transformations to a polar state set in, one ion is displaced from its original position forming a dipole and giving rise to an electric field in its neighbourhood.

From our considerations it may be inferred that the characteristic features of ordering of thermal dipoles depend essentially on the elastic dipoles induced in the A and O ions. Therefore, the ferro- or antiferroelectric arrangement will depend on the configurations and polarizabilities of the ions. The induced dipoles will not, however, affect the total electric moment of the elementary cell, since its resulting elastic electric moment is zero, as is easily inferred from formulas (5).

It is shown that, in crystals of perovskite-type structure, there are four possible kinds of the thermal dipole arrangements, for thermal dipoles formed by the B ions. One arrangement is a ferroelectric one and the three others are antiferroelectric.

In polar ABO_3 substances, with B ion ferroelectrically active, the ferroelectric arrangement can occur if the polarizability of the A ion is smaller than $18.4 \cdot 10^{-24}$ cm^3 and if simultaneously, the lattice constant is smaller than $5.35 \cdot 10^{-8}$ cm. In known substances, the condition for the ferroelectric arrangement is fulfilled. It is expected that further ferroelectric and antiferroelectric arrangement will be found when considering ABO_3 substances with the A ion ferroelectrically active.

6. Acknowlegements

The authors wish to thank Professors R. S. Ingarden and J. Niklibore for valuable suggestions and discussion. The authors also wish to thank Professor J. Mazur, F. Inst. P., Head of the Low Temperature Laboratory, Institute of Physics, Polish Academy of Science, for his interest and comments.

REFERENCES

Kinase, W., *Progr. theor. Phys.*, **13**, 529 (1955).
Mason, W. P. and Matthias, B. T., *Phys. Rev.*, **74**, 1622 (1948).
Piekara, A., *Proc. Conf. Phys. in Spała*, p. 268 (1954).
Slater, J. C., *Phys. Rev.*, **78**, 748 (1950).
Venevcev, Yu. N. nad Zhdanov, G. S., *Izv. Akad. Nauk SSSR, Ser. fiz.*, **20**, 178 (1956).

TRANSPORT OF CURRENT CARRIERS IN n-TYPE INDIUM ANTIMONIDE AT LOW TEMPERATURES

By J. Kołodziejczak

Institute of Physics, Polish Academy of Sciences, Warsaw

(Received September 29, 1960; translated paper received November 25, 1960)

The electric conductivity, Hall effect, and electron mobility are computed within the temperature range of 0° K to 100° K, account being taken of the non-parabolic structure of the conduction band, the ionic mechanism of scattering, and a weak magnetic field. The dependence of the effective mass on the electron concentration is derived. The transport equation is solved by Mc Clure's general method.

1. Structure of the Conduction Band

According to results due to Kane (1957), strong interaction between the conduction band and the valence band of light holes perturbs the parabolic character of either. Interaction with all remaining bands is considerably weaker and contributes anisotropic corrections to the energy that are negligible at $k^2 \ll 5 \cdot 10^{-4}$ atomic units. The absence of anisotropy in the cyclotron effective mass seems to corroborate the spherical band model (Dresselhaus et al. 1955). Measurements of absorption on free carriers (Spitzer et al. 1957) point to an effective mass of the electrons depending on the concentration of the latter. An identical result was obtained from measurements of the Faraday effect (Smith et al. 1959). The experimental dependence of the effective mass on the electron concentration confirmed the results of Kane's theory. The various energy bands are described by the equation

$$\varepsilon'(\varepsilon' - \varepsilon_g)\,(\varepsilon' + \Delta) - k^2P^2(\varepsilon' + \tfrac{2}{3}\Delta) = 0 \tag{1.1}$$

wherein

$$\varepsilon' = \varepsilon - \frac{\hbar^2 k^2}{2m_0}$$

ε_g is the energy gap at $k=0$, and Δ denotes spin-orbit splitting. The constant accounting for coupling between the conduction band and valence band is defined as follows:

$$P = -i\left(\frac{\hbar}{m_0}\right)\langle S|P_z|Z\rangle \tag{1.2}$$

wherein S and Z are the wave-functions corresponding to either band. For $\Delta \gg kP, \varepsilon_g$, the

expression describing the conduction band assumes the form

$$\varepsilon = \frac{\hbar^2 k^2}{2m_0} + \frac{1}{2}\left\{\varepsilon_g + \left(\varepsilon_g^2 + \frac{8}{3}P^2 k^2\right)^{1/2}\right\} . \tag{1.3}$$

Eq. (1.3) yields an accurate description of the structure of the conduction band at $k^2 \ll 5 \times$ $\times 10^{-4}$ atomic units, corresponding to electron concentrations of less than 10^{19} cm^{-3}.

2. *Transport Equation*

Assuming the existence of a relaxation time and the presence of an external magnetic field, the equation of transport can be written in the form

$$\frac{e}{\hbar}\left(\vec{E} + \frac{1}{c}\vec{v} \times \vec{H}\right) \operatorname{grad}_k f + \frac{f_0 - f}{\tau} = 0 \tag{2.1}$$

with the following notation:
$\vec{E}$ — electric field strength, $\vec{H}$ — magnetic field strength, $\vec{v}$ — electron velocity, f — distribution function, f_0 — distribution function at thermodynamic equilibrium, τ — time of relaxation.

The transport equation (2.1) was solved according to Mc Clure's method, yielding the following components of the conductivity tensor:

$$\sigma_{ik} = \frac{2e^2}{(2\pi)^3}\int d_3k \left(-\frac{\partial f_0}{\partial \varepsilon}\right) \tau S_{ik} \tag{2.2}$$

wherein S_{ik} are the components of a tensor, given by

$$S_{xx} = \sum_{m=1}^{\infty} \frac{2|v_x(m)|^2}{1 + (m\omega\tau)^2}$$

$$S_{xy} = \sum_{m=1}^{\infty} \left\{ \frac{v_x(m)\, v_y(-m) + v_x(-m)\, v_y(m)}{1 + (m\omega\tau)^2} + im\omega\tau \frac{v_x(-m)\, v_y(m) - v_x(m)\, v_y(-m)}{1 + (m\omega\tau)^2} \right\}$$

$$S_{zz} = v_z^2(0) + \sum_{m=1}^{\infty} \frac{2|v_z(m)|^2}{1 + (m\omega\tau)^2} \tag{2.3}$$

ω is the cyclotron frequency, and $v_i(m)$ — the coefficients of the Fourier expansion of the velocity. S_{xz}, S_{zx} and S_{yx} are obtained by varying the indices of $v(m)$. The Fourier coefficients $v_i(m)$ are obtained by solving the equation

$$\hbar\dot{\vec{k}} = -\frac{e}{c}\vec{v} \times \vec{H} \tag{2.4}$$

The velocity of the electron is given by

$$v_i = \frac{1}{\hbar}\frac{\partial \varepsilon}{\partial k_i} = \frac{1}{\hbar}\left\{\frac{\hbar^2}{m_0} + \frac{4}{3}\left(\varepsilon_g^2 + \frac{8}{3}k^2P^2\right)^{-\frac{1}{2}} P^2\right\} k_i \tag{2.5}$$

With the notation

$$\hbar^2 \left\{ \frac{\hbar^2}{m_0} + \frac{4}{3} \left(\varepsilon_g^2 + \frac{8}{3} k^2 P^2 \right)^{-\frac{1}{2}} P^2 \right\}^{-1} \equiv m^* \tag{2.6}$$

Eq. (2.5) can be rewritten as follows:

$$v_i = \frac{\hbar k_i}{m^*} \tag{2.7}$$

Hence, the electron can be considered to be free if its mass is assumed to be given by eq. (2.6).

The solutions of eq. (2.4) are the following:

$$\begin{aligned} v_x &= \frac{c\hbar}{eH} \omega \frac{1}{2} k_p \left[e^{i\omega t} + e^{-i\omega t} \right] \\ v_y &= -\frac{c\hbar}{eH} \omega \frac{i}{2} k_p \left[e^{i\omega t} - e^{-i\omega t} \right] \end{aligned} \tag{2.8}$$

with ω denoting the cyclotron frequency as given by

$$\omega = \frac{eH}{c\hbar^2} \left\{ \frac{\hbar^2}{m_0} + \frac{4}{3} \left(\varepsilon_g^2 + \frac{8}{3} k^2 P^2 \right)^{-\frac{1}{2}} P^2 \right\} = \frac{eH}{cm^*} \tag{2.9}$$

k_p is the projection of the wave vector on the plane perpendicular to the direction of the magnetic field. The following relations hold:

$$k_p = (k_x^2 + k_y^2)^{1/2}; \qquad k = (k_p^2 + k_H^2)^{1/2} \tag{2.10}$$

By (2.8), the following Fourier coefficients are obtained:

$$\begin{aligned} v_x(1) &= v_x(-1) = \frac{c\hbar}{eH} \omega \frac{1}{2} k_p \\ v_y(1) &= -v_y(-1) = \frac{c\hbar}{eH} \omega \frac{i}{2} k_p \\ v_z(0) &= \frac{c\hbar}{eH} \omega k_H \end{aligned} \tag{2.11}$$

All other coefficients vanish.

With eqs. (2.2) and (2.3), the components of the conductivity tensor can now be written as follows:

$$\begin{aligned} \sigma_{xx} &= \sigma_{yy} = C \int_0^\infty A \frac{1}{1 + \tau^2 \omega^2} k^4 dk \\ \sigma_{yx} &= -\sigma_{xy} = C \int_0^\infty A \frac{\tau\omega}{1 + \tau^2 \omega^2} k^4 dk \\ \sigma_{zz} &= \sigma = C \int_0^\infty A k^4 dk \end{aligned} \tag{2.12}$$

wherein

$$C = \frac{h^2 e^2}{12\pi^4}; \qquad A = \left(-\frac{\partial f_0}{\partial \varepsilon}\right) \tau \left(\frac{1}{m^*}\right)^2$$

Subsequently, only the case of so-called weak magnetic fields will be considered, a determined by the condition $\tau\omega \ll 1$. The conductivity tensor components are now given b

$$\sigma_{xx} = \sigma_{yy} = \sigma = C \int_0^{\sim} A k^4 dk \qquad (2.13$$

$$\sigma_{yx} = -\sigma_{xy} = C \int_0^{\infty} A \tau \omega k^4 dk$$

3. *The Conductivity Tensor at Low Temperatures*

The scattering mechanism predominant throughout the temperature range of 0 – 100 K is that of scattering on ionized impurities. The relaxation time for the case under consider ation is (Barrie 1956):

$$\tau = \frac{\hbar \varkappa^2}{2\pi e^4 N} k^2 \frac{d\varepsilon}{dk} \left\{ \ln (1 - \xi) - \frac{\xi}{1 - \xi} \right\}^{-1}$$

$$\xi = \frac{4k^2}{q^2} \qquad (3.1$$

with N denoting the concentration of the scattering centres

$\varkappa$ — the dielectric constant, and

q — the screening constant.

The scattering potential is given by

$$V(r) = \frac{e}{\varkappa r} e^{-qr} \qquad (3.2$$

Eq. (3.1) is of a higher degree of accuracy than the Conwell-Weisskopf formula, as it takes into account the screening of the scattering centres by the electrons. The screening constant q is a function of the electron concentration. In order to facilitate subsequent computations it is of advantage to proceed to the integration of the expressions of eq. (2.13) over the energy. Assuming zero energy at the bottom of the conductivity band, eq. (3.1) can be rewritten as follows:

$$\varepsilon = \frac{\hbar^2 k^2}{2m_0} + \frac{1}{2} \left\{ \left[\varepsilon_g^2 + \frac{8}{3} k^2 P^2 \right]^{1/2} - \varepsilon_g \right\} \qquad (3.3$$

The constant P can be determined by comparing the effective cyclotron mass (2.6) with the value measured at cyclotron resonance. Such measurements carried out with samples of a very high degree of purity and at low temperatures (Dresselhaus et al. 1955) yielded an

ffective mass of m_n 0.013 m_0. Considering the high degree of purity of the samples and he low temperatures, this can be assumed to be the mass of the electrons at the bottom of he band of conductivity.

Putting $k = 0$ in the effective mass of eq. (2.6), and equating m^* and m_n, we have

$$P^2 = \frac{3}{4}\,\hbar^2 \varepsilon_g \frac{m_0 - m_n}{m_0 m_n} \tag{3.4}$$

olving eq. (3.3) in k yields

$$k = \frac{m_0}{\hbar}\sqrt{\frac{\varepsilon_g}{m_n}}\{1 + 2\chi\mu - \sqrt{1 + 4\chi(\mu - \mu^2)}\}^{1/2} \tag{3.5}$$

herein

$$\chi = \frac{\varepsilon}{\varepsilon_g}; \qquad \mu = \frac{m_n}{m_0}$$

m_n is the cyclotron mass of the electrons at the bottom of the conductivity band, i.e. at $k = 0$.

Considering that μ is a small quantity amounting to 0.013 (the latter results from measurements of m_n at cyclotron resonance), the root in the brackets in eq. (3.5) can be expanded n a power series. This procedure is fully justified, as the inequality

$$\varepsilon \ll \frac{\varepsilon_g}{4(\mu - \mu^2)} \tag{3.6}$$

s fulfilled even in samples containing the greatest amount of impurities. Indeed, at $\varepsilon_g =$ 0.23 eV the right hand side of the inequality is of the order of 6 eV, whilst the left hand ide, at an electron concentration of 10^{18} cm^{-3}, amounts to 0.16 eV.

Expansion in series yields, in the first approximation,

$$k = \frac{\sqrt{2m_n\varepsilon_g}}{\hbar}[\chi(1 + \chi)]^{1/2} \tag{3.7}$$

whence

$$k^4 dk = \frac{(2m_n\varepsilon_g)^{5/2}}{2\hbar^5}[\chi(1 + \chi)]^{3/2}(1 + 2\chi)\,d\chi \tag{3.8}$$

The effective mass of eq. (2.6) now assumes the form

$$m^* = m_n(1 + 2\chi) \tag{3.9}$$

The relaxation time of eq. (3.1) assumes that of

$$\tau = \frac{\varkappa^2(2m_n)^{1/2}}{\pi N e^4 B}\,\frac{[\varepsilon(1 + \chi)]^{3/2}}{1 + 2\chi} \tag{3.10}$$

with

$$B = \ln(1 + \xi) - \frac{\xi}{1 + \xi}; \qquad \xi = \frac{8m_n}{q^2\hbar^2}(1 + \chi) \tag{3.11}$$

In computing the screening constant q, the method proposed by Dingle (1955) is utilized; however, it was necessary to make allowance therein for the non-parabolic structure of the conductivity band.

The concentration of the electrons is given as follows:

$$n = \frac{2}{(2\pi)^3}\int f_0 d_3 k \tag{3.12}$$

by (3.7), this yields

$$n = \frac{4}{3}\left(\frac{2\pi m_n k_0 T}{h^2}\right)^{3/2}\frac{2}{\sqrt{\pi}}\, L_0^{3/2}(\beta, \eta) \tag{3.13}$$

The $L_k^n(\beta, \eta)$ are integrals defined as follows:

$$L_k^n = \int_0^{\infty}\left(-\frac{df_0}{dx}\right)(x+\beta x^2)^n\,(1+2\beta x)^k\,dx$$

The parameters are defined thus

$$\beta = \frac{k_0 T}{\varepsilon_g}; \qquad \eta = \frac{\zeta}{k_0 T}$$

with k_0 denoting the Boltzmann constant, and ζ — the Fermi level.

The electron concentration about a centre of positive charge is

$$n = \frac{4}{3}\left(\frac{2\pi m_n k_0 T}{h^2}\right)^{3/2}\frac{2}{\sqrt{\pi}}\, L_0^{3/2}(\beta, \eta + V^*) \tag{3.14}$$

with

$$V^* = \frac{eV}{k_0 T}; \qquad V = \frac{e}{\varkappa r}\, e^{-qr}.$$

The excess space charge density is given by the following expression:

$$\varrho = -e\delta n = -e\frac{4}{3}\left(\frac{2\pi m_n k_0 T}{h^2}\right)^{3/2}\frac{2}{\sqrt{\pi}}\left\{L_0^{3/2}(\beta, \eta + V^*) - L_0^{3/2}(\beta, \eta)\right\} \tag{3.15}$$

The potential energy of the electron in the Coulomb field of the centre can be assumed to be small as compared to the kinetic energy. This is justified inasmuch as the probability for an electron passing at a very small distance from the centre is small. With this assumption, the quantity $L_0^{3/2}(\beta, \eta + V^*)$ can be expanded in a series, thus

$$L_0^{3/2}(\beta, \eta + V^*) \simeq L_0^{3/2}(\beta, \eta) + \left|\frac{dL_0^{3/2}}{dV^*}\right|_0 V^* \tag{3.16}$$

The density of space charge is now

$$\varrho = -\frac{4\pi e^2 (2m_n)^{3/2}}{h^3}\,(k_0 T)^{1/2}\, V L_1^{1/2}(\beta, \eta) \tag{3.17}$$

Poisson's equation

$$V^2V = -\frac{4\pi}{\varkappa}\varrho \tag{3.18}$$

must be fulfilled. Substituting the scattering potential of eq. (3.2) and on making r tend to infinity, we have

$$q^2 = \frac{16\pi^2 e^2 (2m_n)^{3/2} (k_0T)^{1/2}}{\varkappa h^3} L_1^{1/2}(\beta, \eta) \tag{3.19}$$

Eq. (3.11) now assumes the form

$$\xi = \frac{\varkappa h\varepsilon(1+\chi)}{e^2(2m_nk_0T)^{1/2} L_1^{1/2}} \tag{3.20}$$

Because of the weak variability of the coefficient B appearing in the formula of the relaxation time, it can be placed before the integral with an energy value corresponding to the maximum sub-integral expression,

$$\xi_{\max} = \frac{\varkappa h(k_0T)^{1/2} L_0^{5/2}}{e^2(2m_n)^{1/2} L_1^{1/2} L_0^{3/2}} \tag{3.21}$$

On ground of the foregoing considerations, the components of the conductivity tensor (2.13) assume the form

$$\sigma_{xx} = \sigma_{yy} = \sigma_{zz} = \sigma = GL_{-2}^3 \tag{3.22}$$
$$\sigma_{yx} = -\sigma_{xy} = G\sqrt{\gamma}\, L_{-4}^{5/2}$$

wherein

$$G = \frac{16}{3}\pi \frac{e^2}{h^3} m_nk_0Tl_0$$
$$l_0 = \frac{2\varkappa^2(k_0T)^2}{\pi Ne^4B}$$
$$\gamma = l_0^2 \frac{e^2H^2}{2m_nk_0T}$$

The quantity B is defined by eq. (3.11).

4. Electric Conductivity and Hall Effect

From the considerations of the preceding section, the electric conductivity and Hall effect in a transversal magnetic field can be computed. The current density depends on the electric field strength as follows:

$$J_x = \sigma_{xx}E_x + \sigma_{xy}E_y \tag{4.1}$$
$$J_y = \sigma_{yx}E_x + \sigma_{yy}E_y$$

Putting $J_y = 0$, and with respect to $\sigma_{xy} = -\sigma_{yx}$, $\sigma_{yy} = \sigma_{xx}$, we have

$$E_y = RJ_xH, \quad J_x = \sigma_H E_x \tag{4.2}$$

R is Hall's constant, and σ_H the electric conductivity in a transversal magnetic field. Both quantities are given by the conductivity tensor components:

$$R = -\frac{1}{H}\frac{\sigma_{yx}}{\sigma_{xx}^2+\sigma_{yx}^2}, \quad \sigma_H = \frac{\sigma_{xx}^2+\sigma_{yx}^2}{\sigma_{xx}} \tag{4.3}$$

For a vanishing magnetic field we have

$$R_0 = -\frac{3\sqrt{\pi}}{8e}\left(\frac{2\pi m_n k_0 T}{h^2}\right)^{-3/2}\frac{L_{-4}^{5/2}}{(L_{-2}^3)^2} \tag{4.4}$$

or

$$R_0 = -\frac{1}{en}\frac{L_0^{3/2}L_{-4}^{5/2}}{(L_{-2}^3)^2} \tag{4.5}$$

and

$$\sigma = GL_{-2}^3 \tag{4.6}$$

The numerical values of the coefficient $\frac{2}{3}\frac{L_0^{3/2}L_{-4}^{5/2}}{(L_{-2}^3)^2}$ corresponding to different β are given in Fig. 1. It is noteworthy that, if $\beta = 0$ is put in the foregoing formulas, the respective expressions for the parabolic band are obtained:

$$R_0 = -\frac{3}{4}\cdot\frac{1}{en}\frac{F_{1/2}F_{7/2}}{(F_2)^2}; \quad \sigma = 3GF_2 \tag{4.7}$$

The functions F_k in the foregoing formulas are Fermi integrals defined as follows:

$$F_k = \int_0^\infty \frac{\lambda^k}{1+e^{\lambda-\eta}}\,d\lambda \tag{4.8}$$

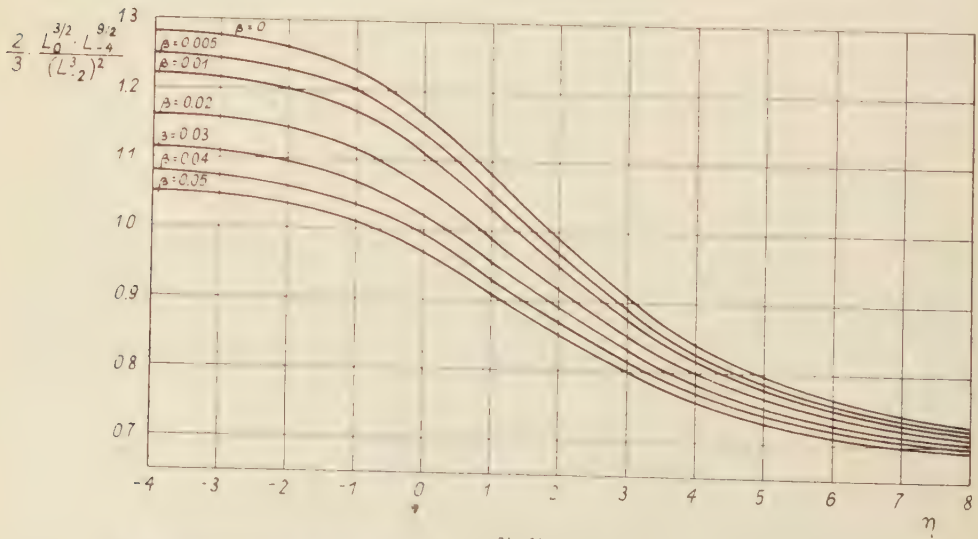

Fig. 1. Dependence of the coefficient $\frac{2}{3}\frac{L_0^{3/2}L_{-4}^{5/2}}{(L_{-2}^3)^2}$ on η, for different values of β.

The numerical values of L_k^n have been assembled in Tables I, II and III.

TABLE I

Values of $L^3_{-2} = \int_0^\infty \left(-\frac{df_0}{dx}\right) \frac{(x+\beta x^2)^3}{(1+2\beta x)^2}\, dx$

η \ β	0	0.05	0.10	0.15	0.20	0.25	0.30
−4	0.109	0.097	0.094	0.094	0.0966	0.0995	0.103
−2	0.798	0.710	0.687	0.689	0.704	0.725	0.751
−1	2.115	1.881	1.822	1.829	1.868	1.927	1.997
0	5.409	4.793	4.645	4.669	4.777	4.935	5.124
+1	12.94	11.50	11.16	11.25	11.55	11.98	12.47
+2	28.33	25.31	24.63	24.96	25.76	26.83	28.06
+4	103.6	89.56	88.54	91.48	96.19	101.8	108.0

TABLE II

Values of $L^{9/2}_{-4} = \int_0^\infty \left(-\frac{df_0}{dx}\right) \frac{(x+\beta x^2)^{9/2}}{(1+2\beta x)^4}\, dx$

η \ β	0	0.05	0.10	0.15	0.20	0.25	0.30
−4	0.957	0.516	0.378	0.313	0.277	0.255	0.240
−2	7.042	3.790	2.779	2.304	2.038	1.873	1.765
−1	18.96	10.22	7.491	6.211	5.496	5.0555	4.767
0	50.33	26.87	19.66	16.29	14.41	13.26	12.51
+1	129.7	68.51	49.97	41.39	36.66	33.77	31.91
+2	318.4	163.8	119.0	98.66	87.57	80.89	76.62
+4	1560	746.7	535.9	447.0	400.7	374.1	358.1

TABLE III

Values of $\frac{2}{3} L_0^{3/2} = \frac{2}{3} \int_0^\infty \left(-\frac{df_0}{dx}\right) (x+\beta x^2)^{3/2} dx$

η \ β	0	0.05	0.10	0.15	0.20	0.25	0.30
−4	0.0161	0.0194	0.0228	0.0265	0.0303	0.0343	0.0385
−2	0.115	0.138	0.163	0.184	0.217	0.246	0.277
−1	0.291	0.345	0.408	0.476	0.548	0.623	0.702
0	0.678	0.833	0.996	1.170	1.354	1.548	1.752
+1	1.396	1.750	2.128	2.534	2.965	3.420	3.889
+2	2.502	3.233	4.032	4.893	5.812	6.787	7.813
+4	5.771	8.198	10.84	13.73	16.85	20.17	23.70

5. Strong Degeneracy

The non-parabolic structure of the conductivity band can produce measurable effects in the case of samples with a high amount of impurities only. High concentrations of the latter, especially at low temperatures, cause strong degeneracy of the electron gas. Indium antimonide, which presents a small effective mass of the electrons, is a material wherein degeneracy can be especially strong. The Hall constant as measured by Putley (1959) in samples of different concentrations of the impurities is temperature-independent throughout the range of 2° K to 100° K. The absence of activation energy resulting can be explained by the existence of an admixture band overlapping the conduction band. The presence of electrons in the conductivity band warrants strong degeneracy even at the lowest temperatures. Obviously, the degree of degeneracy is dependent on the concentration and temperature, and can be determined by solving the following equation with respect to η:

$$\tfrac{2}{3} L_0^{3/2} = 1.24 \times 10^{-13} n T^{-3/2} \tag{5.1}$$

η is the reduced Fermi level.

"Strong" degeneracy is meant to denote the case of $\eta > 4$. At 2° K, all samples with concentrations exceeding 10^{14} cm^{-3} already exhibit strong degeneracy. It can be proved that, for $\eta \to \infty$, $\left(-\frac{df_0}{dx}\right) \to \delta(x - \eta)$. Introduction of the delta function makes the exact computation of the integrals L_k^n possible. Eq. (3.13) yields

$$\zeta = \frac{\varepsilon_g}{2}(\sqrt{\Delta} - 1) \tag{5.2}$$

wherein

$$\Delta = 1 + \frac{1}{2}\left(\frac{3}{\pi}\right)^{2/3} \frac{h^2}{\varepsilon_g m_n} n^{2/3} \tag{5.3}$$

On passing to infinity with ε_g and expanding the root in (5.2) in a power series, the respective expression for the parabolic band is obtained:

$$\zeta = \left(\frac{3}{\pi}\right)^{2/3} \frac{h^2}{8 m_n} n^{2/3} \tag{5.4}$$

The electric conductivity of eq. (4.6) now assumes the form

$$\sigma = \frac{1}{48}\left(\frac{3}{\pi}\right)^2 \frac{h^3 \varkappa^2 n^2}{N e^2 B m^{*2}} \tag{5.5}$$

Herein, the effective mass m^* is given by the concentration:

$$m^* = m_n \left[1 + \frac{1}{2}\left(\frac{3}{\pi}\right)^{2/3} \frac{h^2}{\varepsilon_g m_n} n^{2/3}\right]^{1/2} \tag{5.6}$$

The quantity B is determined by eq. (3.11), except that now

$$\xi_{\max} = \left(\frac{3}{\pi}\right)^{1/3} \frac{\varkappa h^2 n^{1/3}}{4 e^2 m^*} \tag{5.7}$$

Analogical procedure with respect to the Hall constant of eq. (4.5) yields

$$R_0 = -\frac{1}{en} \tag{5.8}$$

The dependence of the effective mass (5.6) on the concentration is shown in Fig. 2. The computations were carried out for $\varepsilon_g = 0.23$ eV and $m_n = 0.013\, m_0$. It will be seen from the graph that, as the concentration exceeds 10^{16} cm^{-3}, the effective mass increases steeply. Experimental values of the mass from measurements of the absorption on free carriers

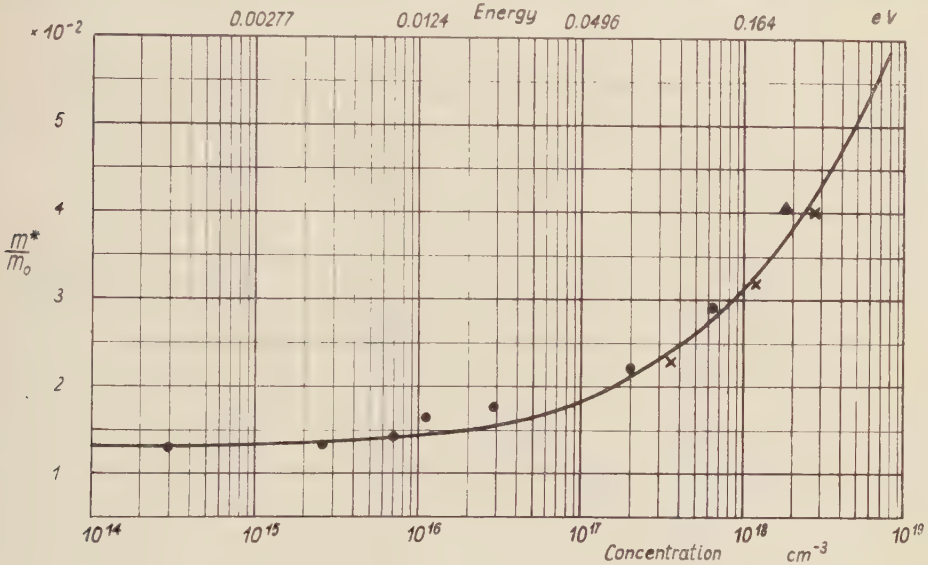

Fig. 2. Effective mass m^* *versus* electron concentration.

(Spitzer and Fan 1957) and of the Faraday effect (Smith et al. 1959) are also shown. Comparison of the conductivity of eq. (5.5) with the experimental results is less conclusive, since this involves an unknown parameter, namely, the concentration of scattering centres N. Assuming the electrons to be scattered on ionized donors and acceptors, we have

$$N = n_d + p_a \tag{5.9}$$

The condition of electric neutrality of the crystal is fulfilled:

$$n + p_a = p + n_d \tag{5.10}$$

with n denoting the electron concentration in the conductivity band,

p — the concentration of holes in the valence band,

n_d — the concentration of ionized donors, and

p_a — that of ionized acceptors.

The assumption of $p = 0$ at low temperatures is reasonable, as all acceptors are ionized by electrons from the donors. Hence, the concentration N amounts to

$$N = n + 2p_a \tag{5.11}$$

Finally, we obtain the following expressions for the electric conductivity and electron mobility:

$$\sigma = \frac{1}{48}\left(\frac{3}{\pi}\right)^2 \frac{h^3 \varkappa^2 n^2}{(N_i + n) e^2 B m^{*2}} \tag{5.12}$$

$$u = \frac{1}{48}\left(\frac{3}{\pi}\right)^2 \frac{h^3 \varkappa^2 n}{(N_i + n) e^3 B m^{*2}} \tag{5.13}$$

wherein:

$$N_i = 2p_a$$

Graphs of (5.12) and (5.13) are shown in Figs. 3 and 4. The computations were carried out for different values of N_i at $\varkappa = 17.5$. The experimental points are those derived from the references. The electron concentration for each sample was determined from eq. (5.8) (from the Hall constant as measured at low temperatures).

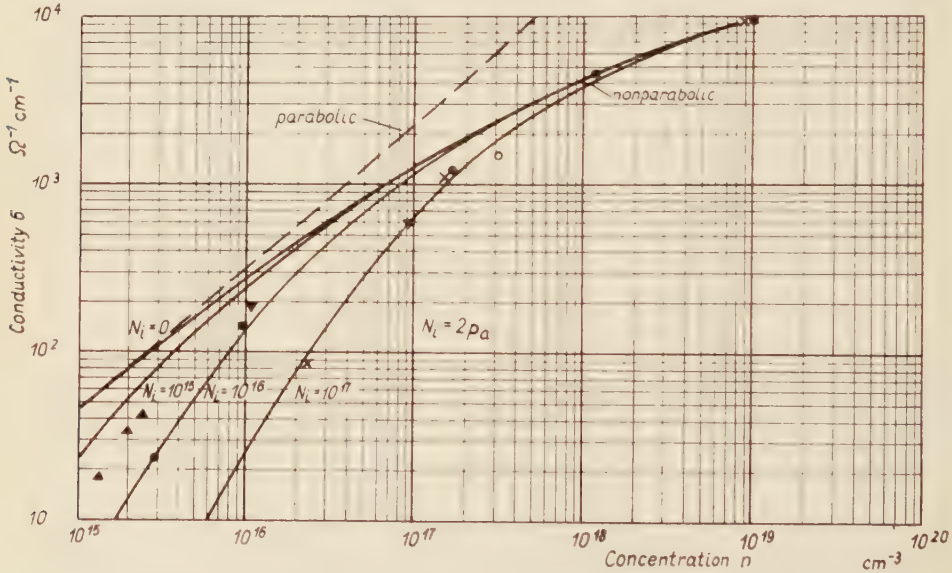

Fig. 3. Electric conductivity *versus* electron concentration, for different values of N_i.
The experimental points are taken from the papers by Putley (1959), Tauc and Matyas (1955) and Frederikse and Hosler (1957).

In samples of a high degree of impurity, the electric conductivity and mobility are temperature-independent throughout the entire interval of impurity conduction. In samples that are of a somewhat higher degree of purity, the conductivity and mobility are found to increase as the temperature is raised. This latter effect is due to the vanishing of degeneracy. The temperature dependence of the conductivity is described by eq. (4.6). Fig. 5 brings graphs computed from that formula for three of Putley's samples. The graphs corresponding

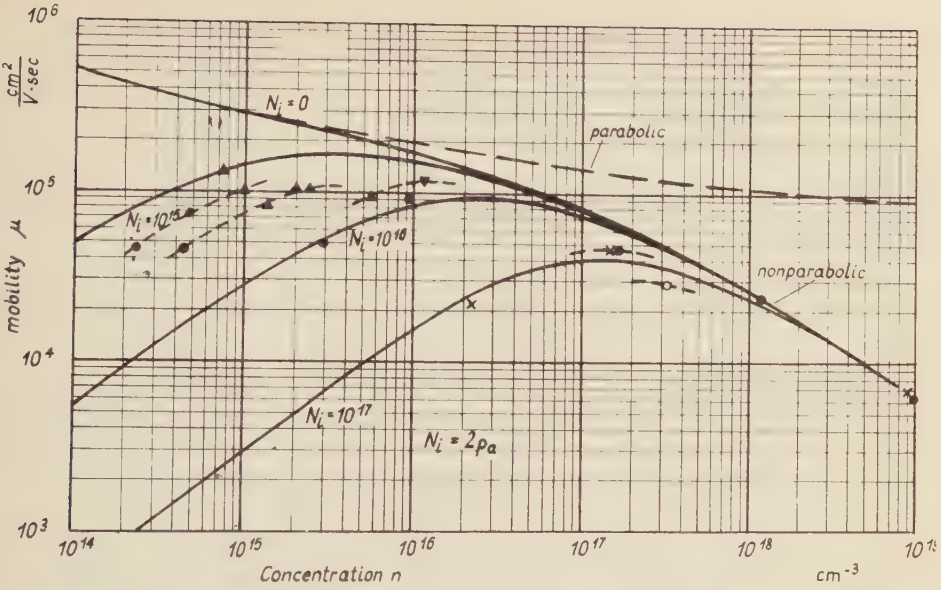

Fig. 4. Mobility *versus* electron concentration, for different values of N_i.
The experimental points are those for conductivity.
The dashed line corresponds to the parabolic band.

to samples of a rather high degree of impurity are in good agreement with the experimental data. The results for the purest sample C48/4 are less consistent, although the shape of the graph is conserved. The graphs were computed on the assumption that the electron concentration is temperature-independent for a given sample throughout the range of impurity conduction. In determining the concentration of the electrons from Hall's constant as measured at the lowest temperatures, one can compute the temperature dependence of the Fermi level from eq. (5.1) and then proceed to compute the graphs of Fig. 5 from eq. (4.6). Lack of consistency with the experimental data in the case of the samples of highest purity can result from an incorrect evaluation of the concentration. The source of error can reside in the fact that, for the magnetic fields of 2000 Oe utilized by Putley, the classical theory of the Hall effect ceases to be valid, as then

$$\hbar\omega \gg \zeta$$

with ω denoting the cyclotron frequency and ζ – the Fermi level. The foregoing inequality, if fulfilled, sets a limit to the applicability of the classical theory. For a concentration of 10^{14} cm^{-3}, Fermi's level is given by a value of 5.98×10^{-4} eV, whereas the Landau splitting amounts to $\hbar\omega = 1.74 \times 10^{-3}$ eV. The quantum effect becomes appreciable here. In the case of samples of higher carrier concentration, the quantum limitation sets in at higher values of the magnetic field strength.

The author wishes to thank Professor Dr L. Sosnowski for directing the present investigation and for his valuable hints. The author is indebted to Dr Dr M. Suffczyński, J. Ginter

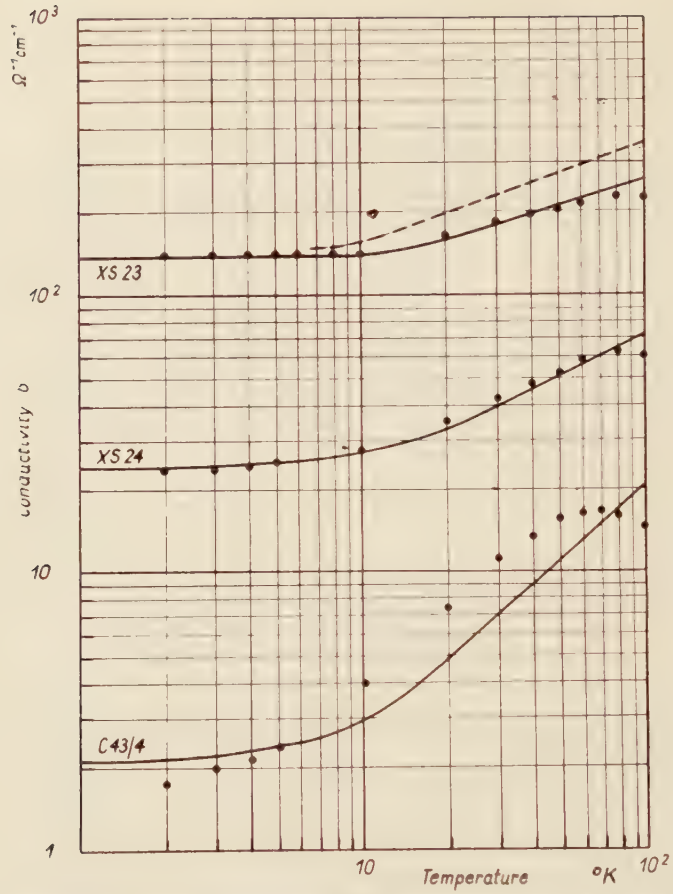

Fig. 5. Electric conductivity *versus* temperature. The experimental points are from Putley's paper.

and J. Rauluszkiewicz for their critical remarks. The author desires to express his special acknowledgement for the effective help provided by Mr. B. Załoga in the field of numerical computation.

REFERENCES

Barrie, R., *Proc. Phys. Soc.* [London], B**69**, 553, (1956).
Dingle, R. B., *Phil. Mag.*, **46**, 831, (1955).
Dresselhaus, G. et al., *Phys. Rev. Letters*, **98**, 556, (1955).
Frederikse, H. P. R., Hosler, W. R., *Phys. Rev.*, **108**, 1136, (1957).
Mc Clure, J. W., *Phys. Rev.*, **101**, 1642, (1956).
Kane, E. O., *J. Phys. Chem. Solids*, **1**, 249, (1957).
Putley, E. H., *Proc. Phys. Soc.* [London], **73**, 280, (1959).
Smith, S. D., Moss, T. S., Taylor, K. W., *J. Phys. Chem. Solids*, **11**, 131, (1959).
Spitzer, W. G., Fan, H. Y., *Phys. Rev.*, **106**, 882, (1957).
Tauc, J., Matyas, M., *Czech. J. Phys.*, **5**, 369, (1955).

LUMINESCENCE IN ELECTRIC FIELDS OF "DRY" OXIDE FILMS ON ALUMINIUM

By J. Wesołowski

Institute of Experimental Physics, Bolesław Bierut University, Wrocław

M. Jachimowski* And R. Dragon

Institute of Physics, Teachers' College, Opole

(Received October 12, 1960)

The electrical and luminescent properties of electrolytically formed "dry" aluminium oxide films were investigated. Cells consisting of an aluminium base with oxide layer and transparent semiconducting coating were subjected to a *D.C.* field.

The light emission from the oxide layers was observed.

The luminescence brightness and cell current were measured *versus* the applied voltage.

The properties of dry aluminium oxide films strongly resemble, on the one hand, those of electrolytic cells and, on the other hand, those of typical electroluminescent cells.

It is therefore assumed that in either case, viz., in that of dry cells and in that of electrolytical cells, the light emission may be considered to represent a process of electroluminescence.

1. Introduction

The luminescence accompanying processes of anodic oxidation of Al, Ta, Zr and some other metals is a phenomenon which has been known and repeatedly described for over 50 years (Güntherschulze 1906; Lavaux 1919; Dufford 1929; Forrest 1930; Sullivan et al. 1931; Güntherschulze et al. 1932, 1934; Betz 1935; Verwey 1935; Rummel 1936; Gumiński 1936; Anderson 1943).

During the last decade and, particularly, in the last few years, this phenomenon received special attention.

Systematic, extensive investigations were carried out and a number of theories aimed at explaining the origins and mechanism of the phenomenon were put forward (van Geel et al. 1950, 1956, 1957; Dekker 1950; Dekker et al. 1950; Charlesbey 1953; Ruziewicz 1956; Smith 1959).

---

* Present address: Institute of Physics, Medical Academy, Cracow.

Aluminium was the metal investigated most extensively. Aluminium plates or foils of various grades of purity, formed the anodes of a suitable electrolytic cell (usually containing an aqueous solution of boric acid or oxalic acid), the other electrode (the cathode) usually being made of platinum.

Let us recall some basic facts described in the literature, i.a. in the paper of van Geel, Pistorius and Bouma (1957), where they are presented in a concise and particularly clear way.

(a). The intensity L of the "anodic" luminescence occuring during the formation of the oxide layer or in a completely formed layer depends on the actual thickness d of the layer and on the density I of the current flowing through the system: Al Al_2O_3 electrolyt.

$$L = \alpha I(\exp \beta d - 1). \tag{1}$$

α and β being constants for a given sample.

(b). At a constant thickness d of the oxide layer, the current density I is a function of the voltage V applied to the electrolytic cell.

$$I = \alpha_1(\exp bV - 1). \tag{2}$$

α_1 and b being constants.

By (1) and (2):

$$L = cI, \tag{3}$$

$$L = a(\exp bV - 1). \tag{4}$$

a, b and c being constants for a given specimen.

(c). The system $Al/Al_2O_3/$ electrolyt is known to exhibit rectifying properties, the blocking direction being that from (Al +) to (electrolyt −). At the opposite polarity, (Al−), larger currents flow through the cell, a gradual deterioration of the structure of the oxide takes place, and the system loses both its rectifying and luminescent properties. A sudden reversal of the polarity, from (Al +) to (Al−), produces short-lasting luminescence, termed "the cathode flash", on the aluminium electrode. The cathode flash occurs only when the Al previously constituted the anode, and can be observed even after an interval of several hours between the removal of the anodic polarization and its sudden reversal.

A subsequent, sudden transition from the state (Al +) to the state (Al−) results in a short-lasting "anode flash" superimposed on the normal, steady anodic luminescence.

The anode flash occurs when the Al previously constituted the cathode, provided the currentless time interval separating the states (Al −), (Al +) does not exceed several minutes.

An anode flash of low intensity also occurs when the anodic system is first short-circuited and then submitted to the previous anodic polarization.

These facts, and many another described in the literature, suggest that we are dealing here with a phenomenon of electroluminescence of the aluminium oxide (Ruziewicz 1956; Curie 1953; Curie et al. 1954; Piper et al. 1958; Smith 1959).

If this is so, aluminium oxide in the "dry" system: $Al/Al_2O_3/$ semiconductor or metal can be expected to exhibit similar properties.

This paper gives an account of some experiments carried out on dry aluminium oxide ells.

Each cell consisted of an aluminium base plate covered with an electrolytically formed xide layer and a transparent film of "*n*" type semiconductor deposited on the oxide.

2. *Apparatus*

2.1. *Luminescent cells*

Aluminium plates (of about 20 cm^2 area), generally of technical purity, were degreased, ashed in distilled water and oxidized anodically in 1—2% aqueous solutions of oxalic cid. Two methods of oxidation were adopted: the constant voltage method and the constant urrent method.

In the first of these, a constant formation voltage is applied to the electrolytic cell ntil the continually decreasing current drops to the low and nearly constant value of the leakage" current.

In the second method, *D.C.* of constant density (in our experiments 2 –5 mA/cm^2) s passed through the system until the increasing voltage reaches the preselected value of ormation.

Formation voltages ranging from 24 to 140 volts were used. The oxidized specimens were washed thoroughly in running and distilled water and dried in air at room temperature. Finally, part of the oxide area was coated with a transparent and conducting CdO or SnO_2 ilm.

Samples intended for CdO coating were mainly oxidized by the constant current procedure.

Cadmium oxide films were deposited by the cathodic reactive sputtering technique n an apparatus similar to that described by J. S. Preston (1950).

Transparent layers of SnO_2 were fumed by the chemical deposition procedure (Fischer 1954; Holland). Notwithstanding the temperatures required in this method ($\approx$500°C), no breakdowns were observed in the majority of specimens throughout the range of voltages used in our experiments. The luminescent cell finally constituted a parallel plate condenser. Voltages were applied to the aluminium base and to the semiconducting film by means of an elastic spring contacting the latter.

There appeared to be little difference in the behaviour of the cells prepared by either method.

2.2. *Luminescence*

Quantitative investigations of the luminescence of oxide films were carried out with a *F. E. U.* 19-*M* type photomultiplier in the simple arrangement of Fig. 1.

The arrangement allowed for simultaneous measurements of both the intensity I_f of the photocurrent, which is proportional to the luminescence brightness L, and the intensity I_c of the current flowing through the cell, as functions of the value and polarity of the voltage applied to the cell.

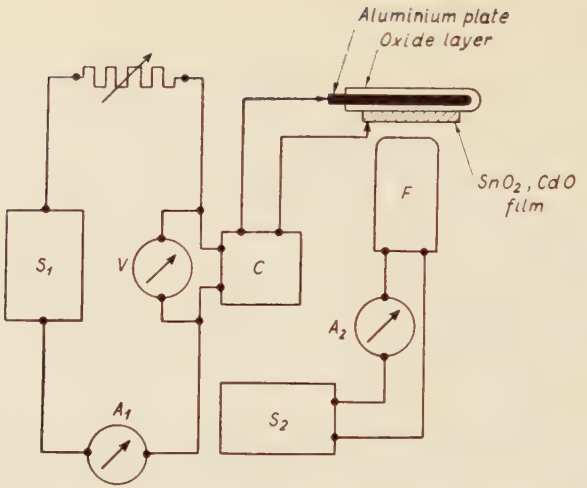

Fig. 1. Block diagram of the apparatus. S_1, *D. C.* voltage source; S_2, supply for photomultiplier; V, voltmeter; C, voltage commutator; A_1, A_2, microammeters; F, photomultiplier.

3. *Experiments and results*

3.1. *Anodic luminescence and flashes*

All experiments were carried out in air at room temperature. Preliminary visual observations showed that the cells prepared as described in Section 2.1 emitted light under the influence of sufficiently high voltages applied in the blocking direction, (Al+).

At the opposite polarity no steady luminescence was observed. Sudden transition from the state (Al+) to the state (Al−) produces a cathode flash which, however, decays at a much slower rate than in the case of an electrolytic cell. A subsequent sudden return to the state (Al+) causes an anode flash, superimposed upon the steady anodic luminescence. This anode flash is also of longer duration than in the electrolyte. The anode and the cathode flashes are mutually dependent in the same way as they are in the electrolyte.

As in the case of the electrolytic cell, the anode flash of low intensity can be observed without previous cathodic polarization, i. e. when the system, upon anodic polarization, is first short-circuited and then subjected to the same polarity again.

3.2. *Relationships between Voltage, Current and Luminescence*

On applying various voltages V to the cells, cell-currents I_c proportional to the current densities I, and photocurrents I_f, were measured. The general trends of the relationships $I_f(I_c)$, $I_f(V)$ and $I_c(V)$ were approximately the same for all the cells hitherto investigated.

As an example, the dependence $I_f(I_c)$, in the blocking direction, for a cell coated with cadmium oxide is shown in Fig. 2.

The relationships $I_f(V)$ and $I_c(V)$ for the same cell and for both the blocking and forward directions of V are shown in Fig. 3.

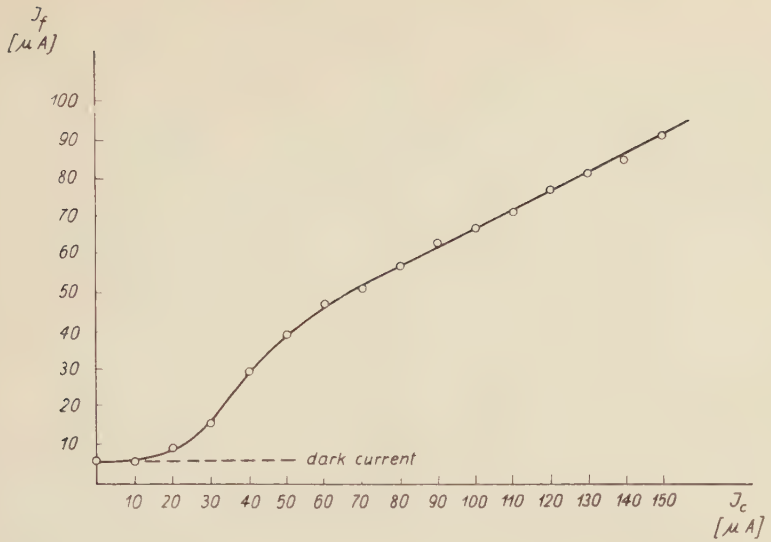

Fig. 2. CdO coated cell. Relation between photocurrent I_f and cell-current I_c.

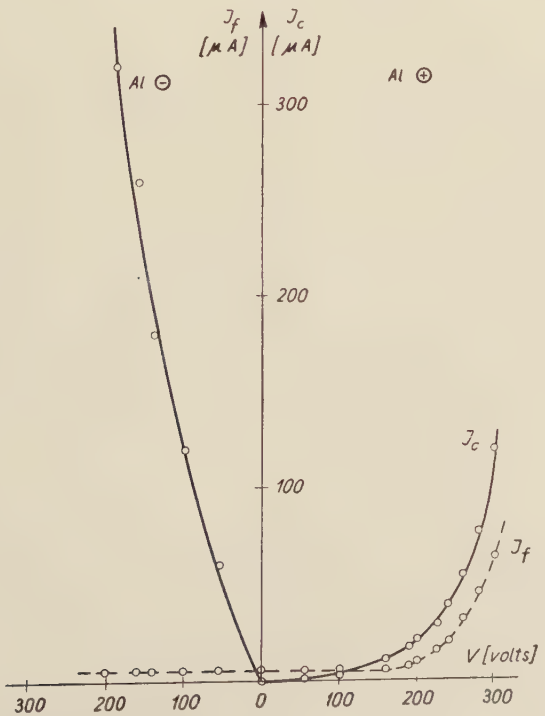

Fig. 3. CdO coated cell. Photocurrent I_f and cell-current I_c against voltage V.

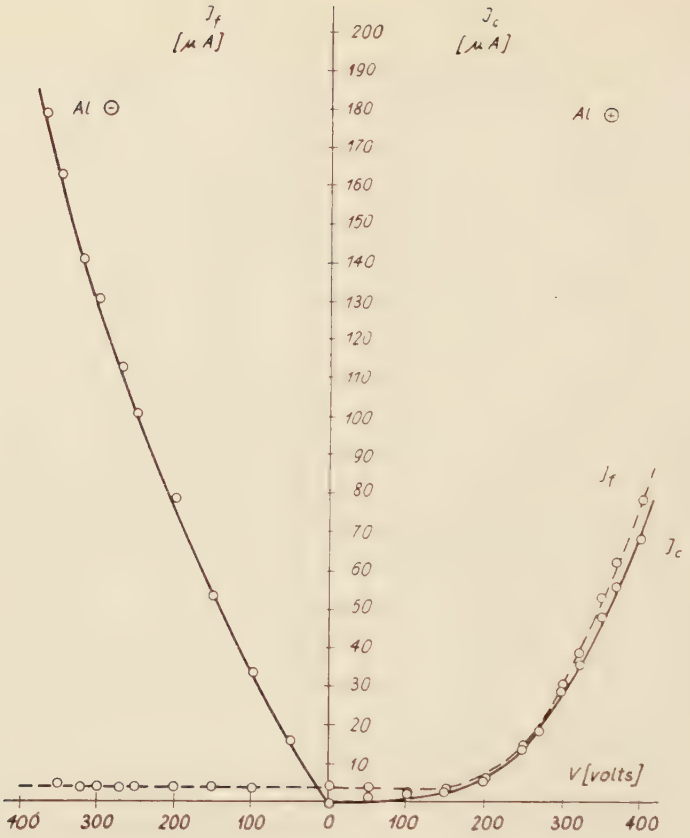

Fig. 4. SnO_2 coated cell. Photocurrent I_f and cell-current I_c against voltage V.

Fig. 4. represents the same dependences as in Fig. 3 for a specimen coated with SnO_2.
The following conclusions can be drawn from the graphs of Figs. 2, 3 and 4:

a) "Dry" luminescent cells show a pronounced property of rectification.

b) For I_f considerably exceeding the dark current the dependence $I_f(I_c)$ is nearly linear; consequently $L = cI$, as in the electrolyte at constant oxide thickness.

c) The shape of the curves in Figs. 3 and 4 suggests an exponential form of the functions $I_f(V)$ and $I_c(V)$.

In Fig. 5, $\log(I_c + a)$ with suitably chosen values of the parameter a, is plotted against V for either cell.

As will be seen from Fig. 5, the relationship between $\log(I_c + a)$ and V may be regarded as linear; hence, by eqs. (2) and (3), the dependence of the luminescence L on V can be represented by a formula of the type

$$L = a(\exp bV - 1).$$

This is the relationship found for the electrolytic cells at constant oxide thickness.

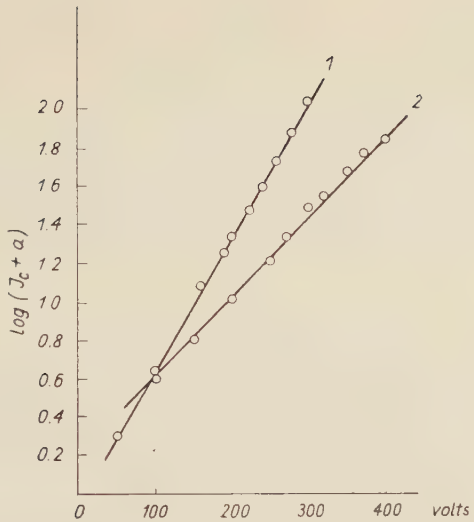

Fig. 5. Log $(I_c + a)$ against V. I_c in microamps. (1), CdO coated cell; (2), SnO_2 coated cell.

The $I_f(V)$ and $I_c(V)$ curves from our experiments present the same general shape as those obtained by D. A. Cusano and F. E. Williams (1956) in their investigations on the photoelectroluminescence of ZnS:Mn, Cl films (Cusano 1955).

For comparison, Fig. 3 from the paper of Cusano and Williams is reproduced here as Fig. 6.

Both types of cells, viz., the Al_2O_3 and the activated ZnS cells, exhibit the properties of rectification and of light emission in electric fields applied in the blocking direction. The only difference consists in the fact that, in the case of ZnS, the blocking direction

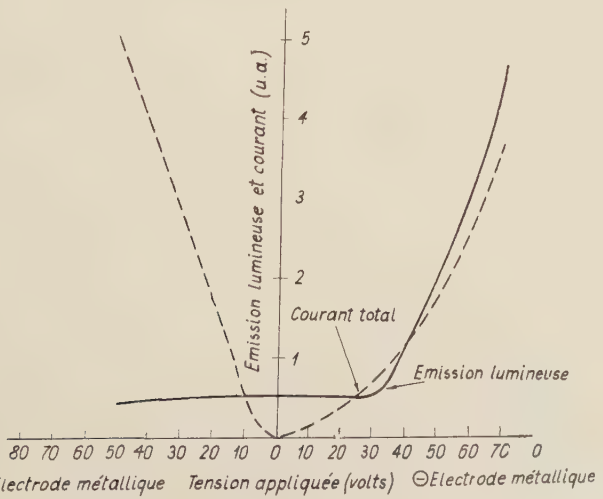

Fig. 6. Repreduction of Fig. 3 from the paper of Cusano and Williams (1956).

is *from* the semiconducting electrode, (TiO_2+), *to* the metal, whereas in our cells the meta is on a positive potential with respect to the semiconductor.

The curves of Figs. 3 and 4, in their general trend, also resemble the analogous curve obtained by A. Fischer (1953) in his investigations of the electroluminescence of Zn(sheets, although the arrangement in Fischer's experiments was entirely different.

Moreover our $I_f(V)$ curves are fairly similar to the analogous curve given by W. A Thornton (1959) in his paper on the electroluminescence of thin activated ZnS films.

4. Concluding Remarks

The fact of light emission from "dry" aluminium oxide films under the influence o strong electric fields, and the close similarity between our $I(V)$ and $L(V)$ characteristics an the analogous ones obtained in typical experiments on electroluminescence make it plaus ible to interpret the phenomena described in this article as electroluminescence effects

On the other hand, the system $Al/Al_2O_3/$ semiconductor behaves in *D.C.* electric field much in the same way as the system $Al/Al_2O_3/$ electrolyte at constant oxide thickness.

Hence it would seem that, in either system, we are dealing with a phenomenon of tru electroluminescence.

It must be emphasized, however, that all our experiments were carried out in atmos pheric air, which necessarily contains water vapour.

This last remark is of importance, as some of our observations revealed a significan rôle played by the humidity in the phenomena here described.

The influence of the humidity of the medium will be the subject of a separate publica tion.

REFERENCES

Anderson, S., *J. appl. Phys.*, **14**, 601 (1943).
Betz, H., *Z. Phys.*, **95**, 189 (1935).
Charlesbey, A., *Proc. Phys. Soc.* [London], **B66**, 317 (1953); *ibid.*, **B66**, 533, (1953).
Curie, D., *J. Phys. Radium*, **14**, 672 (1953).
Curie, G. and Curie, D., *J. Phys. Radium*, **15**, 61 (1954).
Cusano, D. A., *Phys. Rev.*, **98**, 547 (1955).
Cusano, D. A. and Williams, F. E., *J. Phys. Radium*, **17**, 742 (1956).
Dekker, A. J. and van Geel, W. Ch., *Philips Res. Rep.* **5**, 303 (1950).
Dekker, A. J. and Urquahart, H. M. A., *J. appl. Phys.*, **21**, 708 (1950).
Dufford, R. T., *J. Opt. Soc. Amer.*, **18**, 17 (1929).
Fischer, A., *Z. Naturforsch.*, **8a**, 756 (1953); *ibid.*, **9a**, 508 (1954).
Forrest, J. S., *Phil. Mag.*, **10**, 1003 (1930).
van Geel, W. Ch. and Bouma, B. C., *Philips Res. Rep.*, **5**, 461 (1950); *ibid.*, **6**, 401 (1951).
van Geel, W. Ch. and Pistorius, C. A., *Philips Res. Rep.*, **11**, 471 (1956).
van Geel, W. Ch., Pistorius, C. A. and Bouma, B. C., *Philips Res. Rep.*, **12**, 465 (1957).
Gumiński, K., *Bull. Acad. Polon. Sci., Cl. Sci. Math. Nat., sér. A.*, **145**, 457 (1936).
Güntherschulze, A., *Ann. Phys.* [Leipzig], **21**, 929 (1906).
Güntherschulze, A. and Betz. H., *Z. Phys.*, **73**, 586 (1932); *ibid.*, **74**, 681 (1932); *ibid.*, **91**, 70 (1934); *ibid.* **92**, 367 (1934).

Holland, L., *Vacuum Deposition of Thin Films*, Chapman and Hall Ltd. 1956.
Lavaux, J., *C. R. Acad. Sci.* [Paris], **169**, 180 (1919).
Piper, W. W. and Williams, F. E., *Solid State Physics*, **6**, 96 (1958), Academic Press, N. Y.
Preston, J. S., *Proc. Roy. Soc.* [London], **A202**, 449 (1950).
Rummel, T., *Z. Phys.*, **99**, 518 (1936); *ibid.*, **101**, 276 (1936).
Ruziewicz, Z., *Bull. Acad. Polon. Sci.*, Cl. III., **4**, 537, 543 (1956).
Smith, A. W., *Canad. J. Phys.*, **37**, 591 (1959).
Thornton, W. A., *J. appl. Phys.*, **30**, 123 (1959).
Verwey, J. W., *Physica*, **2**, 1059 (1935).

A THEORY OF EXCITON TRANSFER IN ANTHRACENE

By Kacper Zalewski

Institute of Physical Chemistry, Polish Academy of Science, Kraków

(Received October 19, 1960)

A continuity equation describing the motion of localized excitons in an anthracene crystal is proposed. The intermolecular transition probabilities are computed in dipol approximation with a semi-empirical adjustment as used by Dexter. Simpson's experiment is discussed and his phenomenological theory is reexamined.

Introduction

A molecule in an anthracene crystal when excited may return to its ground state, either by emitting a light quantum, or by transmitting the state of excitation to another molecule. A conversion of the excitation energy into lattice vibrations is also possible. This seldom happens, however, as the quantum efficiency of anthracene fluorescence is about 90% (Bowen, Mikiewicz and Smith 1949). A state of excitation travelling from molecule to molecule is called an exciton.

The transfer of excitons in anthracene was studied experimentally by Simpson (1956). In his experiment a thin layer of anthracene was deposited on a glass plate and covered by a layer of anthracene doped with naphthacene. This second layer worked as a detector of excitons because all the excitons entering it were trapped by naphthacene molecules and emitted as a green fluorescence, different from the fluorescence of anthracene. The double layer was illuminated by light falling through the glass plate, perpendicular to the layers. Let us denote the numbers of quanta per second: transmitted through the anthracene layer in the absence of the detector, transmitted by both layers, and emitted by the detector, respectively by: $\alpha_0 I$, $\alpha_1 I$, $\alpha_2 I$, where I is the incident light intensity. If there were no exciton transfer, the transmittivity of anthracene would be independent of the presence of the detector and the equality $\alpha_1+\alpha_2=\alpha_0$ would hold. Actually it has been found that $\alpha_1+\alpha_2$ always exceeds α_0. It means that some of the quanta absorbed by anthracene travel into the detector and are emitted by naphthacene. The difference $S=(\alpha_1+\alpha_2-\alpha_0)I$ is the rate of transfer of excitons into the detector. The dependence of S on the thickness of the anthracene layer was determined by measuring $\alpha_1+\alpha_2-\alpha_0$ for 18 different specimens.

To explain the results, Simpson assumed that the excitons are localized and that the flux of excitons, perpendicular to the surface, is given by the formula

$$S = -D\frac{dn}{dx} \tag{1}$$

where D is a constant, n is the concentration of excitons, and the axis x is perpendicular to the layers. This formula implies that n fulfils a one-dimensional diffusion equation which for the stationary state takes the form

$$\frac{n}{\tau} - D\frac{d^2n}{dx^2} = \varepsilon I e^{-\varepsilon x}, \tag{2}$$

where τ is the mean life-time of an exciton and ε is the absorption coefficient of anthracene for the exciting radiation. For an anthracene layer of thickness d the following boundary conditions were assumed:

$$D\frac{dn}{dx} = 0 \quad \text{for } x = 0, \tag{3a}$$

$$n = 0 \qquad \text{for } x = d. \tag{3b}$$

Equations (3a) and (3b) mean that the flux of excitons from glass into anthracene vanishes and that the detector traps all the excitons which fall into it. This theory explains well the experimental results when D is put equal to $(460\ \text{Å})^2/\tau$.

In this paper a theory of exciton transfer is developed starting from the assumption that each exciton is localized in one molecule at a time. This assumption cannot be strictly valid for it is known that the Davydov splitting, observed also in the anthracene spectrum (Craig and Hobbins 1955), is caused by the delocalization of excitons; however, such a model can be fairly easily handled and leads to some conclusions probably valid for real crystals too.

Theory

Let us assume that the deposited anthracene layers are oriented with the cleavage plane (001) parallel to the surface of the glass. This result was experimentally obtained by Obreimov and Prichotko (1936), and confirmed by Craig and Hobbins (1955). The structure of anthracene crystals was studied by X-ray diffraction by Mathieson, Robertson and Sinclair (1950). According to these authors the anthracene molecules in the crystal are arranged in layers, parallel to the (001) plane. From now on, the word layer is reserved for unimolecular layers, and the whole anthracene layer is referred to as the plate. The distance between successive layers is taken as unit of length.

Let us ascribe labels 1, 2, ... to successive layers, so that layer 1 touches the glass plate, and a layer labelled k is at a distance of $k-1$ units of length from the glass surface. Let the index d label the first layer of the detector, then the layers 1, 2, ... ,$d-1$ consist of pure anthracene, and the layers d, $d+1$, ... belong to the detector. The number of excitons in the i-th layer will be denoted by $n(i)$. In the stationary state the number of excitons produced in a chosen layer together with those which reach it from other layers must equal the

number of light quanta emitted from this layer together with the excitons transmitted from it to other layers. Consequently, assuming that the detector is very thick, we can write the continuity equation as follows:

$$\frac{n(i)}{\tau} + \sum_{k=1}^{\infty} n(i)\, p_{ik} - \sum_{k=1}^{d-1} n(k)\, p_{ki} = \varepsilon I e^{-\varepsilon(i-1)}, \qquad i = 1, 2, \ldots, d-1 \tag{4}$$

where p_{ik} denotes the probability per unit time that an exciton present in the i-th layer will pass to the k-th layer.

In our notation the rate of transfer of excitons to the detector is given by the formula

$$S(d) = \sum_{i=1}^{d-1} \sum_{k=d}^{\infty} n(i)\, p_{ik}. \tag{5}$$

To obtain numerical values of the flux S which can be compared with experiment, we need the coefficients p_{ik} and the numbers $n(i)$. If the p_{ik} are known, $n(i)$ may, in principle, be found by solving equation (4). Thus our next task is to compute the transition probabilities p_{ik}.

Calculation of the transition probabilities p_{ik}

The probability of transition p_{ik} is a sum of the probabilities of transition from a given molecule in the layer i — let us label it ij — to all the molecules kl from the layer k. Thus the problem splits into two parts, first $p_{ij,\,kl}$, the probability of transition between single molecules, is to be computed, next the result must be summed over all the molecules from the layer k (summation over l). It follows from symmetry that the result is independent of j and gives the required coefficient p_{ik}.

In order to compute the transition probability for two molecules, let us assume that it is proportional to the probability computed by the perturbation method in the Born-Oppenheimer approximation. The proportionality coefficient will be assumed to be independent of the relative orientation and distance of the two molecules (Gołębiewski and Witkowski 1959). Thus in the dipole approximation

$$p_{ij,\,kl} = a \frac{|V_{ij,\,kl}|^2}{R^6}, \tag{6}$$

where a is a constant and $V_{ij\,kl}/R^3$ is the interaction energy of the transition dipoles of molecules ij and kl, divided by the square of the dipole moment measured in units Å × electronic charge, thus $|V_{ij,\,kl}|^2/R^6$ is measured in Å^{-6}. The first optical transition of anthracene, which was active in Simson's experiment, is short axis polarized (Craig and Hobbins 1955), consequently the transition dipole of the molecule points along its short axis. The magnitude of the dipole moment influences only the coefficient a.

Formula (6) gives the probability of transition to a single molecule. The summation over all molecules of the layer k which is now to be performed would be very laborious, and was therefore replaced by an integration. The result is

$$\sum_{l} \frac{|V_{ij,\,kl}|^2}{R^6} = 6 \times 10^{-6}\text{Å}^{-6}. \tag{7}$$

The introduction of an integration instead of a summation increases the value of the sum. To get an estimate of the error thus introduced the part of the sum (7) corresponding to molecules kl parallel to the molecule ij was computed by direct summation for $|k-i|=1$. The result is 2.5×10^{-6} Å^{-6} to be compared with the value $2.7\cdot10^{-6}$ Å^{-6} obtained by integration, thus the error is about 10%. Another source of error (Gołębiewski and Witkowski 1959) is the use of dipole approximation. A numerical estimate has shown that this error is of the same order as and of the opposite sign to the first one, thus both errors partly cancel. From formulae (6) and (7), we get

$$p_{ik}=\frac{6\times10^{-6}a}{|i-k|^4}\,\mathrm{sec}^{-1}=\frac{b}{|i-k|^4}\,\mathrm{sec}^{-1}. \tag{8}$$

The constant a is a semi-empirical parameter. For large intermolecular distances it may be estimated (Gołębiewski and Witkowski 1959) from Dexter's (1953) theory. In particular if the average life time of the excitons τ is known, a is given by the formula

$$a=\frac{9\hbar^7c^6\pi S}{8n^6E^6\tau^2}, \tag{9}$$

Here n is the refraction coefficient of anthracene, E is the transition energy from the region where the absorbtion and emission spectra overlap, and S is defined as follows: assuming $f(E)$ and $F(E)$ to be proportional to the numbers of quanta of energy E, respectively emitted or absorbed by the molecule, and $\int f(E)dE=\int F(E)dE=1$, we put

$$S=\int f(E)\,F(E)\,dE. \tag{10}$$

The parameter S causes the most difficulty when applying this theory. It depends critically on the shape of the spectra, and consequently on the method of preparing the crystal (Birks and Cameron 1959). What is more, it is not at all clear whether p_{ik} should depend on S for aromatic hydrocarbons. Northorp and Simpson (1956) deny this on the basis of experiments with the quenching efficiency. It should be borne in mind therefore that the coefficient a, computed from (9), is at best an estimate.

For numerical computations the values: $\tau=6.4\times10^{-9}$ sec (Birks and Cameron 1949), $n=1.6$, $E=3.1$ eV (Bowen 1949), and $S=2\times10^{-2}$ eV^{-1} were assumed. The value of n is estimated from the values for related compounds (Handbook). The value of S is a crude estimate from the graphs given by Bowen (1949 – with no scale of intensities), and Birks and Cameron (1959 – without the absorption spectrum). Substituting these values $a=4.4\times10^{15}$ Å^6 sec^{-1} was obtained, which gives

$$b=2.7\times10^{10}\,\mathrm{sec}^{-1}. \tag{11}$$

There is one more problem to be discussed in connection with formula (8). Up to now shielding has been completely neglected. If we assume on the contrary ideal shielding, only $p_{k,k+1}$ can be different from zero. Actually it should be less than computed by formula (6), but not much less, as the sum (6) converges rather quickly (the largest term yields by itself about 10% of the whole sum). In the following the decrease of $p_{k,k+1}$ caused by shielding is neglected. In the usual theory of sensibilized luminescence shielding is not

included, but it will be shown in the following section that this assumption is necessary to derive the diffusion equation from equation (4). For the sake of brevity the models with and without shielding will be referred to as models (a) and (b) respectively. Both models will be dealt with in the next section.

Discussion of the continuity equation

The system of equations (4) may be solved easily if model (a) is adopted. In this case the equations can be written in the form

$$\frac{n(i)}{\tau} - p_{i,\,i+1}[n(i+1) - 2n(i) + n(i-1)] = \varepsilon I e^{-\varepsilon(i-1)}. \qquad i = 1, 2, \ldots, d-1 \tag{11}$$

where $n(0)$ and $n(d)$ are defined by the conditions

$$p_{i,\,i+1}(n(0) - n(1)) = 0 \qquad n(d) = 0 \tag{12}$$

assuring the equivalence between systems (11) and (4).

It can be verified by direct substitution that the solution of this equation is

$$n(i) = \frac{\varepsilon\tau I e^2}{1 - 4p_{i,\,i+1}\,\tau \sinh^2 \dfrac{\varepsilon}{2}} e^{-\varepsilon i} + C_1 e^{-\eta i} + C_2 e^{\eta i}, \tag{13}$$

where the constants C_1 and C_2 should be computed from conditions (12) and η is the positive root of the equation

$$4p_{i,\,i+1}\tau \sinh^2 \eta/2 = 1. \tag{14}$$

Actually ε is about 7.5×10^{-3} and $p_{i,\,i+1}\tau \approx 250$ (from experiment), thus the operators sinh and e^{ε} may be dropped and (13) passes into the solution of the diffusion equation found by Simpson with

$$D = p_{i,\,i+1} \tag{15}$$

An alternative method of deriving this result is to assume equation (11) as valid for a continuous variable x and to put in (11) and (12) differentials instead of differences. With the assignment (15) equation (2) with boundary conditions (3a) and (3b) is thus obtained.

Formula (15) has been derived taking the distance between neighbouring layers $c' = 9.19$ Å (Mathieson, Robertson and Sinclair 1950) as the unit of length. Changing into ångstroms, we get from (8) and (15) $D = (121\text{Å})^2/\tau$ to be compared with the experimental result $D = (460\text{Å})^2/\tau$. Let us note further that for this model the flux of excitons falls exponentially with increasing thickness of the anthracene plate (Simpson 1956):

$$S = I \frac{\varepsilon\sqrt{D\tau}}{1 - \varepsilon\sqrt{D\tau}} e^{-\varepsilon d}. \tag{16}$$

The solution of system (4) with the assumptions of model (b) is much more difficult. In this paper only an estimate, valid for thick layers, is given. This estimate, however, shows clearly the difference between the implications of models (a) and (b).

Whatever the distribution of excitons in anthracene the flux of excitons streaming into the detector is larger than the flux S_1 computed on the assumption that all excitons are localized in the molecular layer labelled 1. For S_1 we get from formula (5)

$$S_1 = N \sum_{k=d}^{\infty} \frac{b}{|k-1|^4} \approx N \frac{b}{3d^3}, \tag{17}$$

where N is the total number of excitons in anthracene. In unit time anthracene absorbs $I(1-e^{-\varepsilon(d-1)})$ and emits $N/\tau + S$ quanta. Thus for the stationary state

$$N = I\tau(1-e^{-\varepsilon(d-1)}) - S\tau. \tag{18}$$

Substituting into (17) and solving the inequality $S_1 < S$ for S we get

$$S > \frac{b\tau}{3d^3 + b\tau} I(1-e^{-\varepsilon(d-1)}). \tag{19}$$

We see that model (b) predicts a much slower decrease of the flux S with the thickness d of the anthracene plate than model (a).

Conclusions

The assumption that each exciton is localized in one molecule at a time implies equation (4), which is not equivalent in general to the diffusion equation proposed by Simpson. The subsequent calculations depend on whether shielding is taken into account.

In model (a) it is assumed that the shielding is perfect, in the sense that excitons can be transferred between neighbouring molecular layers only. In this case a diffusion equation for the concentration of excitons is obtained and an exponential decay of the exciton flux follows. The transmission coefficient computed by Dexter's theory is about an order of magnitude smaller than required to reproduce the experimental results.

In model (b) shielding is neglected. In this case equation (4) does not reduce to a diffusion equation. The qualitative difference between models (a) and (b) is easily seen for thick anthracene layers. Here model (b) predicts a decrease of the flux, but only with the third power of the layer thickness. If this effect were really observed, it would shed a new light on the band theory of excitons where the applicability of the diffusion equation is assumed (Heller and Marcus 1951).

The theory of this paper was developed neglecting the transfer of excitations by reabsorption of fluorescence. Indeed, Simpson verified that in his experiment this effect is unimportant. For thick plates, however, it must be included, as proved by the observed dependence of the decay time of fluorescence on the size of the anthracene sample (Birks and Little 1953).

REFERENCES

Birks, J. B., Cameron, A. J. W., *Proc. Roy. Soc.*, **249**, 297 (1959).
Birks, J. B., Little, W. A., *Proc. Phys. Soc.* [London], **66**, 921 (1953).
Bowen, E. J., *The Chemical Aspects of Light* Oxford 1949 p. 162.

owen, E. J., Mikiewicz, E., Smith, F. W., *Proc. Phys. Soc.* [London], **62**, 26 (1949).
raig, D. P., Hobbins, P. C., *J. Chem. Soc.*, 2309 (1955).
exter, D. L., *J. chem. Phys.*, **21**, 836 (1953).
ołębiewski, A., Witkowski, A., *Roczniki Chemii*, **33**, 1443 (1959).
andbook of Chemistry and Physics, Ohio Cleveland 1956 ed. 38.
eller, W. R., Marcus, D. L., *Phys. Rev.*, **84**, 809 (1951).
athieson, A. McI., Robertson J. M., Sinclair, V. C., *Acta cryst.*, **3**, 245 (1950).
orthorp, D. C., Simpson, O., *Proc. Roy. Soc.*, **234**, 136 (1956).
bereimov, I. W., Prichotko, A. F., *Phys. Zs. Sow.*, **9**, 48 (1936).
impson, O., *Proc. Roy. Soc.*, **238**, 402 (1956).

POSITRON RADIATION OF Tm^{166}

By J. Żylicz, Z. Preibisz

Institute for Nuclear Research, Polish Academy of Sciences, Warsaw,

S. Chojnacki, J. Wołowski

Institute of Experimental Physics, Warsaw University, Warsaw,

Yu. Norseev

Joint Institute for Nuclear Research, Dubna, USSR.

(Received October 20, 1960)

The Tm^{166} positron spectrum has been examined with a long-lens beta spectrometer fitted with helical baffles for separating the electrons from the positrons. Two components were found of maximum energy 1920 ± 20 keV and 1219 ± 40 keV and relative intensities $1 : (0.092 \pm 0.018)$. The total number of positrons for a decay amounts to about 1%. The decay scheme of Tm^{166} and the applicability of the theory of non-axial nuclei is under discussion.

I. Introduction

Data on positron radiation of Tm^{166} ($T_{1/2} = 7.7$h) can be found in papers by Wilkinson and Hicks (1949), Boskma and De Waard (1959), and Wilson and Pool (1960). According to the first of these, the maximum energy of the positron spectrum amounts to 2.1 MeV (about 0.5% positrons per decay). Boskma and De Waard claim to have found two components of energies 450 ± 80 keV and 1.300 ± 100 keV (relatively 1.8% and 1.3% positrons per decay). Lastly, Wilson and Pool, in a short note announcing the publication of a more detailed paper, report that according to their measurements the maximum energy amounts to 2090 ± 40 keV. In each of the three works pure[1] Tm^{166} was produced and then investigated.

The aim of the present work was: 1. to measure precisely the energies and intensities of the components of Tm^{166} β^+ radiation and thus to solve the inconsistency observed in the data so far published, 2. to discuss the decay scheme, 3. to consider the possibility of applying the theory of non-axial nuclei.

[1] Not in equilibrium with Yb^{166}.

II. Source. Apparatus. Measurements

Isotope Tm^{166} was produced in the spallation process of tantalum nuclei caused by 660 MeV protons from the *JINR* synchrocyclotron. The rare earth elements were chemically separated from the tantalum target irradiated for four hours. Next, the rare earths were separated according to their atomic number by a chromatographic method (Preobrazhensk et al. 1956).

Tm^{166} is produced directly in a spallation reaction or by decay of Yb^{166} ($T_{1/2} = 57$ h) so that either the thulium fraction or ytterbium fraction may be used for measurements. It appears that the use of the ytterbium fraction is more advantageous, as a greater activity

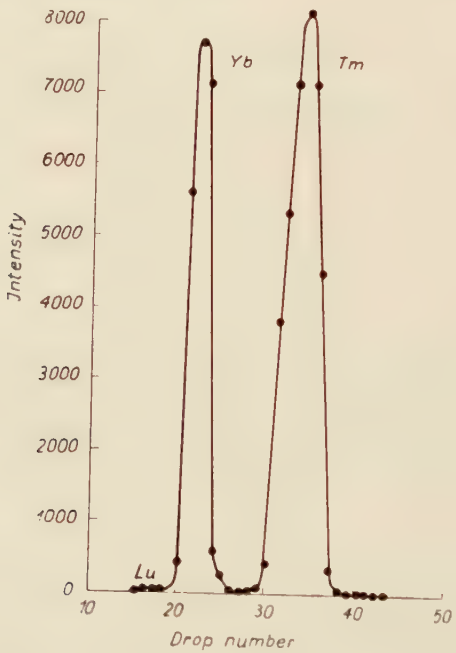

Fig. 1. Results of additional separation of the ytterbium fraction.

slower to expire is obtained. Yb^{166} does not emit positrons and so its presence in the source does not hinder the observation of Tm^{166}. The same can be said of the second long-lived isotope present in this fraction: Yb^{169}.

To avoid any possible contamination, the ytterbium fraction was subjected once again to the chromatographic process shortly after its separation. The results are shown in Fig. 1, where the activity of drops leaving the column is plotted as a function of the drop number. Three peaks are visible: the weak peak of lutecium — the contamination, the basic peak of ytterbium, and the thulium peak — the Tm^{166} produced from Yb^{166} during the time interval between the first and second chemical operation. In the preparation of the source,

ops of the ytterbium peak were used. The drops were evaporated on a thin aluminium foil 36 mg/cm^2) moistened with an insulin solution. When the measurements were started[2] hours after chemical operation, Tm^{166} was already almost in equilibrium with Yb^{166} d its activity amounted to about 0.5 mC.

A spectrometer with a long magnetic lens and baffles for separating the positrons from e electrons (Chojnacki et al. 1960) was used for carrying out the measurements. The mica ndow of the G.M. counter was 1.3 mg/cm^2 thick and did not cause any distortion of the ectrum for particles with energy exceeding 170 keV.

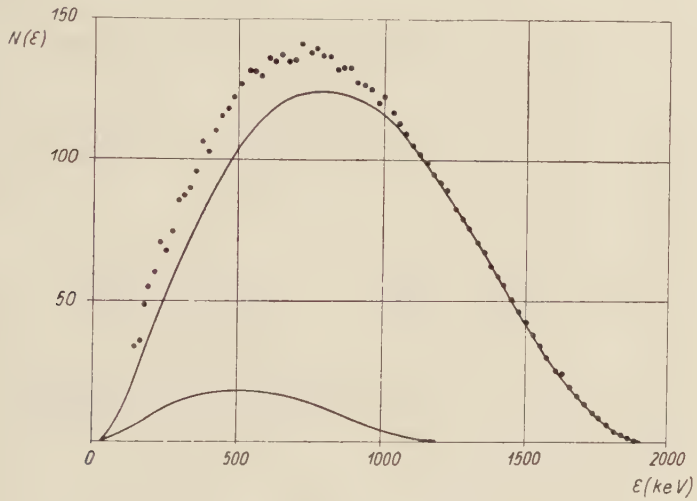

Fig. 2. Energy distribution of Tm^{166} positrons.

Three measurements of the positron spectral distribution were made. Each measure- ent took about four hours, so that small corrections for the expiration of activity with time ere necessary. As an example, Fig. 2 shows the results of one measurement.

It was verified during a period of thirteen days that the activity of the positron radiation minished throughout the entire spectrum in equal proportion with a half-life of 57 h. his result was in agreement with the assumption that the radiation under observation as due to Tm^{166}, the latter being in equilibrium with Yb^{166}.

In addition to the positrons, internal conversion electrons from the Tm^{166} were also easured. Part of the electron spectrum is shown in Fig. 3.

III. Results

Fig. 4 represents the positron spectrum in the form of a Kurie plot. With the assumption an allowed shape of spectrum the analysis yielded two components with maximum energies 1.9 MeV and 1.2 MeV and of relative intensities of 10:1. The presence of a third, less tense component of maximum energy lower than 1 MeV cannot be ruled out.

[2] After moving the isotopes to laboratory in Warsaw.

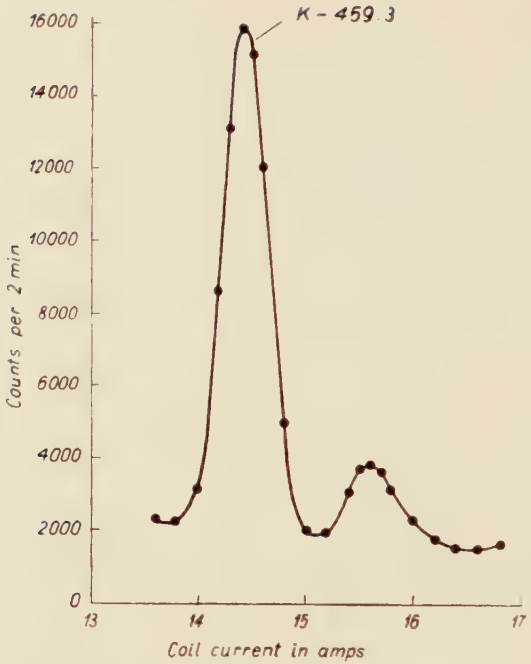

Fig. 3. Part of the internal conversion electron spectrum of Tm^{166}.

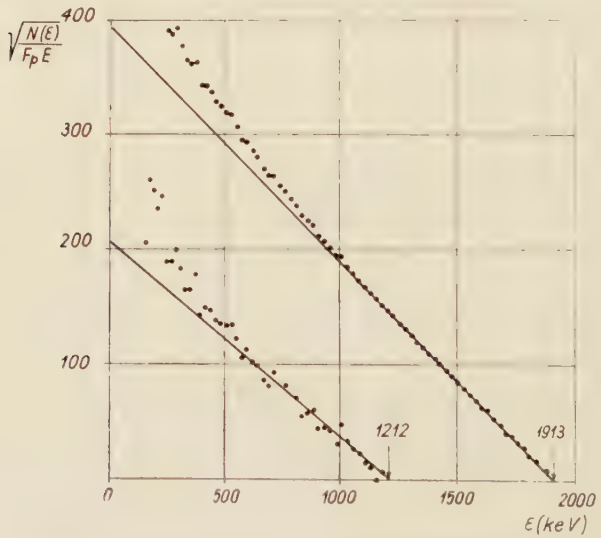

Fig. 4. Kurie plot of the Tm^{166} positron spectrum.

The computation of $\log ft$ for both components required the determination of th
mean number of positrons per Tm^{166} decay. This was deduced from data on the conversio
radiation of this isotope.

1. The ratio of intensities of the β_1^+ component (E_{max} = 1.9 MeV) and of the K-co

rsion line of the 459.3 keV [3] transition was measured:

$$\beta_1^+ : e_{K-459.3} = 1 : (0.079 \pm 0.0095)$$

e K-459.3 line was chosen for the measurement because it is well resolved from the ner conversion lines and its activity is not excessive for measurement with a G.M. unter.

2. On the basis of a paper by Gromov et al. (1959), the absolute intensity of the K-459.3 e was computed at $(6.56 \pm 0.94) \times 10^{-4}$ electrons per decay.

3. From results 1 and 2, the absolute intensity of the β_1^+ component is found to equal $3 \pm 1.6) \times 10^{-3}$ positrons per decay.

The ratio of the probabilities of electron capture and of positron emission (ε/β^+) was lculated using data assembled by Wapstra et al. (1959). These are exact for allowed transi-ons and may serve as a first approximation for first forbidden transitions (probably the nd we dealt with in the present investigation).

The final results of all the measurements and computations are assembled in Ta-e I.

TABLE I

Component	E_{max}(keV)	Relative intensities	Number of positrons per decay	log ft	ε/β^+ (theor.)
β_1^+	1920 ± 20	1	$(8.3 \pm 1.6) \times 10^{-1}$ %	7.9	~ 4
β_2^+	1219 ± 40	0.092 ± 0.018	$(7.6 \pm 2.1) \times 10^{-2}$ %	8.1	~18

IV. Control measurements

Element fractions of the rare earths are separated by the chromatographic method ithout using a carrier; hence, sources prepared from these fractions are of very small ickness. Nevertheless, the spectrum in the low energy region can still be distorted due o electron scattering. In order to estimate the amount of distortion due to apparatus factors n our case, a source was prepared of a neodymium fraction from the tantalum target and ne positron spectral distribution of Pr^{140} obtained from Nd^{140} decay was measured. In Kurie coordinates a straight line was obtained beginning from maximum energy (2362 keV) own to an energy of about 350 keV. This led to the following conclusions: 1. the Pr^{140} ositron spectrum above 350 keV is simple and 2. above this energy electron scattering oes not cause distortion of the spectral distribution. Conversely, in the case of thulium, mall deviations from the straight line in the Kurie plot of the β_2 component (Fig. 4) may lready be observed for energies of about 600 keV.

The positron spectral distribution of pure Tm^{166} separated from an ytterbium fraction as also investigated. The analysis of the Kurie plot confirmed the existence of components β_1^+ and β_2^+. No traceswerefound of a third component; this, however, may be due to low tatistical accuracy.

[3] Here and subsequently the enegies of Tm^{166} γ transitions are quoted according to Jacob et al. (1960).

V. Discussion of the decay scheme

The difference between the maximum energies of the components β_1 and β_2 amoun to 701 ± 45 keV. An analysis of the Er^{166} excited levels scheme (Fig. 5) from the point view of possible ways of positron decay leads to the conclusion that two pairs of levels ar distinguished, namely 80.6 (2^+) keV and 787.1 (2^+) keV (the difference in excitation energ is 706.5 keV), and 265.1 (4^+) keV and 957.2 (4^+) keV (with a difference in excitation energ amounting to 692.1 keV).

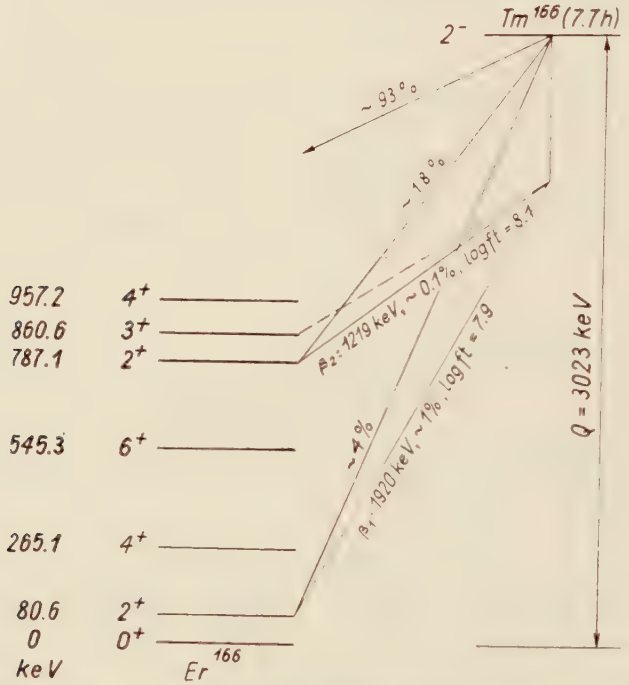

Fig. 5. A possible decay scheme of Tm^{166}. Scheme and energies of excited levels according to Jacob et al. (1960)

The assumption that the components β_1 and β_2 excite 80.6 keV and 787.1 keV levels is in agreement with what was known on isotope Tm^{166} previous to Wilson and Pool's publication (1960), namely 1. that the theoretical aspect (comparison with Tm^{169} and Dy^{163}) suggests spin 2 or 3 and odd parity for the Tm^{166} ground state, and 2. that the experimental data distinguish the first of these values (Gromov and Dzhelepov 1959, p. 65—66). Indeed, if the Tm^{166} ground state is (2^-), then it seems obvious that positron transitions will lead primarily to levels (2^+). Thus we have the first forbidden transition. This is also suggested by the log ft value (see Table I). The decay scheme of this variation is shown in Fig. 5. The transition energy $Q = 3023$ keV does not appreciably differ from the 2700 keV value obtained from the semi-empirical equation by Cameron (1957). Levy's (1957) equation yields the distinctly smaller value of 2230 keV.

Wilson and Pool (1960) report that according to their analysis the principal positron radiation component excites the level 265 (4^+) keV. In this case the transition energy Q would amount to 3207 keV.

VI. Possibility of applying the theory of non-axial nuclei

According to Davydov (1959a), the nucleus of Er^{166} is one of those not possessing the xial symmetry. If this is the case, the first three excited levels (normal) as well as the next hree (abnormal) have a rotational character (Fig. 5). Rotational nuclear excitation has no ppreciable effect on the internal state of the nucleus. In other words, the wave function escribing the internal state of the nucleus is the same for all rotational levels. This allows is to generalize the results obtained by Alaga et al. (1955) and to write the equations for he relative intensities of the β transitions in the case when one transition leads to a "normal" evel and the other to an "abnormal" one (Davydov 1959b). These equations may in principle e applied in the case of Tm^{166} positron radiation. Nevertheless, some difficulties subsist.

1. It is not certain what the spin of Tm^{166} is in its ground state.

2. In general, it should be assumed that the ground state of Tm^{166} is a superposition f states corresponding to different values of the quantum number K. However, there is no heory for odd-odd nuclei (such as Tm^{166}) which would permit us to evaluate the contribu- ion of the particular states.

3. Davydov's (1959b) equations are applicable to transitions of a fixed multipolarity L, whereas in the case of forbidden transitions of the first order $L=0$, 1 and 2 should be exam- ned. It is not possible, however, to predict the ratios of the corresponding matrix elements, i.e. o predict the contributions from the different multipolarities.

Taking into consideration the foregoing difficulties:

1. It is assumed that the Tm^{166} ground state has spin 2 (the most probable value) and odd parity.

2. It is accepted that the ground state of this isotope is a pure $K=2$ state (probably the contribution of other states is much lower).

3. Possible first forbidden transitions are taken into consideration: β' — to a lower level (2^+), β'' — to a higher level (2^+), and β''' — to level (3^+) (Fig. 5) and the different cases of $L=0$, 1 and 2 are examined.

The γ parameter, determining the deviation of the nucleus from axial symmetry amounts to 12.7 for Er^{166}. Knowledge of this number enables us to give the wave functions of the three excited states already mentioned (Davydov and Filippov 1958). These are the following:

$$\psi_{21m} = 1.000\,\Phi_{20} + 0.017\Phi_{22}$$

$$\psi_{22m} = 0.017\,\Phi_{20} + 1.000\Phi_{22}$$

$$\psi_{31m} = \Phi_{32}$$

Φ_{IK} is the wave function of a state with spin I and quantum number K.

The ratios of the reduced probabilities of transitions β' and β''' to the reduced proba- bility of transition β'' are given in Table II for different L.[4])

[4] In the case of $L=2$ equal intrinsic matrix elements of $K=2\to K=2$ and $K=2\to K=0$ transitions were assumed to show, that there is no K-forbidness. However the real intrinsic matrix elements may not be equal.

TABLE II

ratio of reduced probabilities	$L=0$	$L=1$	$L=2$
$\frac{B'(L;\,2\to21)}{B''(L;\,2\to22)}$	2.9×10^{-4}	2.9×10^{-4}	1.0
$\frac{B'''(L;\,2\to31)}{B''(L;\,2\to22)}$	0	0.50	1.8

The ratio of the reduced probabilities $(B_1/B_2)_{exp}$ found experimentally for the components β_1 and β_2 amounts to 1.44. If it is assumed that the β_2 component experimentally observed is a superposition of β'' and β''' transitions and the β_1 and β' components are identical, then

$$\left(\frac{B'}{B''}\right)_{exp} > \left(\frac{B_1}{B_2}\right)_{exp} = 1.44$$

Thus, with the all foregoing assumptions it is not possible to obtain a sufficient degree of consistency between the theoretical and experimental data.

VII. Supplementary note

The present paper was presented at the Conference on Neutron Deficient Isotopes at Dubna in June 1960. During this conference it became known that Tm^{166} positron radiation had also been analysed by Brovtsyn, Gromov, Dzhelepov, Dmitriev, and Nikitin. Their results (as far as we know of a preliminary character) were presented at the Conference on Nuclear Spectroscopy in Moscow in January 1960. Brovtsyn and co-workers found two β^+ components: 2020 ± 20 keV and 1150 ± 100 keV of relative intensities 1:0.17 and stressed the probability of the existence of a third component: 220 keV.

The authors wish to express their thanks to Docent Z. Wilhelmi, Head of the Nuclear Physics Laboratory of the Institute for Nuclear Research in Warsaw, for his kind interest in the present investigation and to Miss I. Jarosiewicz and Mr Z. Brynikowski for their help in the measurements and computations. The authors feel especially indebted to Professor B. Mottelson for his invaluable comments on the discussion.

REFERENCES

Alaga, G., Alder, K., Bohr, A. and Mottelson, B., *K. Danske Vidensk. Selsk. mat.-fys. Medd.*, **29**, No 9 (1955).
Boskma, P. and De Waard, H., *Nuclear Phys.*, **12**, 533 (1959).
Cameron, A. G. W., *Canad. J. Phys.*, **35**, 1021 (1957).
Chojnacki, S., Kopystyński, J., Preibisz, Z., Sosnowski, R., Yutlandov, I. and Żylicz. J., *Pol. Acad. of Sci., Inst. of Nucl. Research, Report* No 148/I-A, Warsaw, April (1960).
Davydov, A. S., *Izv. Akad. Nauk SSSR, Ser. fiz.*, **23**, 792 (1959a).
Davydov, A. S., *Zh. eksper. teor. Fiz.*, **37**, 137 (1959b).
Davydov, A. S. and Filippov, G. F., *Nuclear Phys.*, **8**, 237 (1958).

romov, K. and Dzhelepov, B., *Papers presented at the second conference on neutron deficient isotopes of the rare earth elements*, Joint Inst. of Nucl. Research, Dubna (1959).
romov, K. Ya., Dzhelepov, B. S. and Pokrovski, V. N., *Izv. Akad. Nauk SSSR. Ser. fiz.*, **23**, 821 (1959).
cob, K. P., Mihelich, J. W., Harmatz, B. and Handley, T. H., *Phys. Rev.*, **117**, 1102 (1960).
vy, H. B., *Phys. Rev.*, **106**, 1265 (1957).
eobrazhenski, B. K., Lilova, O. M., Dobronravova, A. N. and Teterin, E. D., *Zhurn. Neorg. Khimii*, **1**, 2294 (1956).
apstra, A. H., Nijgh, G. J. and Van Lieshout, R., *Nuclear Spectroscopy Tables*, North-Holland Publ. Comp., Amsterdam (1959).
ilkinson, G. and Hicks, H. G., *Phys. Rev.*, **75**, 1370 (1949).
ilson, R. G. and Pool, M. L., *Phys. Rev. Letters* (abstracts) **4**, 482 (1960).

SOME EXAMPLES OF INTERACTIONS OF VERY HIGH ENERGY PROTONS WITH HEAVY NUCLEI OF PHOTOGRAPHIC EMULSIONS

By J. Bartke, Z. Czachowska, R. Hołyński and K. Rybicki

Cosmic Ray Department of the Institute of Nuclear Research Cracow — Poland

(Received October 24, 1960)

Three high energy jets ($E_{prim} > 10^{12}$ eV) produced in collisions with nuclei of photographic emulsion are described. In spite of the fact that they are probably produced in central collisions of nucleons with heavy nuclei they show double maximum angular distributions in contradiction with hydrodynamical model.

Introduction

In one of the previous papers of our laboratory (Bartke et al. 1960) it has been pointed out that there exists a double maximum angular distribution in events for which we have evidence, that they are central collisions of nucleons with heavy nuclei. Since this problem seems to be important from the point of view of different models of multiple meson production in very high energy collisions we would like to describe three events of this type.

Experimental

In the scanning for nuclear interactions of cosmic particles three jets of comparatively high energy with great numbers of both evaporation and shower particles have been found: jet I: $26+47p$, jet II: $18+41p$, and jet III: $15+78p$ [1]. The events are characterized by a great multiplicity and high excitation of the target nucleus and can be interpreted as central collisions of nucleons with heavy nuclei (Ag or Br).

Jets I and II have been found during a scanning for jets via electromagnetic cascades in a stack of *Ilford G5* emulsions irradiated in the Po valley in 1957, jet III was found in area scanning in a *NIKFI-R* emulsion stack irradiated near Moscow in 1958.

In all these events we have measured angular distributions of minimum, grey and black tracks. The results of these measurements and their analysis are presented in sec. 2 and 3.

[1] These jets have been referred to in the paper of Gierula et al. (1960), as 171*K*, 168*K*, and 200*K* respectively.

TABLE I

Laboratory angles of secondary particles with respect to the jet axis for jets: I, II, III.

Jet I

Track No	log tan θ	Track No	log tan θ	Track No	log tan θ
1	$\bar{5}.825$	17	$\bar{3}.189$	33	$\bar{2}.987$
2	$\bar{4}.404$	18	$\bar{3}.190$	34	$\bar{1}.056$
3	$\bar{4}.405$	19	$\bar{3}.233$	35	$\bar{1}.174$
4	$\bar{4}.586$	20	$\bar{3}.236$	36	$\bar{1}.321$
5	$\bar{4}.691$	21	$\bar{3}.293$	37	$\bar{1}.355$
6	$\bar{4}.787$	22	$\bar{3}.309$	38	$\bar{1}.433$
7	$\bar{4}.826$	23	$\bar{3}.457$	39	$\bar{1}.559$
8	$\bar{4}.859$	24	$\bar{3}.770$	40	$\bar{1}.573$
9	$\bar{4}.871$	25	$\bar{2}.242$	41	$\bar{1}.712$
10	$\bar{4}.949$	26	$\bar{2}.286$	42	$\bar{1}.746$
11	$\bar{4}.972$	27	$\bar{2}.357$	43	$\bar{1}.764$
12	$\bar{3}.123$	28	$\bar{2}.361$	44	$\bar{1}.860$
13	$\bar{3}.125$	29	$\bar{2}.457$	45	0.061
14	$\bar{3}.125$	30	$\bar{2}.648$	46	0.188
15	$\bar{3}.151$	31	$\bar{2}.879$	47	0.247
16	$\bar{3}.185$	32	$\bar{2}.962$		

Jet II*)

Track No	log tan θ	Track No	log tan θ	Track No	log tan θ
1	$\bar{4}.532$	15	$\bar{3}.447$	29	$\bar{1}.099$
2	$\bar{4}.634$	16	$\bar{3}.462$	30	$\bar{1}.107$
3	$\bar{4}.681$	17	$\bar{3}.613$	31	$\bar{1}.110$
4	$\bar{4}.699$	18	$\bar{2}.204$	32	$\bar{1}.202$
5	$\bar{4}.748$	19	$\bar{2}.249$	33	$\bar{1}.231$
6	$\bar{4}.892$	20	$\bar{2}.263$	34	$\bar{1}.259$
7	$\bar{4}.964$	21	$\bar{2}.290$	35	$\bar{1}.317$
8	$\bar{3}.041$	22	$\bar{2}.536$	36	$\bar{1}.339$
9	$\bar{3}.079$	23	$\bar{2}.539$	37	$\bar{1}.723$
10	$\bar{3}.204$	24	$\bar{2}.543$	38	$\bar{1}.819$
11	$\bar{3}.322$	25	$\bar{2}.637$	39	$\bar{1}.822$
12	$\bar{3}.362$	26	$\bar{2}.789$	40	$\bar{1}.983$
13	3.415	27	$\bar{2}.885$	41	0.244
14	$\bar{3}.447$	28	$\bar{2}.952$		

*) Four tracks not presented in the table ($\theta_1=\theta_2=6.9\times10^{-4}$, $\theta_3=6.2\times10^{-4}$ and $\theta_4=6.9\times10^{-4}$rad.) are considered as electron tracks. A definite determination of the nature of the particles is not possible because of great track density in the inner cone and the development of the electromagnetic cascades in further plates.

TABLE I (continued)

Jet III

Track No	log tan θ	Track No	log tan θ	Track No	log tan θ
1	$\bar{3}.342$	26	$\bar{2}.681$	51	$\bar{1}.134$
2	$\bar{3}.362$	27	$\bar{2}.690$	52	$\bar{1}.134$
3	$\bar{3}.602$	28	$\bar{2}.699$	53	$\bar{1}.146$
4	$\bar{3}.699$	29	$\bar{2}.728$	54	$\bar{1}.218$
5	$\bar{3}.708$	30	$\bar{2}.785$	55	$\bar{1}.281$
6	$\bar{3}.740$	31	$\bar{2}.803$	56	$\bar{1}.295$
7	$\bar{3}.763$	32	$\bar{2}.813$	57	$\bar{1}.305$
8	$\bar{3}.813$	33	$\bar{2}.823$	58	$\bar{1}.308$
9	$\bar{3}.851$	34	$\bar{2}.826$	59	$\bar{1}.337$
10	$\bar{3}.869$	35	$\bar{2}.833$	60	$\bar{1}.337$
11	$\bar{3}.886$	36	$\bar{2}.900$	61	$\bar{1}.340$
12	$\bar{3}.898$	37	$\bar{2}.914$	62	$\bar{1}.342$
13	$\bar{3}.978$	38	$\bar{2}.919$	63	$\bar{1}.378$
14	$\bar{3}.996$	39	$\bar{2}.935$	64	$\bar{1}.515$
15	$\bar{2}.033$	40	$\bar{2}.944$	65	$\bar{1}.593$
16	$\bar{2}.041$	41	$\bar{2}.954$	66	$\bar{1}.613$
17	$\bar{2}.057$	42	$\bar{2}.969$	67	$\bar{1}.677$
18	$\bar{2}.090$	43	$\bar{2}.978$	68	$\bar{1}.681$
19	$\bar{2}.111$	44	$\bar{1}.009$	69	$\bar{1}.683$
20	$\bar{2}.290$	45	$\bar{1}.025$	70	$\bar{1}.686$
21	$\bar{2}.371$	46	$\bar{1}.029$	71	$\bar{1}.825$
22	$\bar{2}.484$	47	$\bar{1}.045$	72	$\bar{1}.868$
23	$\bar{2}.491$	48	$\bar{1}.057$	73	$\bar{1}.939$
24	$\bar{2}.648$	49	$\bar{1}.061$	74	0.455
25	$\bar{2}.658$	50	$\bar{1}.097$	75	0.735

Three tracks are not included since they are emitted backwards.

We have also scanned for secondary interactions. In jet I the scanning has been performed only in the narrow cone (volume containing 23 tracks with the total length of ~110 cm) and no secondary interactions have been found. In jet II we have scanned an area containing 32 tracks with the total length of ~260 cm. Three secondary jets was found i.e. $4+9p$, with $\gamma_c=13$, produced in the distance of 49 mm from the primary interactions by a singly charged secondary emitted with an angle $\theta_L=14'$; (transverse momentum $p_1=1.4$ BeV/c), and also jets $14+(28\pm2)p$, $2.5<\gamma_c<3.1$ and $26+(\geqslant20)p$, $10<\gamma_c<20$. A better determination of the track number and the γ_c — value was not possible because of poor visibility and great distortion in this part of the stack. In the jet III a secondary interaction was found already in the distance of 196μ from the primary interaction point. This secondary interac-

tion $12+6p$ or n was initiated by one of the tracks of the narrow cone. Target diagrams in the distance 600μ, 1000μ and 1400μ from the primary interaction enable to distinguish between the tracks from the secondary interaction and those from the primary.

2. Angular distribution of secondary particles and the determination of the primary energy

For each jet we made a target diagram by measuring the coordinate y and z with respect to one selected track. The polar angles of the tracks of the narrow cone with the jet axis were determinated by measuring the distances of the points on the target diagram from the centre of gravity of this points. In the diffuse cone these angles were determined from the projected angle φ (on the plane of emulsion) and the dip angle ϑ using the formula: $\operatorname{sem}\theta_L = \operatorname{sem}\varphi \cdot \cos\vartheta \cos\vartheta_0 + \operatorname{sem}(\vartheta - \vartheta_0)$, ϑ_0 — being the dip angle of the primary. The results are presented in table I.

From the angular distribution the Lorentz-factor of a system in which there is forward-backward symmetry can be determined as $\gamma_c = \overline{\log \operatorname{ctg} \theta_i}$, θ_i — being the polar angle of the i-th particle with respect to primary particle direction (jet axis).

For nucleon-nucleon collision we obtain the primary energy in the laboratory system from: $E_p = 2\gamma_c^2 Mc^2$ $(\gamma_c \gg 1)$.

In collisions of nucleons with nuclei we must assume a type of mechanism in order to evaluate the primary energy. If we assume that the primary nucleon interacts only with a group of the nucleons of the target nucleus (tunnel model) we obtain for the energy: $E_p = 2n\gamma_c^2 Mc^2$ where n is the number of nucleons in the tunnel. In our events using this model (collisions with Ag or Br) we can assume average $n=4$.

If the angular distribution is presented in terms of $dN/d(\log\tan\theta_L)$ *vs.* $x = \log\tan\theta_L$ we can use as the measure of the anisotropy the dispersion

$$\sigma = \sqrt{\frac{\Sigma(\log\tan\theta_i - \overline{\log\tan\theta})}{n-1}}$$

For the isotropic distribution this dispersion should be $\sigma = 0.39$. Anisotropic distributions are characterized by greater σ-values.

In the table II the E_p, γ_c and σ-values for the events described are presented.

TABLE II

jet	type	γ_c	$E_p = 2\gamma_c^2 Mc^2$	$E_p = 2n\gamma_c^2 Mc^2$	σ
I	$26+47p$	83.1	1.3×10^{13} eV	5.2×10^{13} eV	1.25
II	$18+41p$	58.1	6.4×10^{12} eV	2.5×10^{13} eV	1.10
III	$15+78p$	15.3	4.4×10^{11} eV	1.8×10^{12} eV	0.71

On Figs. 1*a*, *b*, *c*, and 2*a*, *b*, *c*, we present differential and integral angular distributions of the jets in the coordinates $x = \log\tan\theta_L$ and $y = \log\dfrac{F(\theta)}{1-F(\theta)}$ where $F(\theta)$ is the fraction of number of tracks with angles smaller than θ.

It can be seen that the differential angular distribution shows strong anisotropy and a double maximum structure which corresponds to a plateau in the integral dostribution.

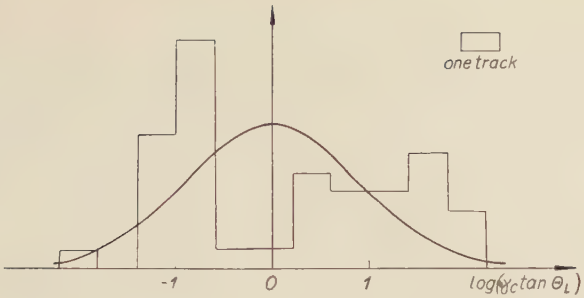

a

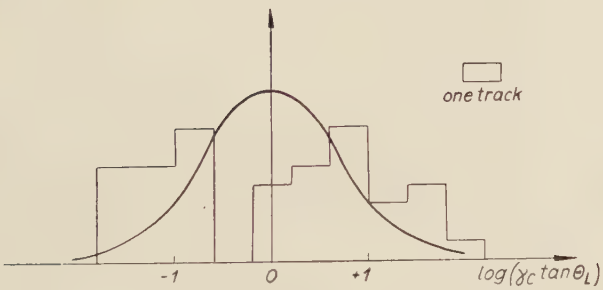

b

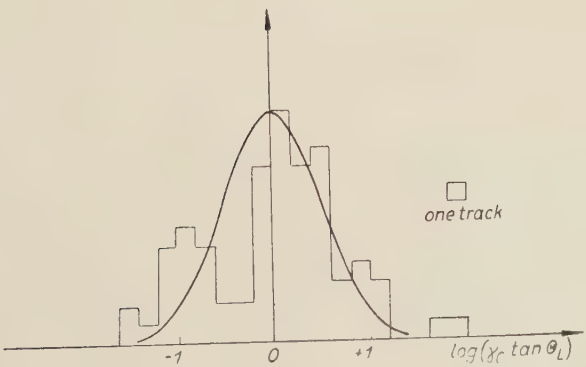

c

Fig. 1a, b, c Differential angular distributions for jets a — I, b — II, c — III. The continuous curve represents the best fit of Gussian curve to the experimental data with $\sigma = 1.25$; $\sigma = 1.09$ and $\sigma = 0.71$ respectively.

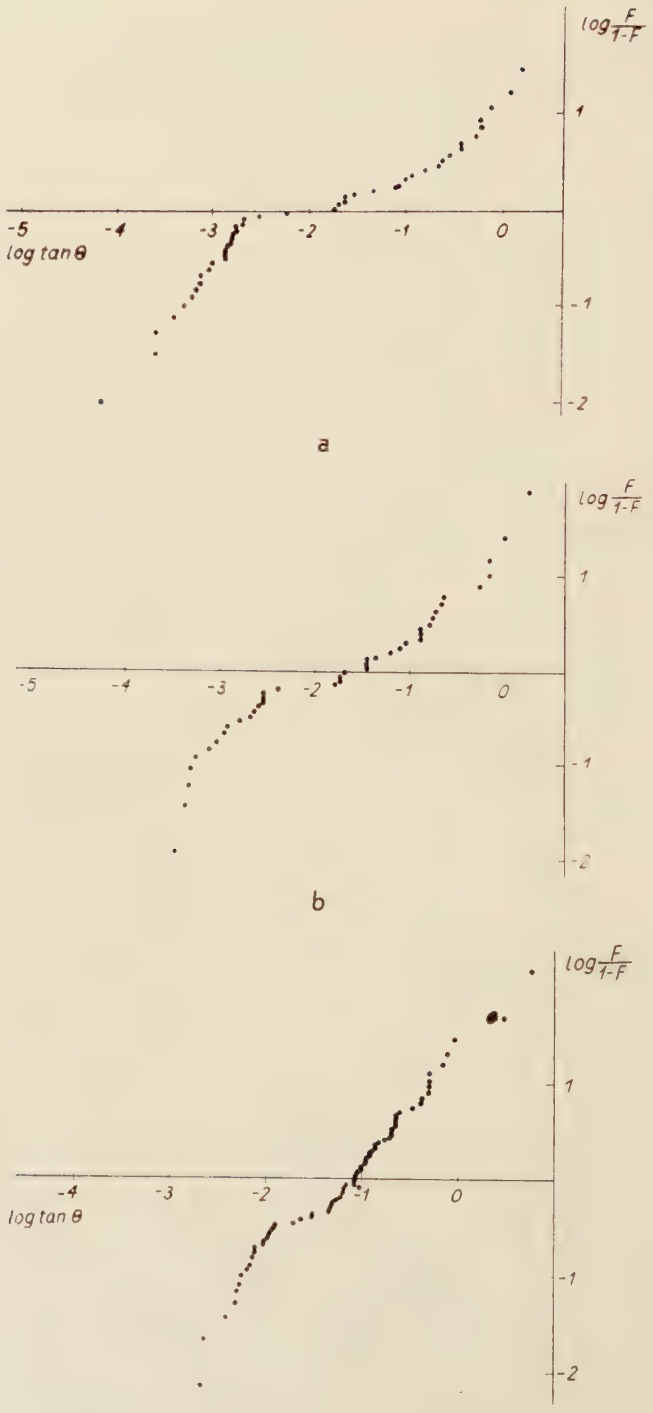

Fig. 2a, b, c Integral distributions for jets a — I, b — II and c — III in Duller-Walker's coordinates.

3. *Angular distributions of black and grey tracks*

We have measured the angular distributions at black and grey tracks for all events. ey have not significant deviations from the isotropic distribution, what may be seen in gs. 3*a*, *b*, *c*. The estimated total energies of black and grey tracks are: jet I: 900 MeV, II: 1400 MeV and jet III: 500 MeV.

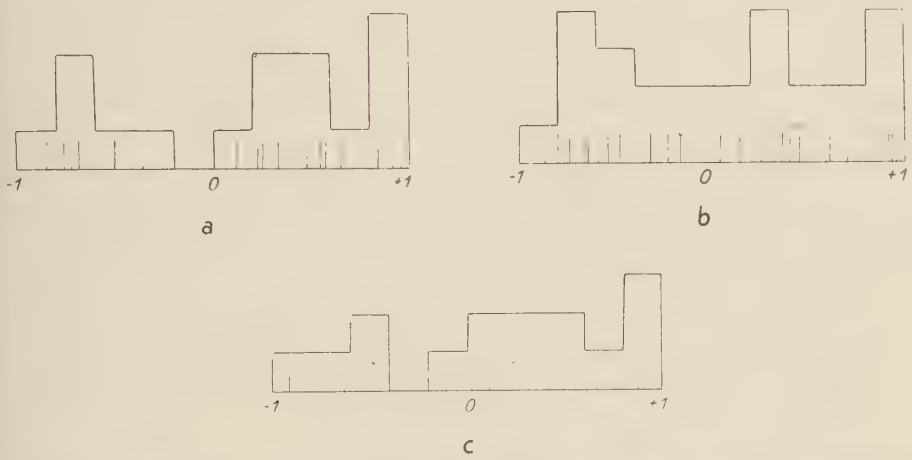

g. 3a, b, c Differential angular distributions of the black and grey tracks for jets a — I, b - II and c — III coordinates $\cos\theta_L$. The continuous and dotted lines correspond to black and grey tracks respectively.

Comparison of the angular distributions of the secondary particles with the predictions of the hydrodynamical model

The hydrodynamical model (Belenkiĭ-Landau 1956, Milekhin 1958) has predicted ıe normal shape of angular distributions with the maximum for *CM*-angle $\theta = \frac{\pi}{2}$, both ›r nucleon-nucleon and nucleon-nucleus collisions.

In the original paper in which the double-maximum distributions had been described Ciok et al. 1958a, 1958b) only nucleon-nucleon collisions were considered. The two-centre ıodel has been introduced for explaining this shape of distributions for n-n collisions. aking into account the possibility for the existence of this type of angular distributions ıe opinion has been expressed (Feinberg 1960) that roughly speaking there are two types f nucleon-nucleon collisions. There are collisions with complete transfer of energy (head-on ›llisions, inelasticity $K=1$) and collisions with incomplete transfer of energy (peripheral ›llisions, inelasticity $K \ll 1$). According to these ideas the hydrodynamical model in its resent form could be applied only to the first type of collisions. But especially favourable onditions for applying of this model are fulfilled for central collisions of nucleons with eavy nuclei.

According to hydrodynamical model these collisions correspond to collisions with the uclear matter of the tunnel which the nucleon shears off the target nucleus. The number

of nucleons in the tunnel is characterized only by the length of the tunnel which is considered as without any structure. The differential angular distribution can, according to this theory be well described by a Gaussian curve: $dN/dx \sim e^{-x^2/2L}$; where $L = 0.56 \ln E/M + 1.6 \times \ln \frac{2}{n+1} + 1.6$. Thus L is a function of the tunnel length and the primary energy.

The analysis of the experimental facts does not confirm the predictions of this model. In the paper Bartke et al. (1960) a statistical analysis of nucleon-nucleus collisions was performed in a large energy interval and it was found that for jets with a primary energy greater than 10^{12} eV and with a great number of evaporations tracks and shower particles there is a strong anisotropy and a double maximum structure.

Taking into account the importance of the existence or not existence of the two-maximum -jets in central collisions with heavy nuclei, we present here in details the three cases from our laboratory which may be considered as central collisions of nucleons with heavy nuclei of photographic emulsion. From these cases I and III was not included in the paper of Bartke et al. (1960) and II was carefully remeasured.

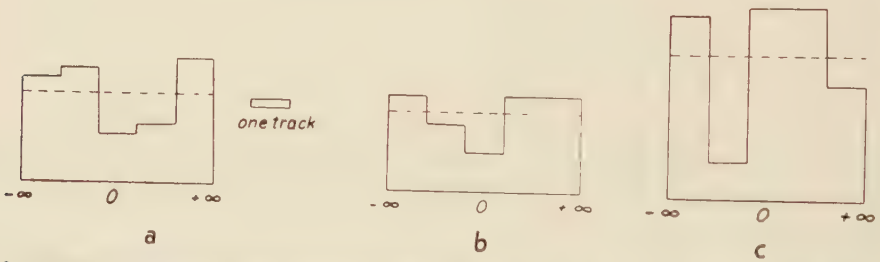

Fig. 4a, b, c Differential angular distributions for jets *a*-I, *b*-II and *c*-III in equal area intervals of the Gaussian function. The Gaussian distribution is given by the dotted straight line.

We have analysed the deviations of the distribution from the normal one in three ways.

1⁰. On Fig. 4*a*, *b*, *c*, the angular distributions of the analysed jets are presented in terms of histograms in coordinates in which equal intervals on the x-axis correspond to equal areas of the normal distribution. The normal distribution curve is in this coordinates a straight line parallel to the x-axis. The deviations from the normal distribution estimated by means of the Pearson's χ^2-test are presented in table III.

2⁰. In the paper of Gierula et al. (1960) the authors introduced a new measure of the deviation predicted by the two-centre model. If we divide the angular distribution in the *C.M.* system into two parts by the value $x = \pm 0.674\sigma$ the number of tracks outside this interval N_e (i.e. those with $|x| > 0.674\sigma$) and the number inside N_i ($|x| < 0{,}674\sigma$) should be equal for the normal distribution. In the case of the double maximum distribution predicted by two-centre model the N_e is greater than N_i. Thus the value $D = \frac{N_e - N_i}{N_e + N_i} = \frac{N_e - N_i}{n_s}$ was proposed as a measure of this deviation, since it should be zero for the normal distribution. In the case of any deviation towards a symmetrical double maximum distribution this value is $0 < D \leq 1$. The level of the significance of the deviation can be computed

m: $\chi^2 = D^2 n_s$. The D values and the significance levels for the jets presented in this per are given in the 3rd and 4th column of table III.

3⁰. The application of the Kolmogorov-Smirnov test (Kolmogorow 1953, Smirnow 59) is a not quite correct procedure since the test in its present form cannot be applied comparing an experimental curve with a theoretical curve with parameters estimated m the experiment. The application of the tables available gives too low values for the viation. Nevertheless we have calculated these values according to this test (4th column le III).

TABLE III

jet	Deviation computed by means of the χ^2-test	D	Deviation computed from $\chi^2(D)$	Deviation computed by means of the Kolmogorov-Smirnov test
	1	2	3	4
I	1.5 st. dev.	0.53	3 st. dev.	2 st. dev.
II	~1 st. dev.	0.41	2.5 st. dev.	1 st. dev.
III	2.5 st. dev.	0.07	~1 st. dev.	1 st. dev.

5. Conclusions

1. It has been confirmed on further events found in our laboratory that in central llisons of nucleons with heavy nuclei for which there is a strong anisotropy we observe double maximum structure significantly different from the normal one.

2. This fact is in disagreement with the hydrodynamical model.

3. This fact would be in agreement with the hypothesis of the superposition of peripheral llisions each described by the two-centre model, if the "core" for "central" nucleon-ucleon collisions was much smaller than the nucleon radius.

It is a great pleasure for us to thank Professors M. Mięsowicz and J. Gierula for continuous idance, permanent discussions and hints during progress of this work.

REFERENCES

rtke, J., Ciok, P., Gierula, J., Hołyński, R., Mięsowicz, M., Saniewska, T., *Nuovo Cimento*, **15**, 18 (1960).
lenkiĭ, S. Z. and Landau, L., *Nuovo Cimento Suppl.*, **3**, 15 (1956).
ok, P., Coghen, T., Gierula, J., Hołyński, R., Jurak, A., Mięsowicz, M., Saniewska, T., Stanisz, O., Pernger, J., *Nuovo Cimento*, **8**, 166 (1958).
ok, P., Coghen, T., Gierula, J., Hołyński, R., Jurak, A., Mięsowicz, M., Saniewska, T., Pernger, J., *Nuovo Cimento*, **10**, 741 (1958).
inberg, E. L., *Uspekhi fiz. Nauk*, **70**, 333 (1960). (Presented also at the Moscow and Kiev conferences).
erula, J., Mięsowicz, M. and Zieliński, P., *Acta phys. Polon.*, **19**, 119 (1960).
erula, J., Mięsowicz, M. and Zieliński, P., to be published in *Il Nuovo Cimento*.
lmogorov, A., *Giornale dell'Instituto Italiano degli Attuari*, **4**, 1 (1953).
ssey, F. J., *American Statistical Association Journal*, 68 (March 1951).
lekhin, G. A., *Zh. eksper. teor. Fiz.*, **35**, 1185 (1958).
irnov, H., *Recueil Mathématique N. S.* **6**, 3 (1959).

ON THE SHAPES OF ALLOWED BETA SPECTRA

By Br. Kuchowicz*

(Joint Institute for Nuclear Research, Dubna, USSR)

(Received October 26, 1960)

The present paper brings a discussion of the small deviations observed in the beta spectra of ^{32}P, ^{90}Y, ^{114}In and ^{22}Na. No explanation thereof exists within the framework of the conventional theory, even assuming the usually dominating nuclear matrix element to be suppressed. Two alternative explanations of the phenomenon are discussed, both of which are tentative and of a somewhat surprising character. The one ascribes the effect to G-nonconserving interactions, whereas the other hypothesis attributes the deviations to a virtual intermediary chiral spinless boson.

1. Small deviations in beta spectra

It would seem that the foundations of beta decay theory are rather well established, as ıe Universal Fermi Interaction explains a considerable number of the phenomena. There ːmain, however, some experimental facts which should be carefully analysed in order to ːcount for details of the theory. The most important among these seem to be the small ːviations which have been observed in beta spectra by Langer's group (Johnson & al., ːamilton & al.). The Fermi-Kurie plots for electron and positron spectra exhibited devia- ːons from linearity which could not be explained by means of Fierz interference terms since, ː present, there is strong experimental support (and even stronger theoretical reasons, too) ːr assuming these terms to vanish. Furthermore, introducing the Fierz interference terms ːould imply opposite directions of the deviations for electron and positron spectra, whereas ːanger and his co-workers found experimentally that in both cases there is an excess of ːw-energy β-particles. In view of the somewhat strange consequences derived in this paper ːd following from the assumption of Langer's results, an experimental reinvestigation ːf the problem can prove to be necessary in order either to obtain support for our hypotheses ːr to show them to be wrong.

The following decays were investigated experimentally:

ː $^{32}\mathrm{P} \xrightarrow{\beta^-} {}^{32}\mathrm{S}$ $(1^+ \to 0^+)$, $\lg ft = 7.9$, allowed G-T transition;

ː $^{114}\mathrm{In} \xrightarrow{\beta^-} {}^{114}\mathrm{Sn}$ $(1^+ \to 0^+)$, $\lg ft = 4.5$, allowed G-T transition;

* On leave of absence from the Institute for Nuclear Research, Warsaw, Poland.

3) $^{22}\mathrm{Na} \xrightarrow{\beta^+} {}^{22}\mathrm{Ne}$ $(3^+ \to 2^+)$, $\lg ft = 7.4$, allowed G-T transition;

4) $^{90}\mathrm{Y} \xrightarrow{\beta^-} {}^{90}\mathrm{Zr}$ $(2^- \to 0^+)$, $\lg ft = 8.0$, first forbidden unique transition[1].

The analysis of experimental spectrum shapes resulted in the introduction of th empirical multiplicative correction term:

$$\left(1+\frac{b}{E}\right)$$

in order to obtain a linear Fermi-Kurie plot of the same type for β^- and for β^+-spectra wit the values of b lying within the interval of 0.2 to 0.4 (in our system of units wherein $\hbar = c = m_e = 1$). It was shown by the present author (Kuchowicz 1959a) that a spectrum shap of the desired type can be obtained under a simple assumption of semiphenomenologic nature (addition of first order corrections in the gradient of lepton fields). The requiremen however, consists in fitting into a regular theory, without any ad hoc assumptions.

II. Numerical estimations within the framework of the conventional theory

It is well known that we have usually to deal in unique beta transitions with only on decisive energy-independent nuclear matrix element (M_{GT} or B_{ij}), which plays the rol of a multiplicative factor in constructing the Fermi-Kurie plot. With respect to the trans tions mentioned, this is approximately true only in the case of the first forbidden decay o $^{90}\mathrm{Y}$ and in that of the allowed decay of $^{114}\mathrm{In}$, whereas the two other allowed G-T decay exhibit too high values of $\lg ft$, which is an argument in favour of the suppression of th usually dominant matrix element. Thus, a series of additional correction terms usuall considered irrelevant can be of comparable magnitude, even leading to a change of th resulting spectrum shape. In the conventional treatment of the $(V-A)$ interaction, followin additional terms for allowed G-T transitions occur:

$$\int \gamma_5 \vec{r}, \qquad \int \vec{\alpha} \times \vec{r}, \qquad \int \vec{\sigma} r^2, \qquad \int (\vec{\sigma} \cdot \vec{r})\, \vec{r}$$

It was shown (Kuchowicz 1959b) that, in ordinary decays (in which $\lg ft$ does no exceed 4), these corrections are vanishingly small. This result can be adapted to the deca of $^{114}\mathrm{In}$, whereas the two other decays (with matrix elements lesser by two orders of magni tude) escape this treatment and require a more thorough analysis.

From the well known relation, valid for allowed transitions:

$$|C_F M_F|^2 + |C_{GT} M_{GT}|^2 = \frac{1}{ft} \cdot \frac{2\pi^3 \ln 2 \cdot \hbar^7}{m_e^5 c^4} \qquad (1$$

we shall now estimate the Gamow-Teller matrix element (with value $C_{GT} = C_A$ given by Goldhaber (1958)). This matrix element amounts to 7.10^{-3} for $^{32}\mathrm{P}$ and $12.5 \cdot 10^{-3}$ for $^{22}\mathrm{Na}$. We use the standard formula for the spectrum shape:

$$\mathcal{N}(E)dE = \mathcal{F}_0 \cdot pEq^2 \left\{ (|C_A|^2 + |C'_A|^2) \left[\left| \int \vec{\sigma} \right|^2 - \frac{2}{3} \mathrm{Re} \left\{ \left(\int \vec{\sigma} \right)^* \left(\int \vec{\sigma} r^2 \right) \right\} \right] (E_0 - E) \times$$

[1] In a paper published recently by Hamilton, Langer and Smith (Phys. Rev. **119**, 772 (1960)) their results have been extended upon the positron decay of $^{89}\mathrm{Zr}$.

$$\times \left(\frac{E_0}{2} - \frac{5}{6}E + \frac{1}{3E} - \xi\right)\Big] - \frac{4}{9}\,\mathrm{Re}\left\{\left(\int\vec{\sigma}\right)^{*}\left(\int(\vec{\sigma}\cdot\vec{r})\,\vec{r}\right)\right\}(E_0 - E)\left(E - \frac{1}{E} + 3\xi\right) +$$

$$+ \frac{2}{3}\,\mathrm{Im}\left\{\left(\int\vec{\sigma}\right)^{*}\left(\int\gamma_5\vec{r}\right)\right\}\left(E_0 - \frac{1}{E} + 3\xi\right)\Big] + \frac{2}{3}\,\mathrm{Re}\,(C_A^{*}C_V^{\prime} + C_A^{\prime *}C_V)\times \qquad (2)$$

$$\times\,\mathrm{Re}\left[\left(\int\vec{\sigma}\right)^{*}\left(\int\vec{\alpha}\times\vec{r}\right)\right]\left(E_0 - 2E + \frac{1}{E} - 3\xi\right)\Big\}\,dE$$

and the approximate form of the nuclear matrix elements given by Morita (1959). According to the large ft-value, we assume that the matrix element $\int\vec{\sigma}$ is approximately one percent of its value for ordinary favoured transitions. Thus, the ratios $|\int\gamma_5\vec{r}|/|\int\vec{\sigma}|$ etc. are multiplied by a factor of the order of 10^2. Nevertheless, what we obtain is not simply a spectrum proportional to $\left(1 + \frac{b}{E}\right)$, since the terms in $\int\vec{\sigma}r^2$, $\int(\vec{\sigma}\cdot\vec{r})\,\vec{r}$ and $\int\vec{\alpha}\times\vec{r}$ obviously imply energy dependence of a different type (terms proportional to E and E^2) which failed to be observed hitherto. Only in one very special case do we obtain a spectrum of the desired empirical shape for ^{32}P. This occurs if we take into account only the additional matrix element $\int\gamma_5\vec{r} \approx 0.0009 \cdot 10^2 \int\vec{\sigma}$; we obtain $b \sim 0.29$. Even under this rather artificial assumption of considering only one correction term no agreement with experiment can be achieved in the case of the positron decay of ^{22}Na, since the coefficient b does not exceed 0.05 for the ratio $|\int\gamma_5\vec{r}|/|\int\vec{\sigma}|$ taken from the reasonable interval of values $(0 \div 0.1)$.

No explanation of the deviations in the beta spectra within the framework of conventional corrections thus seems possible even in the case of the l-forbidden transitions. It seems to be a mere accident that for one possible value of $\int\gamma_5\vec{r}$ we obtained the empirical correction for ^{32}P, since similar estimations fail to yield even approximately the correction factor for the positron decay of ^{22}Na. There arises the problem: How to explain the deviations on a solid basis, not by assuming ad hoc unnatural cancellations of matrix elements, and without the necessity of introducing a different explanation for each experimental case. Besides, it is of interest to mention that there is one more phenomenon in beta decay that cannot be explained theoretically. Namely, experimental values of the longitudinal polarization of β-particles were found to be by about 10% lower than the theoretical value $-v/c$ (Mikaelan and Spivak 1959). A reinvestigation of the problem by the same authors led them to the conclusion that the polarization had been systematically underestimated; nevertheless, deviations from the theory, of the order of about 5% still remain. This problem seems to be closely related to the former one and, maybe, they might be solved simultaneously.

In what follows, two tentative explanations of the deviations under consideration will be given, both of which are no more than the first step of a more detailed analysis to be carried out subsequently, and both requiring further support. One of these alternative explanations reduces deviations observed to possible G-nonconserving interactions, whereas the second will be seen to draw conclusions from the hypothesis of an intermediary chiral boson.

III. G-nonconserving interactions

In order to explain the deviations in the beta spectra, let us consider the most general transition matrix element for a nucleon decay in Weinberg's notation (1958):

$$M = [\bar{u}_e \gamma_\lambda (1+\gamma_5)\, u_\nu]\, [\bar{u}_p (f_V \gamma_\lambda + g_V \sigma_{\lambda\mu} k^\mu + i h_V k_\lambda)\, u_n] + \\ + [\bar{u}_e i\gamma_5 \gamma_\lambda (1+\gamma_5)\, u_\nu]\, [\bar{u}_p (f_A i\gamma_5 \gamma_\lambda + g_A k_\lambda \gamma_5 + i h_A \sigma_{\lambda\mu} \gamma_5 k^\mu)\, u_n] \qquad (3)$$

The effect of strong interaction is described by means of the 6 form factors f_A, f_V etc., which are functions of $k^2 = k^\lambda k_\lambda$, k_λ being the 4-momentum transfer. If time reversal holds and final state interactions are neglected, the form factors in (3) are real.

Weinberg divided the primary weak interactions into two classes according to the G-transformation[2] properties of the strongly interacting currents. It was shown that, for nucleon processes, the terms with h_A and h_V can arise only from the second-class interactions which are absent in the Feynman-Gell-Mann theory. The presence of these interactions would break the deep relation between the weak interactions and isotopic spin suggested by Feynman and Gell-Mann. We shall subsequently see that there is a test for the existence of such interactions.

Let us consider the beta decay of complex nuclei, assuming that the main contribution to the nuclear matrix elements comes from the structure of the nucleon rather than of the nucleus[3].

The relativistic form of the S-matrix element is given in Table I. We apply the Foldy-Wouthuysen transformation, and the nucleon operators are taken in the nonrelativistic form as by Alaga & al. (1958). In Table I we have 4-component nucleon spinors, whereas

TABLE I

Relativistic form of the S-matrix element for nucleon decay

Lepton covariant	General form of the nucleon covariant for	
	pure Fermi transitions	pure G-T transitions
V $L(1) = [u_e^+(1+\gamma_5)\, u_\nu]$	$[u_p^+(f_V + g_V \vec{P}\cdot\beta\vec{\alpha} + h_V E_0 \beta) u_n]$	$[u_p^+(g_V \vec{P}\cdot\beta\vec{\alpha})\, u_n]$
V $L(\vec{\alpha}) = [u_e^+ \vec{\alpha}(1+\gamma_5)\, u_\nu]$	$[u_p^+(f_V \vec{\alpha} + g_V E_0 \beta\vec{\alpha} + h_V \vec{P}\beta) u_n]$	$[u_p^+(f_V \vec{\alpha} + g_V E_0 \beta\vec{\alpha} + i g_V \vec{P} \beta\vec{\sigma}) u_n]$
A $L(\vec{\sigma}) = [u_e^+ \vec{\sigma}(1+\gamma_5)\, u_\nu]$	$[u_p^+(i h_A \vec{P} \times \beta\vec{\alpha})\, u_n]$	$[u_p^+(f_A \vec{\sigma} - g_A \vec{P}\beta\gamma_5 - h_A E_0 \beta\vec{\sigma} + i h_A \vec{P} \times \beta\vec{\alpha})\, u_n]$
A $L(\gamma_5) = [u_e^+ \gamma_5 (1+\gamma_5)\, u_\nu]$	—	$[u_p^+(-f_A\gamma_5 - g_A E_0 \beta\gamma_5 - h_A \vec{P}\cdot\beta\vec{\sigma})\, u_n]$
Nonrelativistic form of the nucleon operators	$\vec{\alpha} = \dfrac{\vec{P}}{2M}$ $\beta = 1$	$\vec{\alpha} = -\dfrac{i}{2M} \vec{P} \cdot \vec{\sigma}$ $\gamma_5 = \dfrac{\vec{P}\cdot\vec{\sigma}}{2M}$ $\beta = 1$

[2] The G-transformation is defined as the product of charge symmetry and charge conjugation.

[3] This means that we consider only the decay of a physical nucleon inside the nucleus, neglecting the possibility of "exchange" or cooperative effects in complex nuclei. Since, for high Z, Coulomb effects destroy G-invariance, both first- and second-class interactions are retained.

in Table II, where the nonrelativistic form of the S-matrix element is given, we have two-component nucleon spinors and $\vec{\sigma}$ is a Pauli matrix in nucleon space.

In subsequent treatment, the dependence of the form factors on the four-momentum will be disregarded for a specific transition, these being treated as constants (which may, however, differ from one decay to another). A rough guess would yield the magnitude of

TABLE II

Nonrelativistic form of the S-matrix element for nucleon decay

Lepton covariant	Nonrelativistic form of the nucleon covariant for	
	pure Fermi transitions	pure G-T transitions
V $L(1)$	$\left\{u_p^+ \left[f_V + h_V E_0 + \underline{\frac{1}{2M} g_V \vec{P}^2} \right] u_n \right\}$	—
V $L(\vec{\alpha})$	$-\left\{u_p^+ \left[\left(\frac{1}{2M} f_V - h_V + \underline{\frac{1}{2M} g_V E_0} \right) \vec{P} \right] u_n \right\}$	$i \left\{u_p^+ \left[\left(\frac{1}{2M} f_V + g_V - \underline{\frac{1}{2M} g_V E_0} \right) \vec{P} \cdot \vec{\sigma} \right] u_n \right\}$
A $L(\vec{\sigma})$	—	$\left\{u_p^+ \left[\left(f_A - h_A E_0 - \underline{\frac{1}{2M} h_A \vec{P}^2} \right) \vec{\sigma} + \underline{\frac{1}{2M} (-g_A + h_A) (\vec{P} \cdot \vec{\sigma}) \vec{P}} \right] u_n \right\}$
A $L(\gamma_5)$	—	$-\left\{u_p^+ \left[\left(\frac{1}{2M} f_A + h_A + \underline{\frac{1}{2M} g_A E_0} \right) (\vec{P} \cdot \vec{\sigma}) \right] u_n \right\}$

The terms underlined are second order correction terms discarded in further cosiderations.

the constants g and h at least about one order of magnitude lower than that of f. We shall therefore disregard those terms in Table II wherein the g and h constants are multiplied by $\frac{1}{2M}$ (here M is the nucleon mass in units of electron mass).

In order to obtain all desired formulae it is sufficient to adapt the results of Alaga's paper after a suitable change of notation[4]. Alaga's terms with the nuclear matrix element T_{12} (for l-forbidden transitions) are omitted in order to simplify the discussion.

[4] In Alaga's formulae (1)... (9) we effect the following substitutions (with the new constants on the right hand side):

a) for Fermi transitions:

$$g_2^2 \to |f_V + h_V E_0|^2$$

$$\frac{1}{M} g_2^2 \to 2\mathrm{Re}\left[(f_V + h_V E_0) \left(\frac{1}{2M} f_V + h_V \right)^* \right]$$

The problem of the relative signs for β^-- and β^+-transitions may be easily solved i Weinberg's Theorem I is taken into account. By this theorem, a change of the sign of h' and h_A in the interference terms follows for β^+-decay, and the final formulae for the spectrum shape are as follows:

a) for Fermi transitions (0→0):

$$\mathcal{N}_0(E)dE = \mathcal{F}_0(\pm Z, E)pEq^2 \left| \int 1 \right|^2 \left\{ |f_V|^2 \pm 2\mathrm{Re}\,(f_V h_V^*)\, E_0 + |h_V|^2 E_0^2 + \right.$$

$$\left. + \left[\frac{1}{M} |f_V|^2 \pm 2\mathrm{Re}\,(f_V h_V^*) \left(1 + \frac{E_0}{2M}\right) + 2E_0 |h_V|^2 \right] \left(E_0 \pm 2\xi - \frac{1}{E} \right) \right\} dE \qquad (4$$

b) for Gamow-Teller transitions ($\Delta J=1$):

$$\mathcal{N}_1(E)\,dE = \mathcal{F}_0(\pm Z, E)\,pEq^2 \left| \int \vec{\sigma} \right|^2 \left\{ |f_A|^2 \mp 2\mathrm{Re}\,(f_A h_A^*)\, E_0 + |h_A|^2 E_0^2 + \right.$$

$$+ \frac{1}{3} \left[\frac{1}{M} |f_A|^2 \pm 2\mathrm{Re}\,(f_A h_A^*) \left(1 - \frac{E_0}{2M}\right) - 2E_0 |h_A|^2 \right] \left(E_0 \pm 2\xi - \frac{1}{E} \right) + \qquad (5$$

$$\left. + \frac{1}{3} \cdot 2\mathrm{Re} \left[(f_A \mp h_A E_0) \left(\frac{1}{2M} f_V^* + g_V^* \right) \right] \right] \left(E_0 - 2E \mp 2\xi + \frac{1}{E} \right) \right\} dE$$

The upper signs are for β^--decay, the lower ones — for β^+-decay. The spectrum shap for a $\Delta J=0$ (not 0→0) transition is given by the sum of expressions (4) and (5). By analog to the formulae for the spectrum shapes, angular correlation formulae can be derived fro expressions (3) and (8) in Alaga's paper (1958).

Langer's empirical shape correction factor is readily derived from (4) and (5). Let u assume for the time being, in order to simplify the respective expressions, that the constant f_V etc. may be considered to be real numbers, and that the following estimation is correct

$$|h_V| \gg \frac{1}{M} |f_V|$$

$$|h_A| \gg \mathrm{Max} \left(\frac{1}{M} |f_A|, \quad \frac{1}{M} |f_V|, \quad |g_V| \right) \qquad (6$$

b) for Gamow-Teller transitions:

$$g_4^2 \to |f_A - h_A E_0|^2$$

$$\frac{1}{M} g_4^2 \to 2\mathrm{Re} \left[(f_A - h_A E_0) \left(\frac{1}{2M} f_A + h_A \right)^* \right]$$

$$\frac{1}{M} g_2 g_4 \to 2\mathrm{Re} \left[(f_A - h_A E_0) \left(\frac{1}{2M} f_V + g_V \right)^* \right]$$

Three other constants g_1, g_3 and g_5 have to be put equal to zero. If the S, T and P interactions will come to b considered once more, the formula presented by Alaga (1958) can be also adapted so as to take into accou the additional terms for tensor interaction given by Weinberg (1958). We have applied here Alaga formulae with some sign corrections. It is the author's duty to thank Dr Tadić for sending him th corrigendum to Alaga's paper.

It follows that a part of terms in (4) and (5) may be omitted and that the spectrum shape is proportional to $pEq^2\left(1+\frac{b}{E}\right)$, wherein

a) for Fermi transitions:

$$b_F = \frac{-2x_F(x_F E_0 \pm 1)}{1+4x_F(\xi \pm E_0)+x_F^2 E_0(3E_0 \pm 4\xi)}$$

$$x_F' = \frac{h_V^s}{f_V}$$

b) for Gamow-Teller transitions:

$$b_{GT}' = \frac{-2x_{GT}(x_{GT}E_0 \mp 1)}{3+4x_{GT}(\xi \mp E_0)+x_{GT}^2 E_0(E_0 \mp 4\xi)}$$

$$x_{GT}' = \frac{h_A}{f_A}$$

The upper (lower) signs are for $\beta^-(\beta^+)$-decay.

The result thus obtained is important, though somewhat strange: There is some indication that, in β-decay, we have an admixture of G-nonconserving interaction of the order of ten percent. For $x_{GT} = -0.25$ [5]) we obtain $b \sim 0.42$, 0.16 and 0.12 resp. for ^{22}Na, ^{32}P and ^{114}In, which is consistent with the experimental values. This explanation of Langer's results is still, however, no satisfactory argument in favour of the existence of G-nonconserving interaction, and we must wait with final conclusions until more experimental data become available. Especially spectrum shapes for pure G-T and Fermi emitters should be carefully investigated in order to obtain further information on possible deviations.

IV. The hypothesis of the intermediary singlet boson in beta decay

In a series of papers by Tanikawa and co-workers (Tanikawa 1957, Tanikawa and Watanabe 1959, Oneda and Tanikawa 1959) a two-stage process is proposed for Fermi interaction, to the effect that the latter is transmitted by some Bose fields with zero spin having only renormalizable interactions with the Fermi particles. The Yukawa model of beta decay was modified so that the Bose field possessed a source consisting of a nucleon and a lepton. Similar modifications have been carried out with respect to other decays. The effective four-fermion interaction in β-decay is of the experimentally well established $(V-A)$ form:

$$H_F = g^2 \overline{\psi}_p \gamma_\mu (1+\gamma_5)\, \psi_n \overline{\psi}_e \gamma_\mu (1+\gamma_5)\, \psi_\nu + \text{H.c.} \tag{7}$$

This interaction results by eliminating the B-field from the basic Hamiltonian:

$$H_S = g[\overline{\psi}_p(1-\gamma_5)\, \psi_e^c B + \overline{\psi}_n(1-\gamma_5)\, \psi_\nu^c B] + \text{H.c.} \tag{8}$$

where B is a complex scalar neutral field with the same chirality as its factor in the Hamiltonian H_S. ψ^c is the charge conjugate spinor $C\overline{\psi}$.

---

[5] The agreement of the theory with the experimental results for the ratio $|h_A|/|f_A| \sim \frac{1}{4}$ may be regarded as a post hoc justification of the estimation of eq. (6).

Some time ago various elegant methods and principles have been proposed for obtaining the desired *U.F.I.* of $(V-A)$ form (Feynman and Gell-Mann 1958, Behrends 1958, Sakurai 1958). None of these, however, could yield the experimental ratio of the axial vector and vector parts of the Universal Fermi Interaction. It was always -1 instead of the experimental value -1.25 for C_A/C_V. One possible objection against the method proposed here for introducing the $(V-A)$ interaction is the same as the one to be raised against other elegant principles from which this interaction can be deduced, viz.: it likewise leads to a C_A/V_V ratio equal to -1 instead of -1.25.

The intermediary boson hypothesis should not be regarded, however, as a mere artificial complication of the present situation. One argument in favour of this hypothesis is that it explains in a straightforward manner the deviations in the beta spectra. In the energy spectrum of the β^- particles, in addition to the usual factor $\mathcal{F}_0 E p q^2$ (in standard β-decay theory notation), we obtain the factor

$$\Phi = (M_B^2 - M^2 + 2ME)^{-2} \tag{9}$$

from the intermediate meson propagator. Here M_B, M and E are the meson mass, nucleon mass and electron energy, respectively. For a suitable value of the meson mass we can obtain a spectrum shape of the desired type. There will be an excess of low energy β-particles of both signs and the deviations in the Fermi-Kurie plot may agree to a high degree of accuracy with the deviations observed experimentally (Johnson 1958, Hamilton 1958). In order to illustrate this thesis we include a table of the values of

$$\Im = \sqrt{\frac{N(E)}{pE\mathcal{F}_0}}\, q^{-1} \tag{10}$$

which, on multiplication by $q = E_0 - E$, should yield the Fermi-Kurie plot. The values are given for a β-transition in which the maximum β-particle energy E_0 is equal to 5 (in $m_e c^2$ units). This value of E_0 is of the order appearing in Langer's experiments (Johnson 1958, Hamilton 1958), where it amounted to e.g. 4.9 for ^{114}In and 1.34 for ^{32}P.

The numerical values in Table III are given with the accuracy to a common multiplicative factor chosen so as to yield unity for the spectrum end.

TABLE III

Values of the quantity $\Im$ for a hypothetical β-decay with $E_0 = 5$

E	$\Im$ from the formula with the empirical correction $\left(1 - \frac{b}{E}\right)$		$\Im$ from the formula with the theoretical correction factor (9) for the boson mass M_B			
	$b=0.2$	$b=0.3$	$1875\, m_e$	$1900\, m_e$	$1925\, m_e$	$1950\, m_e$
1	1.07	1.11	1.11	1.06	1.045	1.035
2	1.03	1.04	1.08	1.045	1.035	1.025
3	1.02	1.02	1.05	1.03	1.02	1.015
4	1.005	1.015	1.025	1.02	1.01	1.01
5	1	1	1	1	1	1

It is reality concluded from Table III that the possible existence of an intermediary boson of mass $\sim 1900\, m_e$ is able to account satisfactorily for the deviations in beta spectra observed.

V. Concluding remarks

In proposing the foregoing alternative explanations for the deviations in beta spectra, the author did not intend to exhaust all the theoretical possibilities, but aimed at confining attention to those only which seemed the simplest in the present stage, when the scarcity of experimental data provides no possibility of distinguishing between them.

The author wishes to express his gratitude to prof. I. A. Smorodinsky for his enlightening discussions of the subject.

REFERENCES

Alaga, G., Šips, L., Tadić, W., *Nuclear Phys.*, **6**, 305 (1958), also a later corrigendum.
Behrends, R. E., *Phys. Rev.*, **109**, 2217 (1958).
Feynman, R. P., Gell-Mann, M., *Phys. Rev.*, **109**, 193 (1958).
Goldhaber, M., *Proceedings of the 1958 Annual Int. Conf. on High Energy Physics at CERN*, Geneve 1958, p. 241.
Hamilton, J. H., Langer, L. M., Smith, W. G., *Phys. Rev.*, **112**, 2010 (1958).
Johnson, O. E., Johnson, R. G., Langer, L. M., *Phys. Rev.*, **112**, 2004 (1958).
Kuchowicz, B., *Inst. Nuclear Research (Warsaw), Report* 94/VII; *Bull. Acad. Polon. Sci., Sér. sci. math. astron. phys.*, **7**, 509 (1959 a).
Kuchowicz, B., *Inst. Nuclear Research (Warsaw), Report* 116/VII (1959 b).
Mikaelan, L. A., Spivak, P. Ie., *Zh. eksper. teor. Fiz.*, **37**, 1168 (1959).
Morita, M., *Phys. Rev.*, **113**, 1584 (1959).
Oneda, S., Tanikawa, Y., *Phys. Rev.*, **113**, 1354 (1959).
Sakurai, J. J., *Nuovo Cimento*, **7**, 649 (1958).
Tanikawa, Y., *Phys. Rev.*, **108**, 1615 (1957).
Tanikawa, Y., Watanabe, S., *Phys. Rev.*, **113**, 1344 (1959).
Weinberg, S., *Phys. Rev.*, **112**, 1375 (1958).

GAMMA-VIBRATIONAL LEVELS IN ^{166}Er

By E. Bożek, H. Niewodniczański, S. Ogaza, S. Szymczyk, T. Walczak, I. A. Yutlandov*

Institute of Nuclear Physics, Polish Academy of Sciences, Cracow

(Received November 10, 1960)

Directional correlation measurements in ^{166}Er for the gamma-gamma cascade 779.8—80.59 keV were performed. The values of spin $I=3$ and the quantum number $K=2$ for the energy level 860.2 keV could be determined. The deformation of the ^{166}Er nucleus in the ground state and in the gamma-vibrational state, as well as the rotational-vibrational interaction of energy levels in this nucleus, are discussed.

1. Introduction

In the course of the last year some measurements were performed [1—6], on the basis of which level schemes for ^{166}Er in the decay of ^{166}Tm were proposed. One group of authors [1, 3, 6] based their proposals on measurements of energies and partly also intensities of conversion electrons, another group [2, 4, 5] — on gamma-gamma coincidence experiments. All these experiments are consistent with the presence in ^{166}Er of a ground state rotational band with excited levels at about 80 keV (0,2+), 265 keV (0,4+) and 545 keV (0,6+). However, in the case of the next group of levels, the agreement of different authors in interpreting them is not so good. Boskma and De Waard [2] proposed a gamma-vibrational level (2,2+) at 862 keV with a first rotational state (2,3+) at 957 keV. The other authors [1, 3, 4, 5, 6] suggest the gamma-vibrational level at 788 keV and two rotational states at 862 keV (2,3+) and 957 keV (2,4+). It is very important to know whether there exists in ^{166}Er a gamma-vibrational level and if so, to know the exact positions of the levels. These informations would allow us to say something about the deformation of the nucleus in the excited states as well as about the rotational-vibrational interaction. The experimental branching ratios of transitions from the levels in question to those belonging to the ground state band fit better the proposal of a γ-vibrational band with the band head at 788 keV and two rotational states above it [4]. The accuracy of the measurements is however too low to confirm unambiguously this interpretation. The accuracy of the determination of the conversion coefficients is also too low to give the exact multipole order of transitions to the ground state band.

---

* Joint Institute for Nuclear Research, Dubna, SSSR.

One can only say that the experimental results do not exclude the possibility of this transitions to be of the $E2$ type.

The investigations reported in this paper were undertaken in order to obtain the spin and K values of at least one of the levels 788, 862 or 957 keV by means of the gamma-gamma directional correlation measurements.

2. Experimental

For the angular correlation measurements in ^{166}Er ytterbium sources were used which were obtained by irradiation of Ta targets with 660 MeV protons in the synchrocyclotron of the Joint Institute for Nuclear Research in Dubna (USSR). The chromatographically seperated Yb fraction was then purified twice in the chromatographic column. The ytterbium lactate was evaporated on an aluminium foil. The diameter of the source was less than 1.5 mm. The measurements in Cracow started two days after the irradiation.

Two scintillation counters with *RCA* 6810 *A* photomultipliers and NaJ(Tl) crystals $1\frac{1}{2}'' \times 1''$ were used. The resolution time of the fast-slow coincidence circuit $2\tau = 3.75 \times 10^{-8}$ sec.

The correction factors for the finite angular resolution of both counters were determined experimentally, before the correlation measurements started, applying the method of Lawson and Frauenfelder [7]. For this purpose gamma rays of the ^{60}Ni cascade were used. The width of the collimated gamma ray beam was measured with a NaJ(Tl) crystal 2 mm × 2 mm × 7 mm. The whole width of the beam at a 410 mm distance from the end of the collimator was 7.2 mm. The angular effieiencies $\varepsilon^{\mathrm{I}}(\alpha)$ and $\varepsilon^{\mathrm{II}}(\alpha)$ for both scintilation counters were measured at a distance of 76 mm between the source and the frontal surfaces of the crystals, the two photopeaks of ^{60}Ni being selected with a single channel analyzer. The integrals $I_{2\nu} = \int P_{2\nu}(\cos\alpha)\varepsilon(\alpha)\sin\alpha\, d\alpha$ were evaluated numerically. So obtained values of $I_2/I_0 = 0.970$ and of $I_4/I_0 = 0.900$ differ from the theoretical ones, for the same distance and the γ-ray energy 1250 keV [8] only by 0.3% and 1.7% respectively. These deviations are smaller than the experimental errors, thus for the solid angle correction in the correlation experiments in ^{166}Er we used the theoretical coefficients given by Stanford and Rivers [8].

The gamma ray spectrum in the decay ^{166}Yb (58h) $\rightarrow$ ^{166}Tm (7.7h) $\rightarrow$ ^{166}Er is very complicated and the half-time is rather not very long. Therefore, we were forced to chose such a γ-γ cascade for the spin determination of levels in question for which a good selection of the transitions is possible and also the differences in the anisotropy values for different spins of the initial state are as large as possible. The table I gives the anisotropy values for γ-γ cascades in which the first γ-ray corresponds to the transitions starting from the 786.7, 860.2 or 957.0 keV levels, and the second γ-ray corresponds to transitions between the levels of the ground state rotational band in ^{166}Er nucleus (fig. 1). Assuming, that the upper level band is connected with γ-vibrations ($K = 2^+$) and that the selection rules for the quantum number K are exactly fulfilled, we can accept that both transitions in the cascades are of the $E2$ type. In table I only the values of spins proposed by Boskma and De Waard [2], as well as the others [1, 3, 4, 5] are taken into account. One can see from this table, that the cascades best suited for the determination of the spins of the initial levels

by correlation measurements are the following ones: 876.3—80.59 keV, 594.9—184.5 keV and 779.8—80.59 keV. Unfortunately, a sufficiently good selection of the 876.3 and 594.9 keV transitions is by scintillation methods impossible, thus only the cascade 779.8—80.59 keV is suitable for measurements.

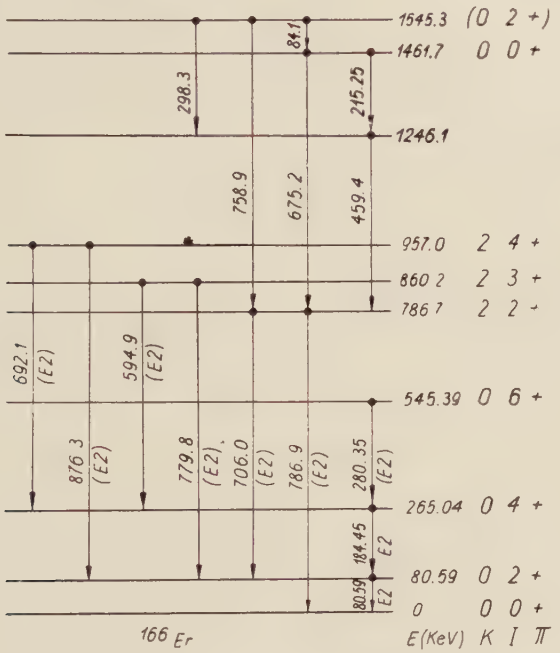

Fig. 1

The correlation measurements for the 779.8—80.59 keV cascade were performed at a distance of 73 mm between the source and the frontal faces of the crystals. Care was taken when discriminating the γ-rays corresponding to the transition 779.8 keV to select this as good as possible from γ-rays corresponding to transitions 758.9 keV (tripple cascade 758.9—876.3—80.59 keV) and 876.3 keV (cascade 876.3—80.59 keV) (fig. 1). A thick

TABLE I

Theoretical values of anisotropy A for cascades $I_i(E2)I(E2)I_i$.

Energy of transitions in cascade (keV)	692.1—184.5		876.3—80.59		594.9—184.5		779.8—80.59		706.0—80.59	
Spin sequence $I_i—I—I_f$	4—4—2	3—4—2	4—2—0	3—2—0	3—4—2	2—4—2	3—2—0	2—2—0	2—2—0	—
Anisotropy A(%)	−7.43	−9.30	+16.6	−33.3	−9.30	+38.3	−33.3	+7.69	+7.69	—

absorber Pb-Cu-Cd protected the crystal in order to cut off the low energetic γ-rays. On the crystal of the second counter, selecting the 80.59 keV transition, another Pb-Cu-Cd absorber was placed, the thickness of which was selected experimentally to give a strong reduction of the X-ray peak and only a small weakening of the 80 keV photopeak. A narrow channel width of the channel analyzer was set on the top of the 80 keV photopeak. The source was centered until the single counting rates in both detectors for different positions of the moveable counter were constant to less than 0.5%. Every 10 minutes the position of one counter was changed from 90° to 180° and back, and coincidences as well as single counting rates in both channels were recorded.

The following anisotropy of the gamma-gamma cascade 779.8—80.59 keV was obtained:

$$A = -(20.9 \pm 2.8)\%$$

The exact correction of this result for the coincidences of overlapping cascades is impossible because of the complicated γ-spectrum in the ^{166}Yb decay. Nevertheless, the approximate calculations based on coincidence and single counting rates, setting the channels of the analyzers on the peaks and near by the peaks, show that the result being obtained may be considered to be lowered by less than 1%.

3. Discussion

After the correction for the finite angular resolution in our experiments, the theoretical anisotropies for the cascade $I_i \xrightarrow{779.8\ \text{keV}} 2+ \xrightarrow{80.59\ \text{keV}} 0+$ in ^{166}Er are $A = -29.80\%$ for $I_i = 3$ and $A = +4.13\%$ for $I_i = 2$. Our result points rather the $3-2-0$ sequence, although the experimental value is too low. However, the intermediate state 80.59 keV has a measured half-life $T_{\frac{1}{2}} = 1.7 \times 10^{-9}$ sec [9], and the ^{166}Er nucleus is strongly deformed. The quadrupole interaction in the intermediate state will thus have a strong smearing out effect on the correlation pattern. This effect accounts partly for the deviations between the theoretical and experimental anisotropies.

Marklund et al. [10] have measured γ-γ directional correlations in ^{166}Er from the ^{166}Ho (27h) decay, with the same intermediate state 80.59 keV. They used aqueous solutions of holmium trichloride as sources. These authors give the values for the attenuation factors $G_2 = 0.63 \pm 0.03$ and $G_4 = 0.69 \pm 0.03$. Assuming the same attenuation in our case the anisotropy in the cascade 779.8—80.59 keV for $I_i = 3$ is expected to be $A = -19.49\%$. This value is in agreement with our result within the experimental errors.

Up to now we have assumed that the 779.8 keV transition is a pure $E2$ radiation. Let us now discuss the possible admixture of $M1$ in this transition. Without taking into account the attenuation of the correlation caused by the finite angular resolution and by the quadrupole interaction in the intermediate state, we obtain for the anisotropy the value $A = -23.31\%$ for the initial spin $I_i = 2$ and a 20% admixture of $M1$ radiation and $\delta < 0$ in the 779.8 keV transition. If the 860.2 keV level is connected with γ-vibrations ($K = 2^+$), this high admixture of $M1$ radiation is rather improbable. If the spin of the 860.2 keV level $I_i = 3$, then a 1% admixture of $M1$ gives $A = -41.19\%$ for $\delta > 0$ and $A = -22.38\%$ for $\delta < 0$. In the first case the attenuation has to be very strong, in the second case — neglectable to fit the experi-

nental result. Larger admixtures of $M1$ are giving larger deviations from the theoretical alue $A=-33.35\%$ for pure $E2$ transitions. Thus we can accept that the 779.8 keV transiion is a pure $E2$ one. A possible admixture of $M1$ radiation is less than 1%.

The anisotropy measurements of the cascade $I_i \xrightarrow{779.8\ \text{keV}} 2+ \xrightarrow{80.59\ \text{keV}} 0+$ point that the 360.2 keV level has a spin $I_i=3$ and $K=2$. That means, it is the first excited level of the otational band connected with the γ-vibrational level 786.7 keV (2,2+).

Fig. 1 represents the incomplete level scheme of ^{166}Er. The new energy values of levels were calculated on the basis of mean values of transition energies given by Jacob et al. [3] nd Grigoriev et al. [6]. This level scheme contains three excited rotational levels in the round state band and three members of the gamma-vibrational band.

In the ^{166}Ho (27h) decay a beta-vibrational level (0,0+) in ^{166}Er at 1460.2 keV was eported [10]. The level at 1461.7 keV excited in the decay of ^{166}Tm [3, 5, 6], may be identical vith the level (0,0+). It is also possible that the level 1545.3keV [4, 5, 6] is another rotational tate (0,2+) connected with β-vibrations.

On the basis of the proposed level scheme, and using the rotational energy formula

$$E_I = E_0 + A[I(I+1) - K(K+1)] - B[I(I+1) - K(K+1)]^2 \qquad (1)$$

where E_0 is the energy of the band head, $A=\hbar^2/2J$ with J — moment of inertia of the nucleus, 3 — the rotational-vibrational interaction coefficient, we are able to calculate the constants 1 and B for the ground state band and the beta and gamma vibrational bands.

The hydrodynamical approximation gives the rotational-vibrational coefficient for he ground state band:

$$B_{\text{th}} = \left(\frac{\hbar^2}{2J}\right)^3 \left(\frac{12}{(\hbar\omega_\beta)^2} + \frac{4}{(\hbar\omega_\gamma)^2}\right) \qquad (2)$$

where $\hbar\omega_\beta$ and $\hbar\omega_\gamma$ are the excitation energies of beta and gamma vibrations respectively.

The calculated values of A and B for the ground state band and for beta and gamma ibrational bands, as well as the factor $b=B_{\text{th}}/B_{\text{exp}}$ for the ground state band are shown n table II. From this table it is seen that $A=\hbar^2/2J$ is somewhat larger for the ground state

TABLE II

Moments of inertia and rotational-vibrational interactions in ^{166}Er nucleus.

$A=\frac{\hbar^2}{2J}$ (keV)			B_{exp} (eV)		$b=\frac{B_{\text{theory}}}{B_{\text{exp}}}$
ground state band	γ	β	ground state band	γ	ground state band
13.50	12.29	1.90*	12.4	9.5	2.39 0.14

* Calculated with $B=0$

and than for the γ-vibrational band. If the simple formula $J=3B_1\beta^2$, connecting the moent of inertia J with the deformation β, is approximately valid, then one can say that the ^{66}Er nucleus is still more deformed in the excited state than in the ground one.

The ratio $b = B_{th}/B_{exp}$ for the ground state band in ^{166}Er is somewhat larger than th value $b = 2.12$ proposed by Sheline [11] to be a constant for all nuclei.

The authors are indebted to Mr. Chojnacki and Mr. Yu. Norseev for the work don with the preparation of sources. Thanks are also due to Miss Z. Konieczna, Miss M. Mięsowic and Mr. G. Zapalski for their valuable assistance in the course of measurements.

REFERENCES

[1] Gromov, K. Ya., Dzhelepov, B. S., Pokrovskiĭ, W. N., *Izv. Akad. Nauk SSSR*, **23**, 821 (1959).
[2] Boskma, P., De Waard, H., *Nuclear Phys.*, **12**, 533 (1959).
[3] Jacob, K. P., Mihelich, J. W., Harmatz, B., Handley, T. H., *Phys. Rev.*, **117**, 1102 (1960).
[4] Bożek, E., Niewodniczanski, H., Ogaza, S., Szymczyk, S., Norseev, Yu. V., *Acta phys Polon.*, **20**, 257 (1961)
[5] Wilson, R. G., Pool, M. L., *Phys. Rev.*, **119**, 262 (1960).
[6] Grigoriev, E. P., Gromov, K. Ya., Dzhelepov, B. S., to be published.
[7] Lawson, J. S., Frauenfelder, H., *Phys. Rev.*, **91**, 649 (1953).
[8] Stanford, A. L., Rivers, W. K., *Rev. sci. Instrum.*, **30**, 719 (1959).
[9] Strominger, Hollander, Seaborg, *Rev. mod. Phys.*, **30**, 585 (1958).
[10] Marklund, I., Van Nooijen, B., Grabowski, Z., *Nuclear Phys.*, **15**, 533 (1960).
[11] Sheline, R. K., *Rev. mod. Phys.* **32**, 1 (1960).

PHASENSPRUNG IM BRENNPUNKT

Von A. Rubinowicz

Polnische Akademie der Wissenschaften

(Eingegangen am 28. November 1960)

Im Jahre 1938 hat der Verfasser auf Grund der Kirchhoffschen Theorie der Beugung und unter teilweiser Benutzung geometrischer Methoden bewiesen, dass der Phasensprung im Brennpunkt eine geometrisch-optische Erscheinung ist. Er tritt nämlich bereits in der nach den Gesetzen der geometrischen Optik konstruierten einfallenden Lichtwelle auf. Es wird nun für diese Tatsache ein mit Hilfe rein analytischer Methoden durchgeführter Beweis angegeben und es werden weitere Plausibilitätsbetrachtungen über die Entstehung des Phasensprunges im Brennpunkte mitgeteilt.

In einer vor längerer Zeit veröffentlichten Abhandlung hat der Verfasser (Rubinowicz 1938) gezeigt, daß der Phasensprung im Brennpunkt ein geometrisch-optisches Phänomen ist. Er ist nämlich bereits in der nach den Gesetzen der geometrischen Optik zu definierenden einfallenden Lichtwelle vorhanden. Der Beweis dieser Behauptung wurde unter Zugrundelegung der Kirchhoffschen Beugungstheorie durchgeführt. In Übereinstimmung mit den Youngschen Anschauungen über die Entstehung der Beugungserscheinungen wurde nämlich die durch das entsprechende Kirchhoffsche Integral gegebene Wellenbewegung in eine im Sinne der geometrischen Optik definierte einfallende Lichtwelle und eine von dem beugenden Rande ausgehende Beugungswelle aufgespalten. Dies wurde in Anlehnung an eine früher vom Verfasser (Rubinowicz 1917) vorgenommene Zerlegung der Wellenbewegung durchgeführt, die im Falle einer divergierenden Kugelwelle durch das Kirchhoffsche Integral dargestellt wird. Dieses Verfahren erfordert aber kompliziertere geometrische Betrachtungen[1], die nicht jedermanns Sache sind, so daß es gerechtfertigt erscheinen mag, einen mit Hilfe der im allgemeinen gebräuchlicheren analytischen Methoden durchgeführten Beweis der damaligen Ergebnisse mitzuteilen. Wir tun dies nun nach dem Muster eines später vom Verfasser (Rubinowicz 1953) für eine divergierende Kugelwelle angegebenen analytischen Verfahrens zur Zerlegung der durch das Kirchhoffsche Integral gegebenen Wellenbewegung in eine einfallende und eine Beugungswelle. Im Anschluß

[1] Die geometrischen Betrachtungen, die in meiner Arbeit über die Beugung einer divergierenden Kugelwelle (Rubinowicz 1917) sowie in der Arbeit über den Phasensprung (Rubinowicz 1938) enthalten sind, können mit Hilfe der Vektorrechnung etwas einfacher dargestellt werden. Vgl. die in Vorbereitung befindliche englische Ausgabe der „Beugungswelle" (Rubinowicz 1957).

an diese im Sinne der Youngschen Vorstellungen vorgenommene Aufspaltung der Wellenbewegung sollen auch neue Plausibilitätsbetrachtungen über die Entstehung des Phasensprunges im Brennpunkte angegeben werden.

§ 1. Das Vektorfeld des Kirchhoffschen Ansatzes und sein Vektorpotential

Sei f eine Fläche, die eine durch den beugenden Rand B begrenzte beugende Öffnung in einem Schirme S verschließt (vgl. Abb. 1). Durch f hindurch möge eine konvergierende Lichtwelle mit dem Brennpunkt F einfallen. Die auf diese Weise entstehende Wellenbewegung wird in der Kirchhoffschen Beugungstheorie (vgl. etwa Rubinowicz 1957) auf der Seite des beugenden Schirmes, auf der sich der Brennpunkt F befindet, durch das Integral

$$u(P) = \frac{1}{4\pi} \int_f \left\{ \frac{e^{ikr}}{r} \frac{\partial}{\partial n} \left(\frac{e^{-ik\varrho}}{\varrho} \right) - \frac{e^{-ik\varrho}}{\varrho} \frac{\partial}{\partial n} \left(\frac{e^{ikr}}{r} \right) \right\} df \tag{1.1}$$

beschrieben. Dabei wird hier der Zeitfaktor $\exp(-i\omega t)$ vorausgesetzt. $\vec{\varrho} - \overrightarrow{FQ}$ bzw. $\boldsymbol{r} - \overrightarrow{PQ}$ bedeutet die Entfernung eines Punktes Q auf der die Beugungsöffnung verschließenden Fläche f vom Brennpunkte F bzw. vom Beobachtungspunkte P.

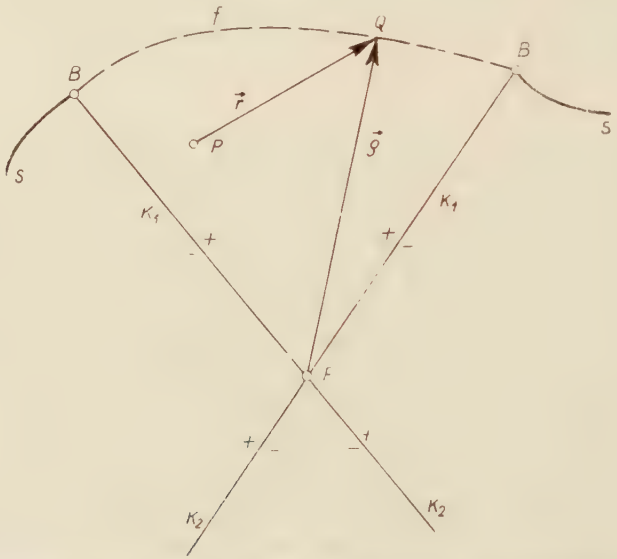

Abb. 1. Zweidimensionale schematische Darstellung der Beugung einer konvergierenden Kugelwelle. S ist der Schirm, B der beugende Rand, f eine die Beugungsöffnung verschliessende Fläche, F der Brennpunkt, P ein Beobachtungspunkt, Q ein Punkt auf der Fläche f; K_1 bzw. K_2 sind die Schattengrenzen des vorderen bzw. rückwärtigen Lichtkegels. Durch + bzw. − wird die positive bzw. negative Seite der Schattengrenze bezeichnet.

Um die Wellenbewegung (1.1) im Sinne der Youngschen Beugungstheorie umzuformen, bemerken wir, daß der Integrand in (1.1) durch die Normalkomponente des Vektorfeldes

$$\boldsymbol{V}(Q) = \frac{1}{4\pi} \left\{ \frac{e^{ikr}}{r} \operatorname{grad} \frac{e^{-ik\varrho}}{\varrho} - \frac{e^{-ik\varrho}}{\varrho} \operatorname{grad} \frac{e^{ikr}}{r} \right\} \tag{1.2}$$

auf der Fläche f gegeben wird, wenn wir es als Funktion des Punktes Q auffassen, der nun und in den zunächst folgenden Überlegungen irgend einen Raumpunkt bedeuten soll. Da e^{ikr}/r und $e^{-ik\varrho}/\varrho$ als Funktionen von Q aufgefaßt Lösungen der Schwingungsgleichung $\Delta u + k^2 u = 0$ sind, so ist $\operatorname{div} \boldsymbol{V} = 0$. Es muß sich daher das Vektorfeld $\boldsymbol{V}$ durch ein Vektorpotential $\boldsymbol{W}$ darstellen lassen, so daß

$$\boldsymbol{V} = \operatorname{rot} \boldsymbol{W}. \tag{1.3}$$

ist. Gelingt es nun das Vektorpotential $\boldsymbol{W}$ anzugeben, so ist die Wellenbewegung $u(P)$ (1.1) in der Gestalt

$$u(P) = \int_f \operatorname{rot}_n \boldsymbol{W} df$$

darstellbar. Die Umformung des Flächenintegrals (1.1) für $u(P)$ in ein die Beugungswelle darstellendes Randintegral über den beugenden Rand B wird dann unmittelbar durch den Stokesschen Integralsatz gegeben.

Um nun das Vektorpotential $\boldsymbol{W}$ zu berechnen, bemerken wir, daß mit Rücksicht auf $\operatorname{grad} \varrho = \vec{\varrho}/\varrho$ und $\operatorname{grad} r = \boldsymbol{r}/r$ das Vektorfeld $\boldsymbol{V}$ (1.2) nun die Gestalt

$$\boldsymbol{V} = -\frac{e^{ik(r-\varrho)}}{4\pi r\varrho}\left\{\left(\frac{ik}{\varrho} + \frac{1}{\varrho^2}\right)\vec{\varrho} + \left(\frac{ik}{r} - \frac{1}{r^2}\right)\boldsymbol{r}\right\} \tag{1.4}$$

erhält.

Da die Vektoren $\vec{\varrho}$ und $\boldsymbol{r}$ ihren Beginn in den Punkten F und P haben, so müssen die Vektoren $\boldsymbol{V}$ des Vektorfeldes (1.4) stets in einer durch diese beiden Punkte gehenden Ebene E liegen. Das Vektorpotential $\boldsymbol{W}$ darf demnach keine in der Ebene E liegenden Komponenten besitzen. Würde dies nämlich der Fall sein, so müßte das aus (1.3) berechnete Vektorfeld $\boldsymbol{V}$ nach der Definition der Rotation auch in den zu den Ebenen E senkrechten Richtungen nicht verschwindende Komponenten aufweisen. Wir dürfen daher für das Vektorpotential $\boldsymbol{W}$ den Ansatz

$$\boldsymbol{W}(Q) = \boldsymbol{r} \times \vec{\varrho}\, g(Q) \tag{1.5}$$

machen, wo $g(Q)$ eine skalare Funktion des Punktes Q ist.

Mit Rücksicht auf die Beziehung $\operatorname{rot}(\boldsymbol{r} \times \vec{\varrho}) = 2(\boldsymbol{r} - \vec{\varrho})$ folgt dann aus (1.3)

$$\boldsymbol{V} = g \operatorname{rot}(\boldsymbol{r} \times \vec{\varrho}) + (\operatorname{grad} g) \times (\boldsymbol{r} \times \vec{\varrho}) = 2(\boldsymbol{r} - \vec{\varrho})\, g + \boldsymbol{r}(\vec{\varrho} \operatorname{grad} g) - \vec{\varrho}(\boldsymbol{r} \operatorname{grad} g). \tag{1.6}$$

Beachten wir, daß

$$2g + \boldsymbol{r} \operatorname{grad} g = \frac{1}{r^2}\boldsymbol{r} \operatorname{grad}(r^2 g)$$

ist, und eine analoge Beziehung mit $\vec{\varrho}$ und ϱ statt $\boldsymbol{r}$ und r besteht, so können wir (1.6) auch in der Gestalt

$$\boldsymbol{V} = \boldsymbol{r}\frac{1}{\varrho^2}(\varrho \operatorname{grad}(\varrho^2 g)) - \vec{\varrho}\frac{1}{r^2}(\boldsymbol{r} \operatorname{grad}(r^2 g))$$

darstellen. Setzen wir diesen Ausdruck für $\boldsymbol{V}$ gleich dem Ausdrucke (1.4) und multiplizieren wir die erhaltene Beziehung vektoriell einmal mit $\boldsymbol{r}$ und das andere Mal mit $\vec{\varrho}$, so ergeben

sich schließlich für die Funktion g die beiden Differentialgleichungen

$$\frac{e^{ik(r-\varrho)}}{4\pi}\,\frac{r}{\varrho}\left(\frac{ik}{\varrho}+\frac{1}{\varrho^2}\right)=\boldsymbol{r}\ \mathrm{grad}\,(r^2 g). \tag{1.7a}$$

$$-\frac{e^{ik(r-\varrho)}}{4\pi}\,\frac{\varrho}{r}\left(\frac{ik}{r}-\frac{1}{r^2}\right)=\vec{\varrho}\ \mathrm{grad}\,(\varrho^2 g). \tag{1.7b}$$

Um zunächst eine Lösung der ersten Differentialgleichung d. h. (1.7a) zu finden spalten wir von der in (1.7a) auftretenden Funktion $r^2 g$ den Exponentialfaktor $\exp ik(r-\varrho)$ ab, setzen also

$$r^2 g = e^{ik(r-\varrho)} f. \tag{1.8}$$

Diese Maßnahme wird durch die Tatsache nahegelegt, daß ein Exponentialfaktor bei allen Differentiationen erhalten bleibt und daher (1.7a) durch den Ansatz (1.8) von dem Exponentialfaktor $\exp ik(r-\varrho)$ befreit wird.

Mit Rücksicht auf

$$\boldsymbol{r}\ \mathrm{grad}\,(r-\varrho)=\frac{1}{\varrho}\,[r\varrho-\boldsymbol{r}\vec{\varrho}]$$

sowie den Ansatz (1.8) erhalten wir für die rechte Seite der Differentialgleichung (1.7a) den Ausdruck

$$\boldsymbol{r}\ \mathrm{grad}\ r^2 g = e^{ik(r-\varrho)}\,\frac{ik}{\varrho}\,[r\varrho-\boldsymbol{r}\vec{\varrho}]\,f + e^{ik(r-\varrho)}\,\boldsymbol{r}\ \mathrm{grad}\,f. \tag{1.9}$$

Setzt man (1.9) in (1.7a) ein, so tritt auf beiden Seiten der so erhaltenen Beziehung

$$\frac{1}{4\pi}\,\frac{r}{\varrho}\left(\frac{ik}{\varrho}+\frac{1}{\varrho^2}\right)=\frac{ik}{\varrho}\,[r\varrho-\boldsymbol{r}\varrho]\,f+\boldsymbol{r}\ \mathrm{grad}\,f \tag{1.10}$$

die Konstante k nur einmal und zwar nur in der ersten Potenz auf. Nimmt man nun an, daß in der Funktion f die Konstante k nicht mehr enthalten ist, so erhält man die beiden Beziehungen

$$f=\frac{1}{4\pi}\,\frac{r}{\varrho}\,\frac{1}{r\varrho-\boldsymbol{r}\vec{\varrho}}, \tag{1.11a}$$

$$\boldsymbol{r}\ \mathrm{grad}\,f=\frac{1}{4\pi}\,\frac{r}{\varrho^3}. \tag{1.11b}$$

Unter den gemachten Voraussetzungen wird somit die Funktion f durch den Ausdruck (1.11a) gegeben, muß jedoch auch noch die Beziehung (1.11b) erfüllen. Dies ist in der Tat der Fall, wie man mit Hilfe der aus $\mathrm{grad}\,r\varrho=\boldsymbol{r}+\vec{\varrho}$ folgenden Relation

$$\boldsymbol{r}\ \mathrm{grad}\,\frac{\varrho}{r}\,[r\varrho-\boldsymbol{r}\vec{\varrho}]=-\frac{1}{r\varrho}\,[r\varrho-\boldsymbol{r}\vec{\varrho}]^2$$

bestätigt.

Aus (1.8) und (1.11a) ergibt sich schließlich, daß die Funktion

$$g = \frac{1}{4\pi} \frac{e^{ik(r-\varrho)}}{r\varrho} \frac{1}{r\varrho - \boldsymbol{r}\vec{\varrho}} \tag{1.12}$$

eine Lösung der Differentialgleichung (1.7a) ist.

Dieser Ausdruck für g muß auch noch die Differentialgleichung (1.7b) befriedigen. Dies ist in der Tat der Fall, weil ja (1.7a) bei Vertauschung von $\boldsymbol{r}$, r und $\vec{\varrho}$, ϱ sowie Vorzeichenänderung von $\imath$ in (1.7b) übergeht, während sich dabei die durch (1.12) gegebene Funktion g nicht ändert.

Zu den obigen Ausführungen sei noch bemerkt, daß man den gleichen Ausdruck (1.11a) für die Funktion f erhält, wenn man voraussetzt, daß f zwar von k abhängt, jedoch in eine nach fallenden Potenzen von k fortschreitende Potenzreihe entwickelbar ist. Setzt man nämlich[2]

$$f = \sum_{n=0}^{\infty} f_n k^{-n} \tag{1.13}$$

in (1.10) ein, so erhält man für die Funktionen f_n die Beziehungen

$$[r\varrho - \boldsymbol{r}\vec{\varrho}]\, f_0 = \frac{1}{4\pi} \frac{r}{\varrho}, \tag{1.14a}$$

$$\frac{i}{\varrho}\,[r\varrho - \boldsymbol{r}\vec{\varrho}]\, f_1 = \frac{1}{4\pi} \frac{r}{\varrho^3} - \boldsymbol{r}\,\mathrm{grad}\, f_0, \tag{1.14b}$$

$$\frac{i}{\varrho}\,[r\varrho - \boldsymbol{r}\vec{\varrho}]\, f_{n+1} = -\,\boldsymbol{r}\,\mathrm{grad}\, f_n \quad (n \geqq 1). \tag{1.14c}$$

Aus (1.14a) folgt, daß f_0 die durch (1.11a) gegebene Gestalt hat. Da infolgedessen f_0 die Relation (1.11b) erfüllt, so ergibt sich aus (1.14b) daß $f_1 = 0$ ist. Setzt man $f_1 = 0$ in die Rekursionsformel (1.14c) für $n = 1$ ein, so folgt daß auch $f_2 = 0$ ist. Benützt man die gleiche Relation (1.14c) der Reihe nach für $n = 2, 3, 4, \ldots$ so kann man schließen, daß auch alle übrigen f_n verschwinden und daher die Funktion f (1.13) durch (1.11a) gegeben wird.

§ 2. Die Beugungswelle

Aus (1.3) und (1.5) folgt, daß die durch den Kirchhoffschen Ansatz (1.1) gegebene Wellenbewegung auch in der Gestalt

$$u(P) = \int_f \mathrm{rot}_n\, (\boldsymbol{r} \times \vec{\varrho} g)\, df \tag{2.1}$$

darstellbar ist, wobei g durch (1.12) gegeben wird.

---

[2] Der gleiche Ansatz (1.13) kann auch im Falle der Beugung einer divergierenden Kugelwelle (Rubinowicz 1953, 1957) zur Auflösung der dort auftretenden zu (1.11a) und (1.11b) analogen Gleichungen verwendet werden.

Bei der Anwendung des Stokesschen Satzes auf (2.1) sind nun die beiden Fälle zu unterscheiden:

(a) In keinem Punkte der die beugende Öffnung verschließenden Fläche f wird das durch (1.5) und (1.12) definierte Vektorpotential $\boldsymbol{W}$ unendlich.

(b) Es ist ein solcher singulärer Punkt Q_0 auf der Fläche f vorhanden.

Um festzustellen in welchen Fällen solche singuläre Punkte Q_0 auftreten, bemerken wir: Damit $\boldsymbol{W}$ unendlich wird muß der Nenner $r\varrho - \boldsymbol{r}\vec{\varrho}$ in g (1.12) verschwinden, d.h. es muß $r\varrho - \boldsymbol{r}\vec{\varrho}$ sein. Das kann nur eintreten, wenn die beiden Vektoren $\boldsymbol{r}$ und $\vec{\varrho}$ die gleiche Richtung und den gleichen Sinn haben. Es verschwindet jedoch dann auch der Vektor $\boldsymbol{r} \times \vec{\varrho}$. Um das Verhalten von $\boldsymbol{W}$ in einem solchen Falle zu untersuchen bezeichnen wir mit β den Winkel zwischen den beiden Vektoren $\boldsymbol{r}$ und $\vec{\varrho}$, so daß

$$\frac{|\boldsymbol{r} \times \vec{\varrho}|}{r\varrho - \boldsymbol{r}\vec{\varrho}} = \frac{\sin\beta}{1-\cos\beta} = \operatorname{ctg}\frac{\beta}{2} \tag{2.2}$$

wird. Falls jedoch die beiden Vektoren $\boldsymbol{r}$ und $\vec{\varrho}$ die gleiche Richtung und den gleichen Sinn haben, so wird $\beta = 0$ und daher der Ausdruck (2.2) unendlich.

Der Fall paralleler Vektoren $\boldsymbol{r}$ und $\vec{\varrho}$ kann nur eintreten (vgl. Abb. 1), wenn der Beobachtungspunkt P eine solche Lage hat, daß die durch ihn und durch den Brennpunkt F hindurchgehende Gerade die Fläche f in einem Punkte trifft, der wie oben mit Q_0 bezeichnet werden möge. Beobachtungspunkte P, denen solche singuläre Punkte Q_0 auf der Fläche f entsprechen, befinden sich somit auf Geraden, die durch den Brennpunkt F hindurchgehen und die Fläche f schneiden. Die Gesamtheit aller dieser Geraden liegt jedoch innerhalb des Doppelkegels, dessen Scheitel mit dem Brennpunkt F zusammenfällt, und dessen Mantel aus allen durch F und den beugenden Rand B hindurchgehenden Geraden besteht. Diesen Doppelkegel, in dem alle Beobachtungspunkte liegen, denen singuläre Punkte Q_0 auf der die Beugungsöffnung verschließenden Fläche f entsprechen, wollen wir als den Lichtkegel bezeichnen. Seine Mantelfläche soll die Schattengrenze heißen. Wie sich nämlich in § 3 herausstellen wird, tritt in dem Lichtkegel auch eine Wellenbewegung auf, die wir als die einfallende Lichtwelle bezeichnen können. Der Halbkegel, dessen Basis durch die Fläche f gegeben wird, soll im folgenden der vordere Lichtkegel, der andere Halbkegel der rückwärtige Lichtkegel heißen.

Wir beschäftigen uns zunächst mit dem Falle (a), wo der Beobachtungspunkt P außerhalb des Lichtkegels liegt. Da dann der Integrand in (2.1) keinen singulären Punkt Q_0 auf der Fläche f besitzt, liefert die Anwendung des Stokesschen Satzes auf (2.1) nur ein Integral über den beugenden Rand B des Schirmes S, welches mit Rücksicht auf (1.12) gegeben wird durch

$$u_B = \frac{1}{4\pi}\int_B \frac{e^{-ik\varrho}}{\varrho}\,\frac{e^{ikr}}{r}\,\frac{(\boldsymbol{r}\times\vec{\varrho})\,\boldsymbol{ds}}{r\varrho - \boldsymbol{r}\vec{\varrho}}\,. \tag{2.3}$$

Dieser Ausdruck stellt eine von dem beugenden Rande B ausgehende Wellenbewegung dar und ist daher im Sinne der Youngschen Vorstellungen über die Entstehung der Beugungserscheinungen als die Beugungswelle anzusprechen. Aus der oben gemachten Voraussetzung (a) folgt, daß der Beobachtungspunkt P außerhalb des Lichtkegels liegt, also in einem

Raumgebiet, das als der Schattenraum bezeichnet werden kann. Bei der Annäherung des Beobachtungspunktes P an einen Punkt P_0 der Schattengrenze wird der Integrand in der Beugungswelle u_B (2.3) unendlich. Und zwar findet dieses Unendlichwerden für jenes Randelement $\boldsymbol{ds}_0$ statt, das auf der Verbindungsgeraden des Brennpunktes F mit dem Punkte P_0 liegt. Für den $\boldsymbol{ds}_0$ auf dem beugenden Rande entsprechenden Punkt werden nämlich die beiden Vektoren $\boldsymbol{r}$ und $\vec{\varrho}$ einander parallel. Dies hat aber mit Rücksicht auf (2.2) ein Unendlichwerden des Integranden in (2.3) zur Folge. Diese Tatsache bewirkt daß die Beugungswelle u_B (2.3) in der Schattengrenze nicht stetig ist, nämlich hier einen Sprung besitzt, der, wie im nachfolgenden Paragraphen klar werden wird, notwendig ist um den entgegengesetzt gleichen Sprung der einfallenden Welle zu kompensieren.

Bezüglich der weiteren Diskussion des Ausdruckes (2.3) für die Beugungswelle u_B verweisen wir auf die früheren diesbezüglichen Publikationen des Verfassers (Rubinowicz 1938, 1957). Hier findet der Leser auch die entsprechenden Näherungsformeln für die Beugungswelle (2.3).

§ 3. Einfallende Lichtwelle

Liegt der Beobachtungspunkt P innerhalb des vorderen oder rückwärtigen Lichtkegels, so schneidet die durch P und den Brennpunkt F hindurchgehende Gerade die Fläche f, so daß hier ein singulärer Punkt Q_0 des Vektorpotentials $\boldsymbol{W}$ auftritt. Wir haben es dann mit dem Falle (b) des § 2 zu tun. Bei der Anwendung des Stokesschen Satzes auf (2.1) müssen wir daher das Kurvenintegral nicht nur über den beugenden Rand B sondern auch über eine den singulären Punkt Q_0 auf der Fläche f umgebende Kurve K erstrecken. Während jedoch der Umlaufssinn des Kurvenintegrals über den beugenden Rand B mit der Normalenrichtung auf der Fläche f durch die Rechtsschraubenregel gekoppelt ist, wird der Zusammenhang zwischen dem Umlaufssinn auf der Kurve K und der Normalenrichtung auf dem aus der Fläche f durch die Kurve K herausgeschnittenen Flächenstück durch die Linksschraubenregel gegeben.

Das Kurvenintegral über den beugenden Rand B ergibt ebenso wie im Falle (a) die Beugungswelle u_B (2.3). Das nun zusätzlich auftretende Integral über K stellt hingegen die einfallende Lichtwelle und zwar sowohl im vorderen als auch im rückwärtigen Lichtkegel dar. Um dieses Integral über K zu berechnen, wollen wir auf K statt der Bogenlänge s eine neue Integrationsvariable α einführen. Zu diesem Zweck betrachten wir die Schar aller Halbebenen, die durch die durch die beiden Punkte P und F hindurchgehende Gerade begrenzt werden und bezeichnen mit α den Winkel zwischen einer beliebigen Halbebene E und einer fixen Halbebene E_0 dieser Schar.

Um nun den Zusammenhang zwischen $d\alpha$ und dem Randelement $\boldsymbol{ds}$ auf dem beugenden Rande anzugeben, benennen wir mit R die Entfernung der beiden Punkte P und F und mit d den Abstand eines Randelementes $\boldsymbol{ds}$ der Kurve K von der durch die beiden Punkte P und F hindurchgehenden Geraden. Da $\frac{1}{2} Rd$ den Flächeninhalt des Dreieckes F, P, ds bedeutet, so stellt

$$\boldsymbol{N} = \frac{\boldsymbol{r} \times \vec{\varrho}}{Rd} \tag{3.1}$$

einen Einheitsvektor dar, der senkrecht auf der Ebene des Dreieckes $F.\ P.\ ds$ steht. Da $\boldsymbol{N}\boldsymbol{ds} = ds_0$ die Projektion des Randelementes $\boldsymbol{ds}$ auf die Richtung des Einheitsvektors $\boldsymbol{N}$ bedeutet, so ist $d\alpha = ds_0/d$, so daß mit Rücksicht auf (3.1)

$$(\boldsymbol{r} \times \vec{\varrho})\, \boldsymbol{ds} = \pm\, R d^2 d\alpha \tag{3.2}$$

ist. Wir haben die rechte Seite von (3.2) mit dem $\pm$ Zeichen versehen, da wir die Integration über α zwischen den Grenzen 0 und 2π erstrecken wollen. Es gilt dann in (3.2) das positive bzw. das negative Vorzeichen, je nachdem der Winkel γ zwischen dem Vektor $\boldsymbol{r} \times \vec{\varrho}$ und dem Bogenelement $\boldsymbol{ds}$ auf der Kurve K ein spitzer oder ein stumpfer ist. Falls nur die Kurve K eine solche Gestalt hat, daß der Winkel α beim Durchlaufen der Randkurve sich stets nur monoton ändert, kann man leicht aus der Abb. 1 entnehmen, daß γ einen spitzen bzw. einen stumpfen Winkel darstellt, je nachdem sich der Beobachtungspunkt P im vorderen bzw. im rückwärtigen Lichtkegel befindet. Demnach ist in (3.2) das positive bzw. das negative Vorzeichen zu verwenden, je nachdem der Beobachtungspunkt P im vorderen bzw. im rückwärtigen Lichtkegel enthalten ist.

Den Nenner in g (1.12) kann man mit Hilfe der nachstehenden, durch Quadratbildung aus $\boldsymbol{R} = \vec{\varrho} - \boldsymbol{r}$ folgenden Beziehung

$$2[r\varrho - \boldsymbol{r}\vec{\varrho}] = R^2 - (\varrho - r)^2 \tag{3.3}$$

ausdrücken.

Um noch die in (3.2) auftretende Entfernung d durch R, r, ϱ darzustellen, bemerken wir, daß aus der Heronschen Formel für den Flächeninhalt des Dreieckes $F.\ P.\ ds$ sich die Beziehung

$$R^2 d^2 = \tfrac{1}{4}\,[(r+\varrho)^2 - R^2]\,[R^2 - (r-\varrho)^2] \tag{3.4}$$

ergibt, da ja seine Seiten durch R, r, ϱ gegeben werden.

Bei der Anwendung des Stokesschen Satzes auf (2.1) erhält man daher für das über die Kurve K erstreckte Integral mit Rücksicht auf (3.2), (3.3) und (3.4) den Ausdruck

$$\pm\, \frac{1}{8\pi} \int_0^{2\pi} \frac{e^{ik(r-\varrho)}}{r\varrho R}\, [(r+\varrho)^2 - R^2]\, d\alpha. \tag{3.5}$$

Dabei gilt mit Rücksicht auf (3.2) im vorderen Lichtkegel das positive und im rückwärtigen das negative Vorzeichen.

Bezeichnen wir mit r_0 bzw. ϱ_0 die Absolutbeträge der nach dem Punkte Q_0 der Fläche f von P bzw. F aus gerichteten Vektoren, so erhalten wir beim Zusammenschrumpfen der Kurve K auf den Punkt Q_0 im Grenzfalle für $(r+\varrho)^2 - R^2 = (r+\varrho)^2 - (r_0 - \varrho_0)^2$ den Wert $4r_0\varrho_0$. Der Abstand R des Beobachtungspunktes P vom Brennpunkt F wird nämlich im vorderen Lichtkegel durch

$$R = \varrho_0 - r_0 \tag{3.6a}$$

und im rückwärtigen Lichtkegel durch

$$R = r_0 - \varrho_0 \tag{3.6b}$$

gegeben.

Es ergibt sich daher im Grenzfalle des Zusammenschrumpfens für den Beitrag (3.5) des Kurvenintegrals über K zu der durch den Kirchhoffschen Ansatz (1.1) dargestellten Wellenbewegung im vorderen bzw. im rückwärtigen Lichtkegel mit Rücksicht auf (3.6a) bzw. (3.6b) für die einfallende Lichtwelle der Ausdruck

$$u_{E_1} = \frac{e^{-ikR}}{R} \tag{3.7a}$$

bzw.

$$u_{E_2} = -\frac{e^{ikR}}{R}\,. \tag{3.7b}$$

Im vorderen Lichtkegel wird somit die einfallende Lichtwelle (3.7a) durch eine auf den Brennpunkt F hin konvergierende Kugelwelle gegeben, wie man dies gemäß der geometrischen Optik erwartet. Im rückwärtigen Lichtkegel verdient (3.7b) eigentlich nicht die Bezeichnung „einfallende" Lichtwelle, da sie ja doch eine von dem Brennpunkt F aus divergierende Kugelwelle darstellt. Wenn wir sie so benennen, so geschieht es nur um für die beiden durch die geometrische Optik gegebenen Wellenbewegungen u_{E_1} und u_{E_2} eine gemeinsame Bezeichnung zur Verfügung zu haben.

Die einfallende Welle u_{E_1} (3.7a) im vorderen Lichtkegel unterscheidet sich von der einfallenden Welle u_{E_2} (3.7b) im rückwärtigen Lichtkegel durch das Vorzeichen. Es ist somit ein Phasensprung π bereits in der einfallenden Lichtwelle vorhanden. Damit ist unsere Behauptung bewiesen, daß der Phasensprung im Brennpunkt eine geometrisch-optische Erscheinung ist.

Allerdings kann man dagegen geltend machen, daß der durch den Kirchhoffschen Ansatz (1.1) beschriebene Wellenvorgang im ganzen Raume also auch im Brennpunkte F regulär ist. Das bedeutet, daß die in der einfallenden Welle $u_{E_1} + u_{E_2}$ im Brennpunkte F auftretende Singularität durch die Beugungswelle u_B kompensiert werden muß, also im Brennpunkte F selbst gar nicht zur Geltung kommt. Und zwar gilt diese Tatsache ohne Rücksicht auf die Größe der Wellenlänge, bleibt also auch im Grenzfalle $\lambda \to 0$ erhalten.

Diese letztere Tatsache wird dadurch bedingt, daß im Brennpunkte F die Beziehung $r = \varrho$ gilt (vgl. Abb. 1, in der jedoch anzunehmen ist, daß der Punkt Q_0 auf dem beugenden Rande B liegt) und daher gemäß (2.3) von allen Punkten des beugenden Randes die Beugungswelle ohne Rücksicht auf die Größe von λ mit der gleichen Phase eintrifft. In einem Beobachtungspunkte P, der ganz in der Nähe des Brennpunktes F liegt, ändern sich demnach die Phasen der von den einzelnen Punktes des beugenden Randes eintreffenden Beugungswellen nur wenig, so daß die gesamte Beugungswelle u_B hier noch größere, d. h. mit der einfallenden Lichtwelle vergleichbare Werte erreichen kann. Sobald aber λ gegen Null strebt, so werden die Phasen der von den einzelnen Punkten des beugenden Randes kommenden Beugungswellen sich immer rascher ändern und daher immer mehr auslöschen (vgl. z. B. Rubinowicz 1957, S. 166 ff.). Das bedeutet jedoch, daß der Bereich um den Brennpunkt, in dem die Beugungswelle mit der einfallenden Welle vergleichbare Werte annimmt und daher die Wellenbewegung von der durch die einfallende Lichtwelle gegebenen beträchtlich abweicht, zugleich mit λ immer kleiner wird. Dementsprechend wächst der Bereich in dem die geometrisch-optische einfallende Lichtwelle als eine angenäherte Darstellung der gesamten

Wellenbewegung angesehen werden kann, in dem also der Phasensprung sich geltend macht. In diesem Sinne ist somit die Behauptung zu verstehen, daß der Phasensprung eine geometrisch-optische Erscheinung ist.

§ 4. Plausibilitätsbetrachtungen über die Entstehung des Phasensprunges

Nachdem vom Standpunkte der Kirchhoffschen Beugungstheorie der mathematisch strenge Nachweis für die geometrisch-optische Natur des Phasensprunges erbracht ist, drängt sich die Frage nach seinem intuitiven Erfassen von selbst auf. Ich habe zwar in meiner früheren diesbezüglichen Arbeit (Rubinowicz 1938) mit Hilfe von Plausibilitätsbetrachtungen eine Begründung für unsere These gegeben; sie hat jedoch den Nachteil, daß sie nicht voll der Tatsache gerecht wird, daß die Beugungswelle u_B im Brennpunkte F eine Singularität aufweist.

Um Plausibilitätsbetrachtungen durchzuführen, die von diesem Mangel frei sind, gehen wir von der Bemerkung aus, daß durch den Brennpunkt die Schattengrenzen der von allen Punkten des beugenden Randes stammenden Anteile der Beugungswelle u_B hindurchgehen. Nähern wir uns einem Punkte der Schattengrenze, der nicht in unmittelbarer Nähe des Brennpunktes liegt, so bewirkt dies, wie wir es in § 2 auseinandergesetzt haben, für einen bestimmten Anteil der Beugungswelle ein Unendlichwerden des Integranden. Nähern wir uns nun dem Brennpunkt, so nähern wir uns gleichzeitig den Schattengrenzen der von allen Punkten des beugenden Randes stammenden Anteile, wodurch also das Auftreten von Singularitäten in allen diesen Anteilen bewirkt wird. Auf diese Weise wird es verständlich, daß die Beugungswelle im Brennpunkte so stark unendlich wird, daß sie das Unendlichwerden der einfallenden Welle $u_{E_1} + u_{E_2}$ kompensiert.

Wir wollen noch zeigen, wie man auch verschiedene andere Details des Verhaltens der Beugungswelle in der Nachbarschaft des Brennpunktes verstehen kann. Sie muß nämlich zunächst die im vorderen und rückwärtigen Lichtkegel auftretenden und hier verschiedene Vorzeichen aufweisenden Singularitäten (3.7a) und (3.7b) der einfallenden Welle beheben. Außerhalb dieser beiden Lichtkegel muß sie jedoch auch in der Nachbarschaft des Brennpunktes endlich bleiben. Den Schlüssel zum Verständnis dieses Tatbestandes liefert das Verhalten der Beugungswelle wenn wir uns einem Punkte ihrer Schattengrenze von der einen oder der anderen Seite nähern. Die Grenzwerte, die wir in diesen beiden Fällen erhalten, unterscheiden sich nämlich in erster Näherung nur durch das Vorzeichen, haben aber sonst gleiche Absolutbeträge und gleiche Phasen. Der Nachweis dafür kann in dem betrachteten Falle ganz ebenso wie im Falle der divergierenden Kugelwelle (Rubinowicz 1957, S. 194) erbracht werden. Das Auftreten dieses Sprunges der Beugungswelle wird durch die in § 2 besprochene Singularität des Integranden von u_B (2.3) für dasjenige Randelement $\boldsymbol{ds}_0$ bewirkt, das auf der Verbindungsgeraden des Brennpunktes F und des Punktes P_0 auf der Schattengrenze liegt, dem der Beobachtungspunkt P sich nähert. Die Verschiedenheit des Vorzeichens rührt von dem Anteil $(\boldsymbol{r} \times \vec{\varrho})\,\boldsymbol{ds}$ des Integranden in (2.3) her, der zum Randelement $\boldsymbol{ds}_0$ gehört. In der Schattengrenze selbst, wo $\boldsymbol{r}$ und $\vec{\varrho}$ parallel werden, verschwindet nämlich $(\boldsymbol{r} \times \vec{\varrho})\boldsymbol{ds}$ und ändert beim Durchgang durch die Schattengrenze sein Vorzeichen.

Der Bequemlichkeit des sprachlichen Ausdruckes wegen, bezeichnen wir nun diejenige Seite der Schattengrenze eines Randelementes $\boldsymbol{ds}$ als die positive Seite, die vondem vorderen Lichtkegel aus zu erreichen ist. Die andere Seite heiße die negative. Wie aus der Abb. 1 zu entnehmen ist, nähern wir uns nun der positiven bzw. der negativen Seite der Schattengrenze, wenn wir an sie von dem vorderen bzw. rückwärtigen Lichtkegel aus herantreten.

Bei der Annäherung an den Brennpunkt F vom vorderen bzw. rückwärtigen Lichtkegel aus, wird daher das Verhalten der Beugungswelle u_B durch die Grenzwerte auf der positiven bzw. auf der negativen Seite der Schattengrenze bestimmt (vgl. Abb. 1). Dies erklärt die Verschiedenheit der Vorzeichen der Beugungswelle in den beiden Lichtkegeln, die notwendig ist, um die Singularitäten der einfallenden Wellen (3.7a) und (3.7b) im Brennpunkte F zu beheben. Die Tatsache, daß der Grenzwert der Beugungswelle endlich ist, wenn wir uns dem Brennpunkte F aus dem Außenraume der beiden Lichtkegel nähern, erklärt sich daraus, daß wir uns dann gleichzeitig der negativen Seite des vorderen und der positiven Seite des rückwärtigen Lichtkegels nähern (vgl. Abb. 1). Bei der Annäherung an den Brennpunkt F von dem Außenraume der beiden Lichtkegel her, haben somit die Singularitäten verschiedene Vorzeichen und ergeben daher einen endlichen Grenzwert.

Dabei ist noch zu beachten, daß die Beugungswelle u_B (2.3) aus Wellen besteht, die ihre Ausgangspunkte in dem beugenden Rande haben. Sie kann daher nur singuläre Wellen erzeugen, die diese Fortpflanzungsrichtung haben, die also in dem vorderen Lichtkegel auf den Brennpunkt F hin, im rückwärtigen aber von ihm weg gerichtet sind, genau so wie dies bei den einfallenden Wellen (3.7a) und (3.7b) der Fall ist, deren Singularitäten durch die Beugungswelle beseitigt werden.

LITERATURVERZEICHNIS

Rubinowicz, A., *Ann. Phys.* [*Leipzig*], (4) **53**, 257 (1917).

Rubinowicz, A., *Phys. Rev.*, **54**, 931, (1938).

Rubinowicz, A., *Acta phys. Polon.*, **12**, 225 (1953).

Rubinowicz, A., *Die Beugungswelle in der Kirchhoffschen Theorie der Beugung*, Państwowe Wydawnictwo Naukowe, Warszawa (1957).

Warszawa, den 19. November 1960.